Evaluation of the Mark III Spacesuit
An Experimental and Computational Modeling Approach

by

Conor R. Cullinane

B.S. Aeronautical Engineering
Clarkson University, 2013

Submitted to the Harvard-MIT Program in Health Sciences and Technology
in partial fulfillment of the requirements for the degree of

Doctor of Philosophy

at the

MASSACHUSETTS INSTITUTE OF TECHNOLOGY
June 2018

Signature redacted

Author . . . . . .
Harvard-MIT Program in Health Sciences and Technology
Bioastronautics Training Program
May 2, 2018

Signature redacted

Certified by . . . . . .
Leia Stirling, PhD
Assistant Professor
Charles Stark Draper Professor of Aeronautics and Astronautics
Associate Faculty, Institute for Medical Engineering and Science
Thesis Supervisor

Signature redacted

Accepted by. . . . . .
Emery N. Brown, MD, PhD
Director, Harvard-MIT Program in Health Sciences and Technology
Associate Director, Institute for Medical Engineering and Science

Evaluation of the Mark III Spacesuit
An Experimental and Computational Modeling Approach

by
Conor R. Cullinane

Submitted to the Harvard-MIT Program in Health Sciences and Technology
on May 2, 2018 in partial fulfillment of the
requirements for the degree of
Doctor of Philosophy

Abstract

Spacesuit Assemblies (SSAs) provide life support for human operators performing extravehicular activities (EVAs). The overall goal of this research was to investigate three research questions to address gaps in the field of spacesuit assembly (SSA) evaluations: [1] What are the mobility and agility limitations causing operators to experience performance decrements when wearing a SSA?; [2] What is causing operators to experience increased joint torques?; and [3] How does the distributed weight of an SSA, transferred to the operator, affect performance? This research leveraged both experimental and computational modeling capabilities to evaluate SSAs with a human-centered focus, in ways previously unachievable.

The space suit evaluated for this research was NASA's Mark III (MkIII) Planetary Technology Demonstrator SSA, built to test the next generation in planetary exploration capabilities, improving upon Apollo era technology. The hip brief assembly (HBA) is built with three nested bearings, each with a single rotational degree of freedom that together provide the range of motion, walking efficiency, and kneeling capabilities.

An initial investigation, combining a pilot study and supporting modeling, revealed limitations in the current human-SSA system that may impair the operator's mobility/stability and agility. Limitations identified and investigated in this thesis include SSA degrees of freedom (DOFs), the SSA range of motion (ROM) envelope, the bearing resistances, the SSA component's inertial effects, the SSA mass load transfer dynamics, and suit fit. The SSA architecture was modeled as part of the thesis, creating a tool that was useful in the investigation of the human-suit system. The model relied on SSA component geometries and inherent mass/inertia and bearing resistance characteristics to output joint dynamics, rather than requiring those dynamics as an input (which would require extensive experimental setups). The model was used to isolate components that contribute to the measured operator performance degradations and to quantify the extent of their contributions. These investigations lead to suggestions for design requirements and evaluation techniques that can guide future SSA development and evaluations.

Thesis Supervisor: Leia Stirling, PhD
Title: Assistant Professor
Charles Stark Draper Professor of Aeronautics and Astronautics
Associate Faculty, Institute for Medical Engineering and Science

Acknowledgement

When I find myself at an intersection on the road of life, I simply ask myself, "Is it going to be awesome?" If the answer is yes, I take that road. Sometimes, I have to decide between two "awesome" roads, but that is a nice problem to have. When I finished my undergraduate degree at Clarkson University, I had the opportunity to pursue a number of exciting opportunities, one stood out to me as having the highest probability of being "awesome"!

During my time working towards a PhD, I had the opportunity to become a pilot, fly in a jet, fly in a B17, watch *Apollo 13* in the Apollo 13 Mission Control Center, drive the Constellation Lunar Rover, meet many astronauts, run on the vertical treadmill, test exercise equipment in parabolic flight, wear and operate a spacesuit, experience varying levels of gravity in ARGOS, sit in Shuttle/Orion/Soyuz/Dragon/New Shepard spacecraft and simulators, see the neutral buoyancy lab, tour JPL, see many rocket launches, fish the Charles River with an astronaut paddling the canoe, eat astronaut food, mentor as a GRT, get engaged, edit an encyclopedia, start a company, and much more.

I am truly excited to have reached the end of an awesome journey, but I certainly was not on that journey alone! I want to start by thanking Leia Stirling, the best advisor I could have ever asked for. Leia takes the time to understand each of her students and adapt to support them in whatever ways they need. Leia was able to guide my engineering focused mindset, to understand that the engineering was actually a tool used to answer bigger scientific research questions. We do not do engineering for the sake of doing it, but rather we do it to address a need.

I want to thank my entire thesis committee: Dr. Larry Young, Dr. Allison Anderson, and Dr. Dennis Anderson for guiding me towards a successful PhD. To my NSTRF mentor, Richard

Rhodes, thank you for supporting me and helping to smooth the path at NASA for me to perform experiments there. To Shane Jacobs, thank you for being there along the way to provide feedback and insight into the process of spacesuit design.

To everyone at NASA that was there along the way, thank you for the great experiences. I was able to learn from doing, and created numerous fond memories along the way. Specifically, I want to thank Amy Ross, Lindsay Aitchison, Mike Gernhardt, Eric Antonsen, Marlei Walton, Andrew Abercromby, Jason Norcross, Robert Sweet, Dan Nguyen, Scott England, Elizabeth Benson, and Sarah Jarvis.

Thank you to the entire MVL, who welcomed me warmly and is an amazing community. I will never forget the science we achieved, nor the fun we had while doing it. I specifically want to thank Forrest Meyen; I looked forward to going to lab every day when you were there and I learned so much from you. Your mentorship helped me to grow greatly, including in the world of entrepreneurship. A lifelong friend.

I want to thank Eli Kapas and Matt Kane, my best friends and business partners. You have both played a huge role in my life. You were instrumental in my success at Clarkson, which allowed me to come to MIT and continue that success. I already look back in awe of how far we all have come, and I cannot wait to see where we go from here.

I want to thank my family for supporting me throughout my PhD. The process was fun, but it definitely had points where I needed an extra push. Specifically, I want to thank my Mom and Dad, my Nana and Papa, and my brothers and sister. Without all of you, I would not be where I am today, and would have struggled to make it to the end of my PhD. I tend to do things "my way", thank you for embracing that and not trying to change me.

Finally, I want to thank my fiancé Robin! I thought I had it all pretty well figured out before I met you. I was so wrong. You changed the way that I see the world and you make every day easier, including the difficult time when I was working on finishing my PhD! It is difficult to remember or imagine life before you. I have had a blast with you every day since I met you and I awake every day looking forward to the adventures we will embark on! This PhD is only the beginning.

This work was supported in part by the National Space Biomedical Research Institute as part of the mentored research program through the Bioastronautics Training Program (NASA NCC 9-58), by a NASA fellowship through their Space Technology Research Fellowship Program (NNX15AP51H), and by a NASA grant in conjunction with the National Robotics Institute (NNX15AR20G).

Table of Contents

1. Introduction

1.1 Motivation

Human space flight necessitates life support for crewmembers during *extravehicular activities* (EVAs) in the form of *spacesuit assemblies* (SSAs), which should maximize human performance and efficiency, while preventing injury.[23] Operators wearing earlier EVA suits have developed a variety of injuries in a range of locations, including the shoulder and hip.[48,57] Prolonged use has led to erythema, abrasions, muscle soreness/fatigue, paresthesia, bruising, blanching, and edema.[48,57] SSA designs must consider the interaction of mass, volume, walking effort, mobility, agility, and suit fit.[2] In this thesis, experimental and computational analyses are leveraged to investigate the interaction of mass, mobility, agility, and suit fit on SSA operator performance in planetary tasks.

Operating a spacesuit requires operators to exert energy and can often be difficult. Carr et al.[11] and Norcross et. al.[47] looked at differences in metabolic cost between unsuited and suited operations, showing that suited operations increase metabolic costs. The research investigated the contributions of terrain, gravity level, suit *kinematics* (the motion of bodies without references to the forces that cause the motion), and suit *dynamics* (the torques and forces that drive the motion) to metabolic costs. By increasing mobility and agility to reduce deviations from unsuited operator kinematics, injury risk and metabolic cost may be reduced[67], and could extend exploration capabilities (e.g. crewmembers could traverse terrain that is more complex, cover greater distances in a given time, or increase the duration of an EVA).

Inclusion of the human-SSA interactions in the design process systematically drives the design to incorporate human factors from the start, reversing the conventional process where mechanical design is followed by an evaluation of the resulting impact on the operator. In this

thesis, I evaluate how the Mark III (MkIII) SSA architecture affects human operator performance and safety and I suggest methods for improvement for both the MkIII as well as future planetary suits. Spacesuits are specialized, load-bearing, wearable systems that are *tightly-coupled* or highly integrated with their human operators. The tightly-coupled nature means that spacesuit design decisions affecting suit kinematics and dynamics will also change the operator motions through altered human-SSA interactions. This research leverages both kinematic and dynamic analyses within both experimental analyses and computational modeling to achieve insight into design decisions for tightly-coupled human-SSA interactions.

Specifically, the research addresses three main gaps or questions in the field of human-SSA interactions, with broader applicability in the Defense, Medicine, and Private sectors:

[1] What are the mobility and agility limitations causing operators to experience performance decrements when wearing an SSA?

[2] What is causing operators to experience increased joint torques when wearing an SSA?

[3] How does the distributed weight of an SSA, transferred to the operator, affect performance?

Gap [1] was addressed experimentally using comparisons of gait parameters in unsuited and suited ambulation, and supported with modeling. Gap [2] was addressed with modeling of the required hip joint torque in flexion and extension, representing motion from ambulation. Gap [3] was addressed experimentally during static double stance and single stance tasks. The results from

the research for each of the three gaps can be used to suggest updated suit evaluation methods and future SSA design requirements.

When evaluating an SSA, such as the MkIII, there are various experimental evaluation techniques used, but the techniques are not always operationally equivalent. For example, an experiment conducted at Johnson Space Center (JSC) by Valish et al.,[64] was designed to obtain SSA *joint torques*. However, the suit was empty (no human operator) and the applied torque was generated from an externally applied force with the suit strapped to a table. The applied torque, in reality, would have been generated by the human operator from the inside of the suit and applied over a distributed area, rather than a single external point. Modeling could augment the experimentally obtained data for operational relevancy. The model could be used to decompose the joint torques required by the operator to move the suit, to understand the contributing components to the overall torque. Then, changing the model inputs to match operational scenarios could allow for conclusions that are more relevant.

A model was developed as part of this research effort, as a tool to address the three gaps, since a high-fidelity kinematics/dynamics model of the MkIII SSA does not exist. Existing computational techniques for SSAs consist of either kinematic or dynamic analyses. The kinematic analyses produce *functional motion envelopes* including *range of motion* (ROM) and reach capabilities, but have no information about forces or torques. The dynamic analyses use experimental measures of required joint torques and models for *joint hysteresis*, as model inputs, to simulate suit resistances. The dynamics models cannot be extended to new scenarios, such as a change in the orientation of a joint relative to gravity) without collecting new experimental data for each scenario of interest. Instead of using joint torques as a model input, the model developed here combined both kinematic and dynamic representations to output estimates of the joint torques

required to achieve the SSA motion envelopes (Chapter 2). The kinematic functionality of the model is implemented to augment experimental analysis in Chapter 3. The dynamic functionality of the model is implemented in Chapter 4 to decompose the required hip torques.

This research, focused on Aerospace applications, can address the needs outlined within NASA's Technology Area Breakdown Structure, specifically section 11.2.3: Human-System Performance Modeling. The model developed as part of this thesis was leveraged to improve current modeling capabilities at NASA for SSA evaluation. The design tool could reduce time and financial costs associated with SSA suit design, manufacturing, and testing. As NASA gears up for its horizon destination, Mars, addressing the three main gaps in this thesis will promote safe and efficient exploration.

Translational Applications in Defense: Considerable work has been conducted in the area soldier suits for augmenting load carriage capability.[9,29,36,66] These systems are designed to enable the user to carry larger loads with reduced metabolic cost. However, locomotion with these systems is compromised by the rigid architecture used to carry load, which requires the operator to alter their natural motion. Operators must conform to the functional motion envelope mobility restrictions of the tightly-coupled system, much like operating the MkIII SSA. The combination of experimental and computational evaluations implemented in this thesis, to evaluate SSA technologies, would be relevant in addressing similar gaps in Defense.

Translational Applications in Medicine: Lower extremity pathologies in patients with neuromuscular disorders can result in abnormal gaits. The most widely used solution is to combine physical therapy with the use of a passive orthotic rehabilitative wearables.[51] Such passive orthotics can improve gait patterns; however, long-term use can make the user more physically dependent on the device, as the immobilization or misuse of specific muscles may induce weakness

and atrophy,[6,22,30] along with reduced muscle activity over time.[21] Similar to the limitations in SSAs for space exploration and for augmenting load carriage, these systems rely on rigid[8,19,31] to soft[50] mechanical architectures that apply loads to the human through the tightly-coupled interactions. The proposed research could also be extended to rehabilitative wearable design and evaluation, providing a tool to predict the effects of design changes on gait and long term outcomes on patient recovery.

1.2 Literature Review

1.2.1 Mark III (MkIII) Spacesuit Assembly (SSA) Kinematics and Dynamics

Typically, with a *soft-goods* suit such as the Apollo A7L (the suit used for lunar exploration), the bending motion at the joint reduces the volume of the suit and requires work (W) to be done by the operator in the form of an applied joint torque. That work (W), is the force (F) necessary to bend the joint multiplied by the distance (d) through which the force acts.[45] Advanced SSAs, such as the Mark III (MkIII), were designed to increase mobility/agility by eliminating the change in volume associated with bending the joints (Figure 1, 2). The MkIII SSA was developed to evaluate technologies that extend planetary explorer capabilities beyond those of the Apollo A7L.

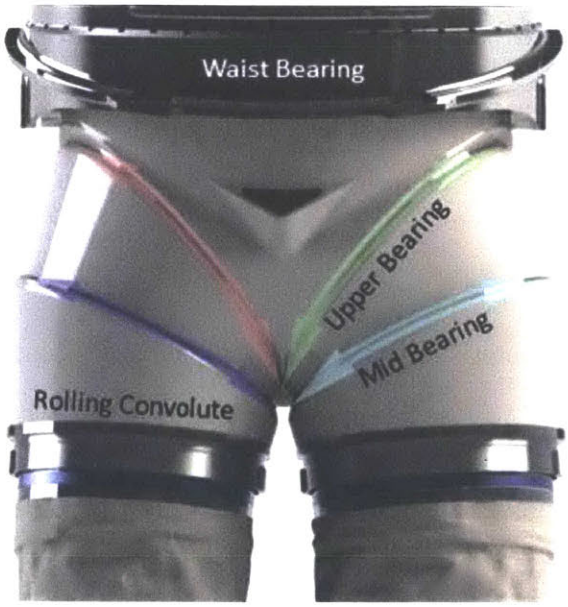

Figure 1: The Mark III (MkIII) Computer Aided Design (CAD) model showing the hip brief assembly (HBA) mobility unit. The depiction of the MkIII suit in this figure was generated from a model of the suit (Chapter 2) that was used to address aims in this thesis.

One technology tested is a hip brief assembly (HBA), that implements a multi-bearing,[13] hard-material (S-Glass, an improved strength E-fiberglass) architecture[7,56] (Figure 1). The upper

(proximal) and mid (distal) bearings provide hip flexion/extension and adduction/abduction. The rolling convolute joint has a bearing that provides rotation for internal and external rotation of each leg, but also a pivot point that provides additional adduction/abduction. Since the mobility is mostly afforded by bearing motions, the HBA provides constant-volume motion.

Although the constant-volume HBA eliminates the Work required to change the volume, there is still an added torque required by the operator to drive the HBA motion from both the resistance in the bearings as well as the weight/inertia of each component. In the soft goods suits, the hip torques were proportional to the angular displacement of the joint because of the changing volume.[45] However, the hip torques in the MkIII are related to the mass/inertial effects of the heavy, rigid suit components as well as the bearing resistances (Chapters 2, 4). Experiments at NASA, comparing the MkIII HBA to the Apollo A7L hip joint, reveal the HBA to have improved performance over its predecessor in two important categories: walking effort, and retrieving a rock sample.[14] However, the HBA has limitations in bent torso stability, standing on one knee, as well as requiring programmed motion.[2]

Another adverse characteristic of the constant volume joints, like the HBA, is that it requires operators to perform pre-determined, *programmed motions* to achieve changes in suit orientation and are inconsistent with natural biomechanics.[15] Cowley et al.[14] computationally estimated the HBA hip rotation to have 84 deg. of flexion, 7 deg. of pure abduction, and 93 deg. of transversely rotated abduction (a complex motion that combines hip flexion with abduction).

Crewmembers spend many hours in a given suit to learn and adapt to the programmed motions and required joint-torques for operational tasks. Training is important for operators to learn to operate a suit and discover ways to map the human joint *degrees-of-freedom* (DOFs) with the suit DOFs and to minimize required torques in an efficient manner.[20] When programmed

motions are not appropriately selected by the operators, the operators may have additional increases in their joint torques as they fight against the suit. If the suit alters natural biomechanics, it may result in increased injury risk over long-term usage inherent in locomotion and utility tasks.[53] Even a small alteration in natural biomechanics can result in injury when amplified through many cycles.[45,42]

There are currently two methods for investigating the complex interaction between human operators and SSAs: Experimental and Computational. To perform either an experimental or a computational investigation, it is necessary to understand both the human and SSA subsystems thoroughly before characterizing the human-SSA system.

1.2.2 Human Kinematics and Dynamics

For the human subsystem, decrements in postural stability can manifest as an increase in variance of the center of pressure (COP) in both X (medial-lateral) and Y (anterior-posterior).[34,49,69] COP is the point through which the ground reaction force vector acts on the surface where the subject is standing.[54] Postural stability decrements can also manifest in the variance of vertical ground reaction force (VGRF) because of a decreased ability to dampen vertical oscillations.[25,32,54] Variance in VGRF has been shown to increase with increased load carriage.[35] Additionally, it has been shown that variance in ground reaction force data can provide improved sensitivity, to the effects of different configurations (independent variables), over COP during quiet stance.[35] This measure will be useful in determining any differences in postural stability for varied levels of coupling, or suit fit (Chapter 5).

Previous unsuited gait studies have explored how typical biomechanics are altered with specific operational tasks. For example, cadence increases while step length and speed decrease when walking backwards (WB) as compared to Walking Forwards (WF).[26,63] It has also been

shown that gait cycle (1/cadence) and stride length are both functions of speed that depend on task, WF or WB.[26] Changes in dynamic base, which is the perpendicular distance between heels during double stance (schematic shown at the bottom of Figure 12), provide insight on overall stability. A wide dynamic base provides improved stability for controlling body mass over the supporting limb. In child development, the dynamic base decreases until the age of 3.5.[62] Within the elderly population the dynamic base increases among those at risk of falling and when walking at faster speeds.[44] As coordination and balance improves, dynamic base decreases.[62] Also, when carrying a load in addition to body mass, such as a 59 kg spacesuit, LaFiandara et al.[37] found a decrease in transverse pelvic rotation and decrease in stride length to maintain speed or increase cadence. Abe et al.[1] postulate that the change in stride length and cadence with load carriage may represent attempts to minimize energy expenditure. Previous analysis by Shorter et al.[60] showed increased circumduction from a hip ROM limitation, similar to the increase in dynamic base seen with the MkIII HBA. The changes reported by Shorter et al. in unsuited gait parameters led to a reduction in efficiency and increase in metabolic cost, even without the added mass and resistances of the suit.

1.2.3 Tightly-Coupled Wearable Systems

The MkIII requires its human operator to apply additional joint torques beyond those required to move their own limbs. A number of experimental studies have been performed to obtain joint torque data associated with operating an SSA.[3,40,41,43,52,55,58,64] There are three experimental methods for obtaining SSA joint torque data including unsuited external forcing, robotically applied internal torque, and suited internally applied torque.[3] In this thesis, experimental analysis from Valish et al.[64], which uses the first method, is leveraged to validate the model developed in Chapter 2. One of the drawbacks between all three methods is that they do not give a good

representation of operational (performing planetary tasks with a human operator) joint torques, but could be useful when augmented with modeling. Along with joint torques, the operator also experiences applied loads from the suit associated with the suit weight.

The weight of the suit can first be broken into two components: the weight transferred to the operator and the *self-supported* weight. Self-support is the fraction of total suit weight that is transferred directly to the ground without requiring the operator's support. Previous work by Carr et al.[10] showed how suit mass and self-support could affect operator biomechanics. They explained, "a space-suited astronaut does not support the entire mass of the space suit during locomotion, because part or all of the mass is supported by the pressure forces of the space suit". For the MkIII architecture, the HBA is a rigid-body system, but both legs are soft-goods. The soft-goods legs connect to the HBA at the rolling convolute joint and continue down to the top of the boot, where they connect at the boot flange, another bearing at the top of the boot. The limit of self-support for the MkIII, based on the architecture, will be the soft-goods legs buckling. The soft-goods rigidity and load-carrying capability comes from the interaction of suit pressure (4.3 psid for the MkIII), the cross sectional area of the soft-goods legs and the tension in the restraint layer. The tension in the restraint layer is based upon the suit weight and suit pressure.

The weight transferred to the operator can be split into two components as well: the weight that is transferred through the designed interaction locations (which in the case of the MkIII SSA, are shoulder straps) and the weight transferred through other non-designed locations (such as the operator's arm contacting the inside of the suit[5,4]). The operator must continually support that fraction of the suit weight as well as overcome the inertial effects associated with the moving mass during dynamic tasks.[24,47] In this thesis, I consider static tasks and examine how the fraction of weight transferred to the operator affects stability. Suited operation requires load carriage as the

operator will support a portion of the space suit weight. Added loads have been shown to decrease postural stability in soldiers.[38,61] I hypothesize that the fraction of suit weight transferred to the operator would also decrease postural stability. Postural stability is defined as a subject's control over their center of mass in both the suited and unsuited configuration.

Indexing, or strategically placed padding between the suit and operator, can be used to adjust suit fit.[27] The thickness and location of that padding can be increased or decreased to make the human-SSA system more or less tightly-coupled, respectively. For example, the suit can become more tightly–coupled with the operator by increasing the thickness of the padding, essentially reducing the gap between the operator and the suit. As discussed, the MkIII drives programmed motions through mobility restrictions, forcing operators to move within a limited motion envelope. Increasing coupling through indexing may force operators to adhere even closer to the mobility limitations inherent in the MkIII architecture.

1.2.4 Modeling Tightly-Coupled Spacesuits

Modeling has many advantages over experimental analysis. With modeling capabilities, questions can be answered or evaluations performed that are impossible or very difficult experimentally. One particular area is in the field of human-SSA interactions. One major drawback is replication of operation conditions along with an inability to measure intricate kinematics and dynamics associated with the human-SSA interaction in real time.

Existing kinematic modeling of human-SSA interactions investigate motion envelope capabilities based on the architecture of that suit, and compare those representations to the motion envelope of the human operators.[14,28,33] Existing dynamics models use experimental measures of required joint torques and models for joint hysteresis, as model inputs, to simulate suit resistances.[39,46,59] The dynamics models cannot be extended to new scenarios without collecting

new experimental data for each scenario of interest. Instead of using joint torques as a model input, the model developed here combined both kinematic and dynamic representations to output estimates of the joint torques required to achieve the SSA motion envelopes (Chapter 2).

Additional modeling uses musculoskeletal modeling to predict the effects of external joint torques, associated with operating an SSA, on the human operator.[17] Unfortunately, musculoskeletal modeling of the human-SSA system is very limited in the interactions that can be modeled, usually only applying torques at the joints or loads at a given point on a bone structure. These models do not account for the distributed nature of the interactions. Further studies use physics-based models to estimate metabolic costs through modeling.[12] Anderson[3] notes:

"...modeling efforts have not focused on how the suit impacts and constrains the wearer and where contact between the human and the suit occurs, which is critical information to reduce EVA injury. A model of that nature would require complicated dynamic simulations and a means by which to validate results, a technology not currently available."

The modeling work put forth in this thesis as a tool to address the aims, is a step towards the advanced modeling capabilities necessary for complete characterization of the human-SSA system. The rigid-body model presented in this thesis includes complicated dynamics of the suit, but leaves room for future modeling efforts in surface contact and interactions, as well as deformable soft goods[59].

1.3 Specific Aims

In this thesis, I will determine shortfalls in the current human-SSA system that may limit the operator's mobility and stability such as the SSA degrees of freedom, the SSA range of motion envelope, the hip bearing resistances, the SSA mass load transfer dynamics, and suit fit. After

identifying limitations in operator performance when suited, the SSA architecture will be investigated to isolate components that contribute to the operator performance degradations and quantify the extent of their contributions. These investigations can form a basis for design requirements that can guide future SSA or other suit (rehabilitative, soldier, private) development.

While targeting research gaps for complex human-suit systems in general, this thesis specifically focuses on aerospace SSAs for extravehicular activities (EVAs). In particular, I evaluated the Mark III (MkIII), a technology demonstrator for the development of the next generation in planetary exploration capabilities. The tightly-coupled human-SSA system implements a multi-bearing, hip-brief assembly (HBA) that provides hip mobility with three bearings, each with a single rotational degree of freedom (DOF).

The first research gap addressed using the MkIII is [1] What are the mobility and agility limitations causing operators to experience performance decrements when wearing an SSA? The measured performance decrement could be attributed to the SSA's functional motion envelope mobility restrictions (kinematic, programmed motion), an increase in required joint torques (dynamics), carrying the distributed weight of the suit (dynamics), suit fit, or a combination (complex interactions). To further understand the interactions, I investigated two additional research gaps for suits; [2] What is causing operators to experience increased joint torques when wearing an SSA?; and [3] How does the distributed weight of an SSA, transferred to the operator, affect performance?

1.3.1 Aim 1: Mobility and Agility Limitations

To identify the mobility (kinematic – resulting in deviations from unsuited biomechanics) and agility (dynamic – resulting in an increase in joint torques as compared to unsuited)

limitations incurred by the existing MkIII SSA architecture and inform future tightly-coupled suit design requirements to avoid similar limitations.

Aim 1.1 To test the hypothesis that the MkIII Hip Brief Assembly (HBA) architecture has DOF limitations that restrict operator mobility and agility. I will also test the hypothesis that there are resistive joint torques that operators must overcome to achieve a desired motion, which also limit operator agility.

Aim 1.2 To measure how much rotational motion the waist bearing affords in the transverse plane during ambulation, to understand how much relief it provides from restrictions introduced by the HBA.

1.3.2 Aim 2: Hip Joint Torque Decomposition

To identify and quantify the MkIII HBA components that contribute to the increase in total hip joint torques required by the operators during ambulation.

Aim 2.1 To identify the contributing components of the SSA that resist motion and require operators to increase their joint torques compared to unsuited, and to measure the specific contributions of each to the overall increase in joint-torque. I specifically decompose the required HBA joint torques into specific component contributions, which an operator must overcome to achieve flexion/extension of the hip during ambulation.

Aim 2.2 To measure the sensitivity of hip joint torque and flexion / extension angle, to model input parameters. This research specifically examined two external forcing profiles, *fleet sizing* (a few discreet sizes to accommodate all users) of the

boots, varied bearing resistances, and gravitational scenarios with multiple magnitude and direction configurations.

1.3.3 Aim 3: Distributed SSA Weight Transferred to the Operator

To quantify the magnitude of the distributed MkIII SSA weight transferred to the operator at the shoulder straps and measure the changes in stability associated with changes in suit fit, or how tightly-coupled the system is.

Aim 3.1 To test the hypothesis that the MkIII SSA self-supports part of its own weight, which increases in double stance as compared to single stance.

Aim 3.2 To test the hypothesis that operators lose postural stability when suited as compared to unsuited, and as they become more tightly-coupled with the suit.

1.4 Thesis Overview

The three main research gaps ([1] What are the mobility and agility limitations causing operators to experience performance decrements when wearing an SSA?; [2] What is causing operators to experience increased joint torques when wearing an SSA?; and [3] How does the distributed weight of an SSA, transferred to the operator, affect performance?) are addressed through a combination of experimental measurements and computational modeling. Chapter 2 presents the development of the computational modeling tool for the MkIII SSA. The model enabled iterative analyses that would typically incur enormous costs through manufacturing and testing of physical components. This tool is an advanced capability, beyond previously existing modeling tools, allowing for the interrogation of a combination of kinematic and dynamic effects. Chapters 3, 4, and 5 present the methods and results of the combined analysis to address Aims 1, 2, and 3 respectively.

Chapter 3 presents the implementation of the model alongside an experimental pilot study that I conducted at Johnson Space Center. The experimental analysis measured gait parameters (e.g. step length, stride length, dynamic base, etc.) for a single subject, both suited and unsuited. Comparing the resulting gait parameters shows that the MkIII SSA restricts operator mobility and agility compared to unsuited performance. The model was then used to supplement the experimental analysis, showing ROM restrictions based on the HBA DOFs, to explain specific results.

Chapter 3 (Aim 1) shows that the MkIII HBA has DOF limitations that restrict performance compared to unsuited. However, the DOF limitations do not explain all of the performance decrement. I was able to identify additional factors that could be contributing: increased hip joint torques associated with the bearing resistances, inertial effects of the SSA component masses, transfer of the distributed suit weight to the operator, and suit fit. Although the specific contributions to the overall performance decrement could not be identified in Chapter 3 (Aim 1), it led to our second and third research gaps. Chapters 4 (Aim 2) and 5 (Aim 3) both investigate specific contributions of the identified factors.

In Chapter 4 (Aim 2), the model is implemented to perform a dynamic analysis of the MkIII HBA to investigate the specific contributions of the bearing resistances and the component masses to the overall increase in hip joint torques seen in Chapter 3 (Aim 1). These resistances are independent of the DOF limitations. If an operator programs their motions to move within the functional motion envelope of the suit, they will still encounter a joint torque associated with the suit mass and bearings. Here, the model allows a decomposition of the overall torque increase into its specific contributing components, otherwise unachievable through experimental analysis alone.

Chapter 5 (Aim 3) investigates the role of the total suit mass and suit fit on the performance decrement compared to unsuited. The weight of the suit is not worn like a backpack, but rather it is distributed all around the operator, much like a shell. Existing literature on load carriage effects on gait are testing weights concentrated in a single area (e.g. the chest or back, much like a backpack). The locations through which the weight of the suit is transferred to the human inside can change with suit fit and could also change gait parameters.

2. Rigid-Body Mark III (MkIII) Space Suit Assembly (SSA) Model

As the development of planetary SSAs progress, it is important to consider the current limitations present in the SSA architectures that drive the human-SSA system interactions and how these can be mitigated to aid future mobility needs. Enabling synergistically integrated SSA designs that allow for optimal performance requires a tool to evaluate mobility and agility of the human-SSA system. In this chapter, I present the development of a rigid-body kinematic and dynamic model of the MkIII SSA.

Existing computational techniques for SSAs consist of either kinematic or dynamic analyses. The kinematic analyses produce functional motion envelopes including range of motion (ROM) and reach capabilities, but have no information about forces or torques. [14,28,33] The dynamic analyses use experimental measures of required joint torques and models for joint hysteresis, as model inputs, to simulate suit resistances. [39,46,59] The dynamics models cannot be extended to new scenarios (architectures, gravity directions, gravity magnitudes, bearing resistances, component masses, etc.) without collecting new experimental data for each scenario of interest. Instead of using joint torques as a model input, the model developed here combined both kinematic and dynamic representations to output estimates of the joint torques required to achieve the SSA motion envelopes. The kinematic functionality of the model is implemented to augment experimental analysis in Chapter 3 (Aim 1). The dynamic functionality of the model is implemented in Chapter 4 (Aim 2) to decompose the required hip torques.

In this thesis, I am interested in the MkIII because it is a planetary suit, designed to provide mobility and agility during planetary tasks. I consider static standing, as well as ambulation. Therefore, I am particularly interested in the components of the MkIII SSA that provide the mobility for standing and walking. Specifically, I am interested in the Hip Brief Assembly (HBA).

The MkIII HBA provides hip mobility with three bearings, each with a single rotational degree of freedom (DOF).

2.1 Generation of Component Part Files

Internal and external laser scans were previously completed at JSC, by Carly Meginnis, for use in developing computer aided design (CAD) models of the Mark III (MkIII) Space Suit Assembly (SSA). The laser scans had been used previously[14] to model kinematic motion envelopes of the Hip Brief Assembly (HBA, Figure 3). For this research, a higher fidelity SSA CAD was needed to understand and evaluate the human-SSA interactions. For example, I needed to understand and account for the inside surface profile of the SSA components as that is the location where the human operator will contact the suit. Additionally, the kinematics of the SSA CAD model needed to match the kinematics of the real suit to achieve accurate outputs and meaningful results.

The laser scan data was split by SSA component, each a point cloud representation (a group of points, each defined in x, y, and z). However, the point clouds were not perfectly isolated by SSA component. Therefore, the first step in processing the laser scan data was to segment the point cloud, using a built-in SolidWorks (Dassult Systems S.A., Vélizy, France) add-in tool (Mesh Prep) to select the points of interest and delete unwanted points in the cloud. Once the points of interest for a given component were segmented, the point cloud was converted into a mesh. The mesh was then converted to an actual part file in SolidWorks, using the tools inside the add-in ScanTo3D.

Each part then underwent a feature recognition process, used to identify evident geometries within the laser scanned SSA component. For example, locations where bearings are located are perfect circles, and the feature recognition detects those locations and superimposes the recognized features over the part. It also detects surfaces, such as flat surfaces. This makes the mating process

in SolidWorks much easier because you can base the mates on the recognized features. However, sometimes the features are not detected, thus they have to be manually adjusted.

This method was repeated for each component of the suit, including the soft-goods sections (legs, arms, and gloves) of the MkIII SSA. While the soft-goods sections of the SSA are deformable, they were represented as rigid-bodies within this model. Only the Arms/Gloves and Legs/Boots were soft-goods in the MkIII. Since I was not concerned with the arms/gloves, those did not matter. However, assuming the legs to be rigid-bodies would and did effect results. I addressed this by simulating multiple knee angles within the model.

To achieve a motion envelope or kinematic profile matching the MkIII, the SSA Rigid-Body SolidWorks Model (Figure 2) mates were strategically chosen. The bearings were represented as two concentric rings. Each ring was manually added to the part files of the SSA components located on either side of the bearing, and was used to define the mate between the two parts, forming a rotating bearing in the SolidWorks assembly. The rings were held concentric, while allowing rotation. Then the surfaces were held coincident to fully define the bearings and provide realistic motion. However, at this point, there was no resistance to motion defined for the bearings.

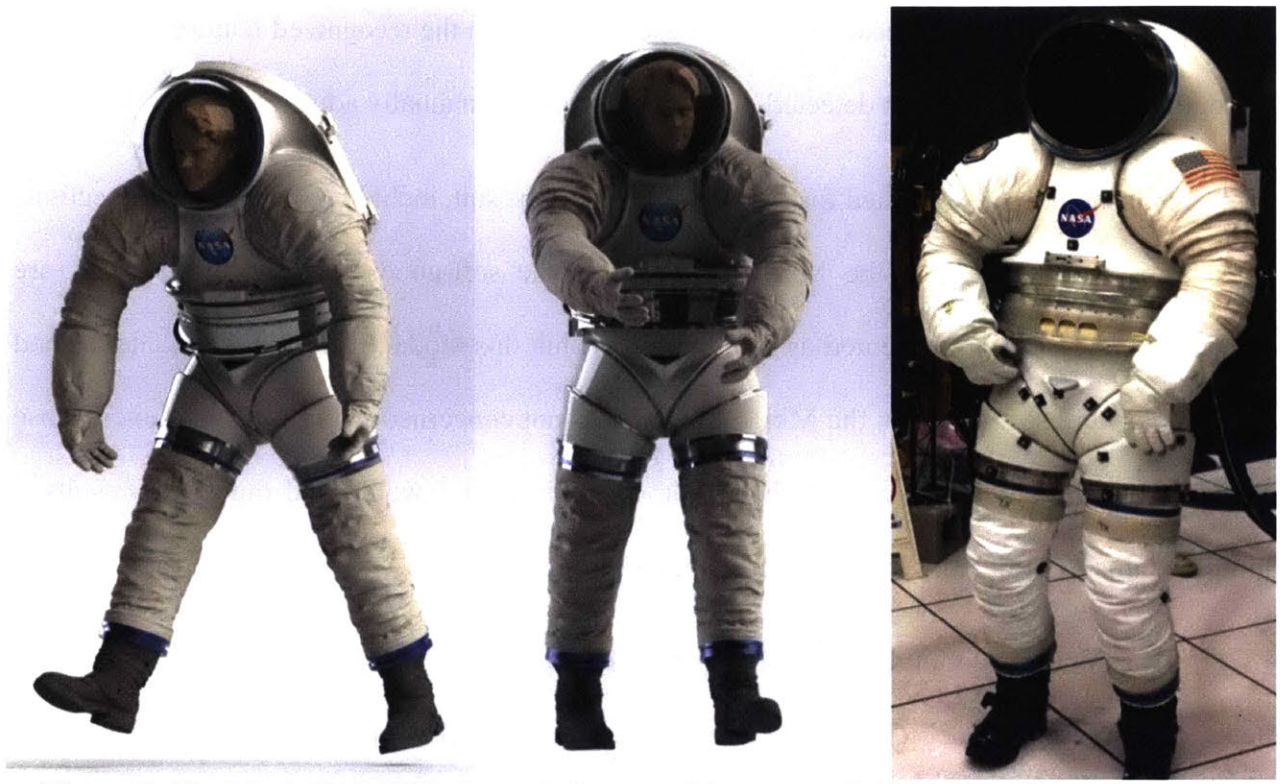

Figure 2: The Mark III (MkIII) Space Suit Assembly (SSA) Rigid-Body SolidWorks Model (Left and Center). The MII SSA (Right).

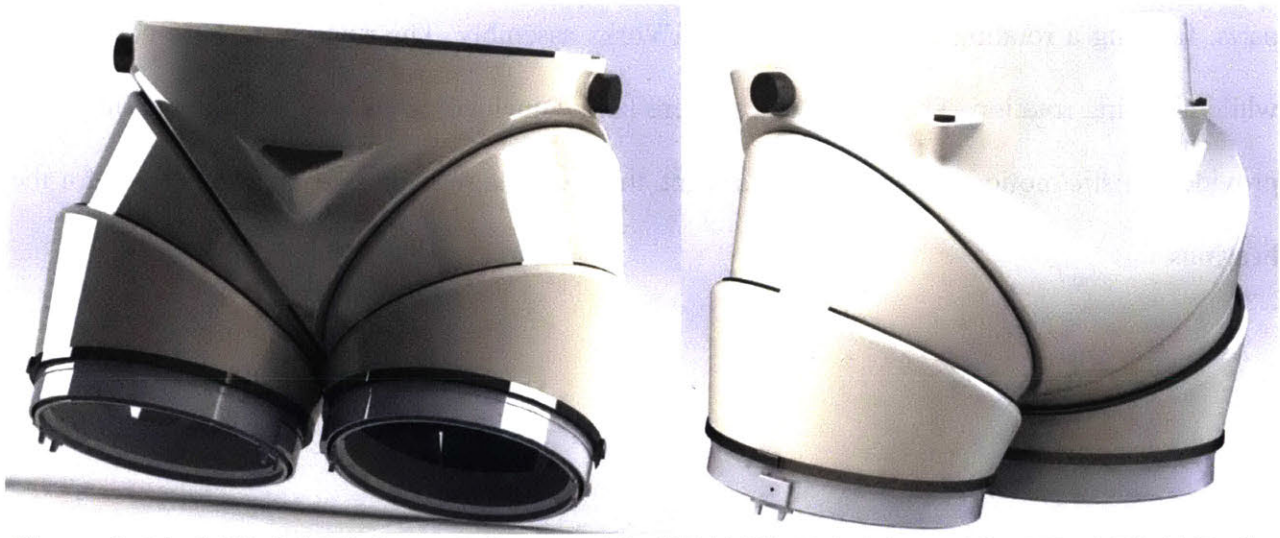

Figure 3: Mark III (MkIII) Space Suit Assembly (SSA) Hip Brief Assembly (HBA) Rigid-Body Model developed in SolidWorks from laser scans.

The MkIII SSA model, even before integrating bearing resistances or suit mass/inertial properties, is useful for kinematic applications such as determining the motion envelope of the

SSA or examining specific dimensions of the suit in a given orientation. The mating in SolidWorks allows the model to show what orientations and motions are achievable, but provide no information on how much torque is required from the operator to achieve those orientations. Therefore, I extended the model to enable high-fidelity dynamics analyses as well by including mass/inertial properties for each component, as well as bearing resistance profiles for each bearing.

2.2 Mass and Inertial Properties

A high-fidelity dynamics analysis requires each component to have accurately represented mass and inertial properties so that the model can accurately calculate forces and torques associated with motion. Each material was initially assumed (since some components are made of multiple materials), and then updated to match experimentally measured component weights in a validation. The updated densities allowed each component mass to match the experimentally measured component mass.

The hard material in the HBA was initially configured as S-Glass, an improved strength E-fiberglass. The bearings were represented as two concentric steel rings. After updating the material properties of the HBA, the material densities of each component were individually adjusted to match experimentally weighed components of the MkIII (Table 1). The experimental and predicted masses were not always equivalent to the model geometric representations. The model did not always represent all the details of the SSA (e.g. fasteners or other small components that cannot be discerned from a laser scan of the surface geometry) or because components were comprised of multiple materials.

Table 1: Component Mass Effects: Assumed and Experimental. The table shows the assumed densities of each relevant Mark III (MkIII) spacesuit assembly (SSA) component. The table also shows the new densities chosen based on the experimental masses of the components that were obtained from the Advanced Suit Development Lab at Johnson Space Center (JSC), where they had measured the weights before this research. The table also highlights the difference between component weights before and after the density adjustments. Finally, the six columns on the right show the principal moments of inertia (P_x, P_y, P_z) before and after the adjustments, which were calculated automatically based on the geometry and densities.

Component	Original Density [lbs/m3]	Updated Density [lbs/m3]	Ratio	Original Model Weight Without Overides [lbs]	Measured Weight [lbs]	Original Px [lbs*in2]	Original Py [lbs*in2]	Original Pz [lbs*in2]	Updated Px [lbs*in2]	Updated Py [lbs*in2]	Updated Pz [lbs*in2]
Briefs	5467.46	5467.46	1.00	8.51	5.10	293.88	301.81	412.23	176.08	180.83	247.00
Proximal Section	5467.46	3275.89	0.60	4.49	2.69	61.42	77.12	125.62	36.80	46.21	75.27
Distal Section	5467.46	3275.89	0.60	3.08	1.85	43.24	47.81	79.09	25.91	28.64	47.39
Upper Bearing	5952.48	5952.48	1.00	0.50	0.50	6.76	6.76	13.50	6.76	6.76	13.50
Mid Bearing	5952.48	5952.48	1.00	0.46	0.46	5.34	5.34	10.67	5.34	5.34	10.67
RC Bearing	5952.48	5952.48	1.00	0.64	0.64	6.52	7.41	13.72	6.52	7.41	13.72
RC Bracket	5952.48	5952.48	1.00	0.93	0.93	8.31	8.49	16.42	8.31	8.49	16.42
Lower Legs	6279.57	3206.77	0.89	6.04	6.80	119.51	220.58	226.96	134.54	248.33	255.52
Boot Flange	2700.00		1.00	1.50	1.50	6.46	9.40	15.20	6.46	9.40	15.20
Boot	6279.57	326.77	0.18	6.08	1.08	11.03	26.36	31.19	4.62	11.04	13.06

The inertial properties were calculated from the part geometries and masses, thus material updates would automatically adjust the inertial properties. This process was completed for the relevant suit components for the lower extremity motion (the HBA composite sections, rolling convolute joint, the lower-leg soft goods, bearings, and boot). Initially, the lower leg soft goods and boot were both assumed as neoprene as a starting point for those components that were made up of multiple materials. When originally scanned at JSC, the boot internal geometry was not scanned, as the internal space was too small, therefore, the model represented the boot as a solid. Therefore, when the boot material was estimated to be neoprene, the mass was greatly over-estimated. The assumed densities were updated to achieve the experimentally measured masses; therefore, the starting estimate of neoprene did not influence the model. I can see with the boot, that the density dropped dramatically here, as the inside of the boot is actually hollow and the overall density had to reflect that to reach the proper mass of the boot.

The component mass/inertial properties are not the only contributors to the required joint torques associated with operating a suit. The other inherent SSA torques come from the bearing resistances associated with the resistance to motion of the spinning bearings. The joints such as the HBA, that obtain mobility from bearings do not have to overcome the work associated with a changing volume inside of the suit, however they do have to overcome the resistance associated with the spinning bearings. Data were collected on the bearing resistance profiles of the bearings in the HBA, necessary for defining the bearing resistance within the model.

2.3 Bearing Resistances

2.3.1 Experimental Characterization

The HBA bearing torque profiles were obtained using a dynamometer (Figure 4) at nominal suit pressure (4.3 psi) with the bearings in an operational configuration. The upper and mid hip bearings were each assessed individually by locking out the other. The upper and mid hip bearings on both the left and right sides were all assessed individually by locking out the remaining bearings. For each bearing, the suit was oriented to align the axis of rotation with the dynamometer while holding that bearing parallel to the ground (Figure 5).

Each trial is defined a 360 deg. rotation. For a given speed, the bearing was rotated 3 times in one sense (CW), then the other (CCW). This was repeated, yielding six trials. For each set, the first trial includes a run-up region (Trials 1, 4) and the third trial includes a run-down region (Trials 3, 6).

Figure 4: Dynamometer (PrimusRSTM) by BTE

The torques required to maintain constant rotation rates of 10, 20, 30, 40, 60, 90, 120, 150, and 180 deg/s were measured for both the clockwise and counterclockwise sense. Each trial is defined as a 360 deg rotation.

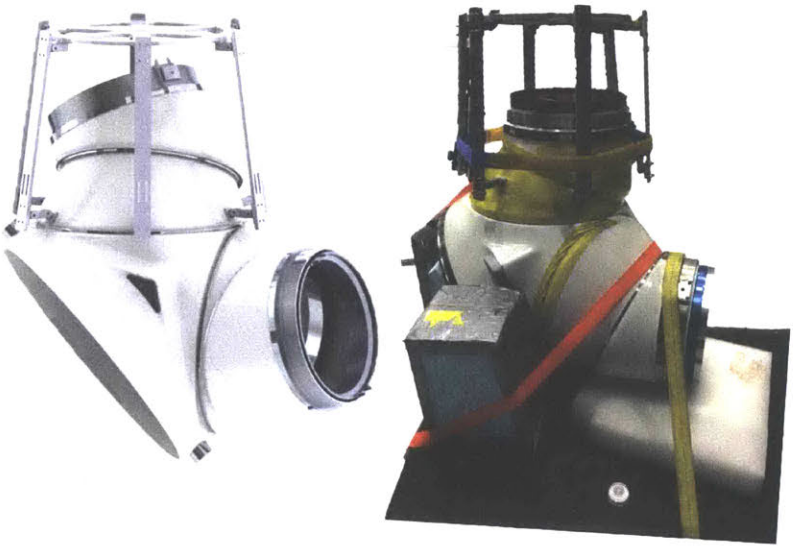

Figure 5: Updated bearing test rig and hip brief assembly (HBA) orientation (Left). Images of the experimental test setup (Right). The bearings were oriented parallel to the ground when being tested to align the axis of rotation with gravity.

The results (Figure 6) show that the torque required generally increases with speed in all cases except when the Left Proximal bearing is rotating at 10 deg/s. Figure 6 shows the average required torque and standard deviation at each angular velocity for each bearing while being rotated CW and CCW. The large sample size of data collected allowed for the determination that the CW and CCW required torques were statistically different ($p<0.005$) everywhere except at 90 deg/s and 120 deg/s for the Left Distal Bearing and 150 deg/s for the Left Proximal Bearing. While this difference in the required torques is detectable, nothing leads us to believe that the difference would be operationally relevant. For both the right and left side, the proximal (upper) bearings had greater average required torques than the distal (mid) bearings at each angular velocity.

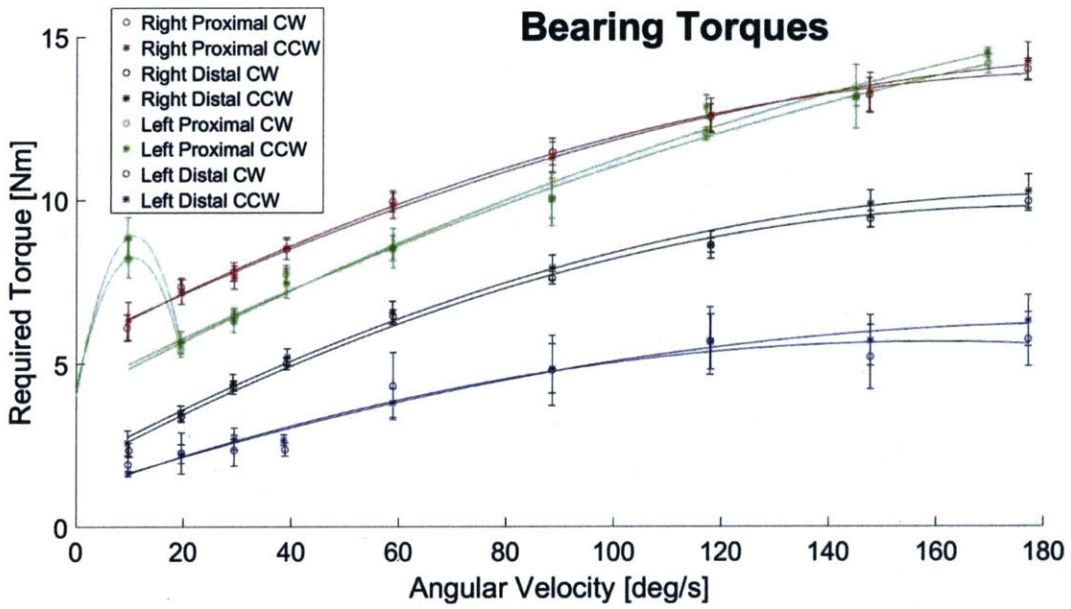

Figure 6: Mean required torque averaged over trial. The red line represents the right upper (proximal) bearing. The green line represents the left upper bearing. The black line is the right mid (distal) bearing, and the blue line is the left mid bearing.

The results show a difference in each bearing (Figure 6). Both the mid bearings have lower required torques than both upper bearings to achieve the same angular velocities. However, the right mid bearing also requires higher torques than the left bearing. The right and left upper

bearings do not have as large a difference as the mid bearings, but the right upper bearing has larger torques up to 120 deg/s while the left upper bearing has larger required torques at 10 deg/s and above 120 deg/s. A parabolic fit was estimated for the data, showing that the relationship between torque and angular velocity is not linearly increasing across the relevant range, as previously thought; however, it is a parabolic curve with the slope decreasing as the velocity increases.

All of the bearings map well to parabolic fits, however the left upper bearing, shown in green) has an initial spike that does not fit with the parabolic fit. When removed from the data, the parabolic representation fits well to the remaining data (Figure 7). This spike at 10 deg/s was not observed in the right upper bearing in either this most recent evaluation or the previous experiment. This most recent study was the first time that data was collected on the left side of the hip brief assembly (the previous study ranging up to 30 deg/s second only measured the right side) and was the first time I saw this spike. The data is not an outlier; it was repeatable within a trial and over multiple trials. The finding sets up future work to determine the cause of the spike. At 10deg/s, the spike in the left upper bearing is most likely related to the inherent viscoelastic properties that are leading to an increasing speed-dependent resistive torque profile.

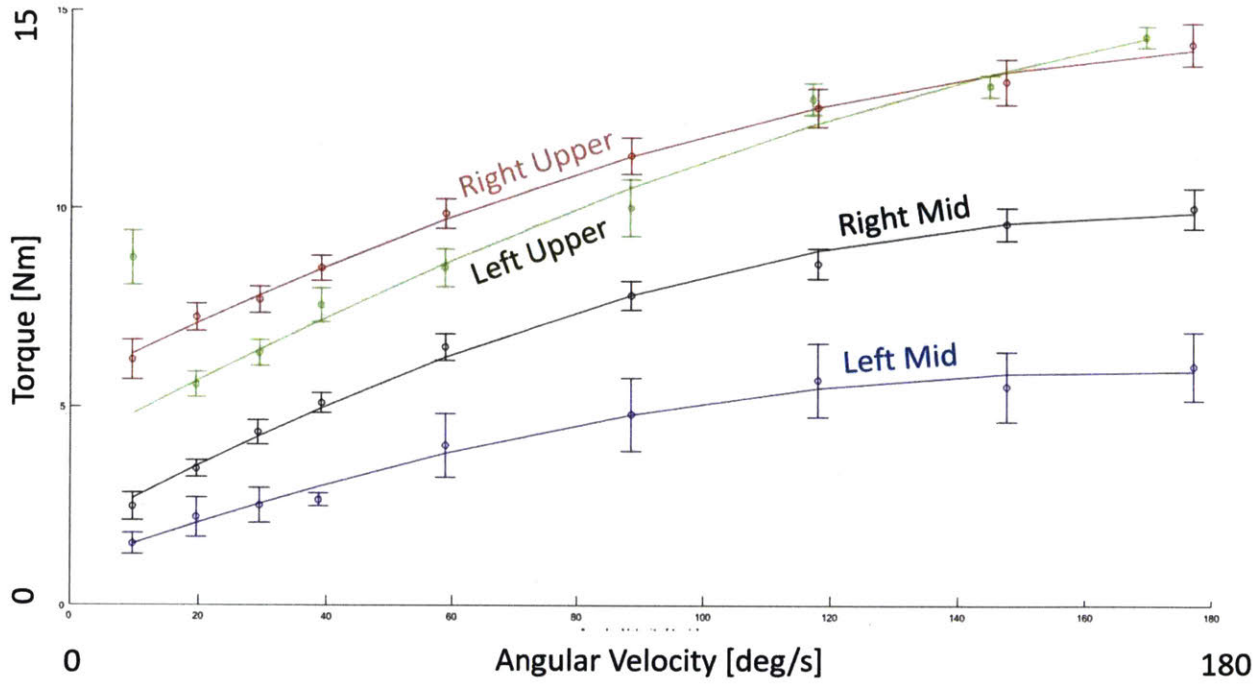

Figure 7: Updated mean required torque averaged over trial with parabolic fits. In this figure, I exclude the spike at an angular velocity of 10 deg/s for the left upper bearing.

Figure 8 shows the right proximal and distal required torques in both the CW and CCW direction, where the color indicates rotational velocity and rotational sense. The left proximal and distal bearings have similar curvatures, therefore, only the data for the right side is shown here. The polar plot representations show the required torques are not uniformly resistant at each angular displacement. Since the curves in Figure 8 are consistent across rotational sense, it helps to confirm the insignificance of rotational sense, and points towards operational considerations for bearing maintenance to avoid wear and tear and non-uniform torques. For a given speed and direction, the required torque varies and the regions where the required torque is above the mean are consistent across trial, representing "sticking points".

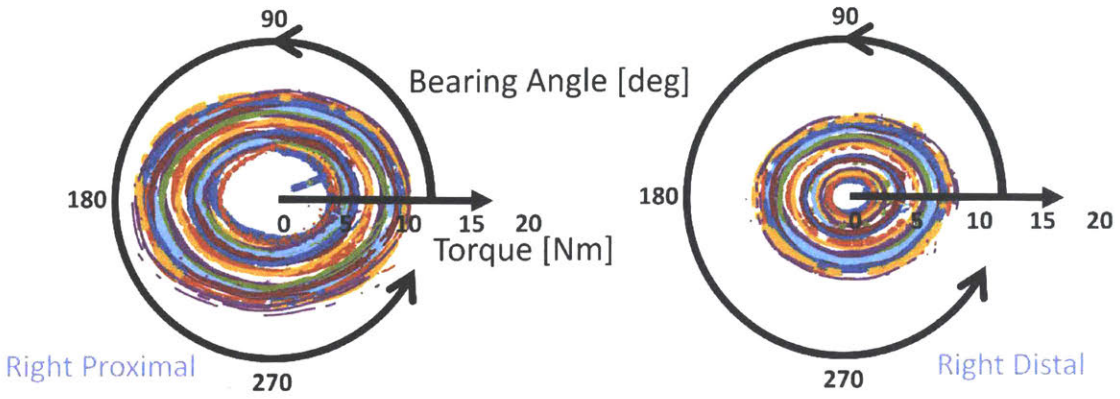

Figure 8: Required torque polar plots. Each color signifies a distinct angular velocity and rotational sense. The two plots are shown to scale, demonstrating for a given angular velocity, the proximal bearing has a greater resistance torque.

One possible explanation for the speed dependency is the geometry of the seals around the races, one seal providing protection from the external elements and the other providing an airtight environment to allow for suit pressurization. The spike that is seen in the left upper bearing could be due to a breakdown in the sealing system that introduces a slow-speed interaction that magnifies the resistive torque. Future work can investigate those hypotheses. Further bearing analyses, including an additional timepoint (Appendix A.1.1), an auditory signal analysis (Appendix A.1.2), and a pressurization analysis Appendix A.1.3) are shown in the appendix.

2.3.2 Model Integration

With a good representation of the bearing resistances throughout the range of angular velocities experienced during ambulation, those representations could be used in the model. The bearing torque vs. angular velocity data (Figure 7) were averaged over trial (360 degree rotations of the bearing) and rotational sense (clockwise vs. counter-clockwise), then represented with polynomial fits. Separate fits were created for both the upper and lower bearings, which were modeled in SolidWorks as reaction torques, creating a motion resistance based on that bearing's

angular velocity. Those two fits are shown below, where T is the bearing resistance torque, and ω is the angular velocity of that bearing.

Proximal / Upper Bearing Resistance Torque Equation:

$$T_{proximal} = -0.0001\omega^2 + 0.0688\omega + 5.8933 \qquad (1)$$

Distal / Mid Bearing Resistance Torque Equation:

$$T_{distal} = -0.0002\omega^2 + 0.0889\omega + 1.9853 \qquad (2)$$

During a motion simulation, the resistance torque magnitude was calculated using the instantaneous angular velocity of the bearing at each time step. Motion was simulated within SolidWorks using the embedded Motion Analysis (MA) toolkit, which uses assembly mates and a physics-based solver to determine the forward dynamics solution of an assembly under load (Figure 9). With the integrated bearing resistance and realistic mass and inertial properties for each SSA component, the model dynamics could be simulated using applied forces as inputs. The model is implemented in Chapter 3 for a kinematics analysis and in Chapter 4 for a dynamics analysis.

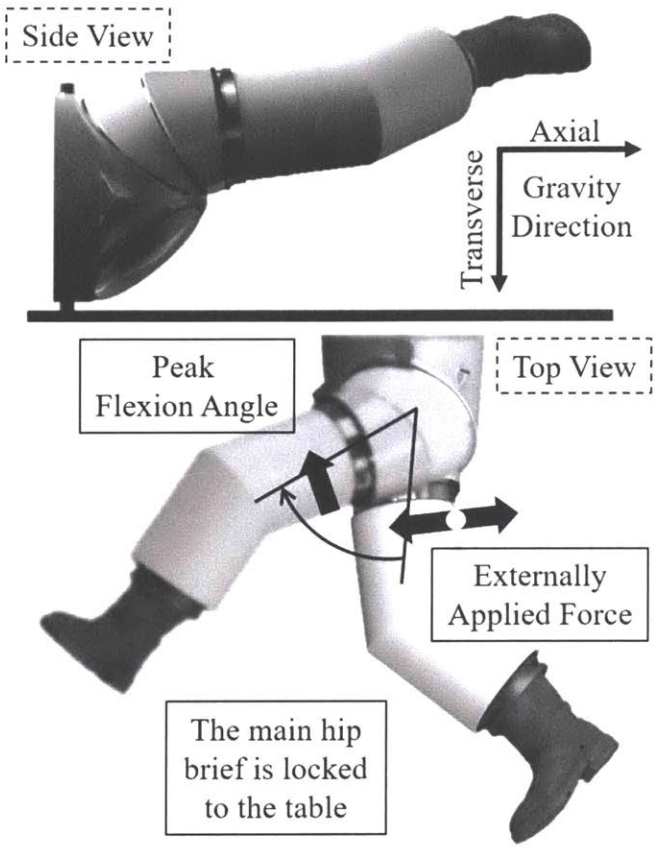

Figure 9: The SolidWorks Motion Analysis rigid-body dynamics model was implemented as shown above to resemble the experimental analyses performed at Johnson Space Center (JSC). The "Top View" depicts the left leg in the neutral, starting position, as well as at peak flexion angle.

2.3.3 Limitations and Future Work

The bearing resistances were based on pooled data and a non-linear regression representing these data. The data used to fit the regression was from a single snapshot in time over an acute 30-hour maintenance schedule, as well as in the lifetime of those bearings. The bearings are sometimes operated with a single seal (for preventing particulate infiltration) and sometimes with dual seals, which may alter the overall resistance to motion. It was not known whether the bearings had a single or dual seal at the time of the experimental testing for Valish et al. [64] or the testing performed in in this Chapter (Chapter 2.3.1). It is also unknown if the bearings that were used in the experiment were more or less resistive than our modeled bearings, or if the regression was

matched. A sensitivity analysis of the joint dynamics (model output) to the bearing resistance is considered in Chapter 4. The current study was a snapshot in time, but performing the same analysis over the 30-hour maintenance cycle of a bearing or over the lifetime of the bearings will yield pertinent information on how the required torque profiles change as the cycles on the bearings increase.

The bearing characterization experiments were performed with the bearings parallel to the ground to eliminate the effects of gravity and off-axis loading. However, in an operational setting, and even during the experimental study at JSC, the bearings would most certainly have had off-axis loading and they were not oriented perpendicular to gravity as they moved through space throughout the experiment. This has a significant effect on the modeling analysis completed in Chapter 4, but is mitigated by applying gravity in multiple directions and magnitudes during the same motion.

Additionally, since the model assumes that the soft-goods components are rigid, the complete motion envelope is not achieved. Any motion or orientation that could be achieved from the deformation of the soft-goods components is not represented.

The model developed in this chapter is implemented in Chapter 3 and in Chapter 4 to address research gaps. In Chapter 3, the kinematic capabilities of the model are leveraged, and in Chapter 4, the dynamic capabilities are leveraged.

3. Mark III Spacesuit Architecture Restrictions: Gait Performance Decrements

Research Gap: What are the mobility and agility limitations causing operators to experience performance decrements when wearing an SSA? The measured performance decrement could be attributed to the SSA's functional motion envelope mobility restrictions (kinematic, programmed motion), an increase in required joint torques (dynamics), carrying the distributed weight of the suit (dynamics), suit fit, or a combination (complex interactions).

Aim 1: To identify the mobility and agility limitations incurred by the existing MkIII SSA architecture and inform future tightly-coupled suit design requirements to avoid similar limitations.

Aim 1.1: To test the hypothesis that the MkIII Hip Brief Assembly (HBA) architecture has DOF limitations that restrict operator mobility and agility. I will also test the hypothesis that there are resistive joint torques that operators must overcome to achieve a desired motion, which also limit operator agility.

Aim 1.2: To measure how much rotational motion the waist bearing affords in the transverse plane during ambulation, to understand how much relief it provides from restrictions introduced by the HBA.

The torque required to rotate the HBA upper and mid bearings was characterized in Chapter 2.3. Coupling these data with measured kinematics may lead to an improved understanding of the underlying programmed motions (pre-planned movements within the motion envelope that the suit allows) and provide future design guidelines for wearable systems. In this chapter, the results are

presented, of a pilot study on locomotion while Unsuited and Suited with the MkIII SSA to address Aim 1.

Aim 1 was formulated to answer the research question: What is the mobility and agility performance decrement incurred when wearing an SSA? The study described here aims to integrate underlying suit component characteristics with the emergent biomechanics of the operator to investigate how an operator's biomechanics are affected by the MkIII, specifically how the HBA architecture effects hip motion. These data are relevant for improving future SSA architectures through design requirements development and evaluation methods.

I hypothesize that **[1]** the MkIII HBA architecture has Degree of Freedom (DOF) limitations that restrict operator mobility and agility. The limitations manifest in effects to both static and dynamic (Walking Forward (WF) and Walking Backward (WB)) gait parameters. **[2]** Based on subjective feedback from experienced suit testers, the waist bearing provides rotational motion in the transverse plane during ambulation, partially alleviating mobility restrictions introduced by the HBA. **[3]** Although the HBA volume does not change during hip joint motion, there is still a resistive speed-dependent torque associated with the spinning bearings. Those torques further diminish the mobility and agility of the operator, requiring increased hip joint torques along the limited DOFs.

3.1 Methods

3.1.1 Subject

This pilot study was performed on a single subject who has similar characteristics as that of an astronaut. The subject was 30 years old and 72 in tall, which falls within the astronaut selection criteria for age (26-46 years old) and height (62-75 in) of astronaut candidates. The subject had extensive experience operating the suit, enabling the assumption of a trained operator.

The subject was cleared with a class I medical to participate as a suit operator. The study protocol was approved by the NASA Johnson Space Center (JSC) IRB and the subject provided written informed consent prior to participation.

3.1.2 Equipment

The study was performed in the Anthropometrics and Biomechanics Facility (ABF) at NASA JSC in 1g. Data were collected using 11 Vicon Bonita cameras, imaging at 100 frames per second. The MkIII was pressurized to nominal suit pressure (4.3 psi) in a tethered configuration (i.e., not with the closed-loop portable life support system (PLSS)). The MkIII in the tethered configuration weighs approximately 59 kg.[2,65] While unsuited, the subject wore a compression shirt and pants.

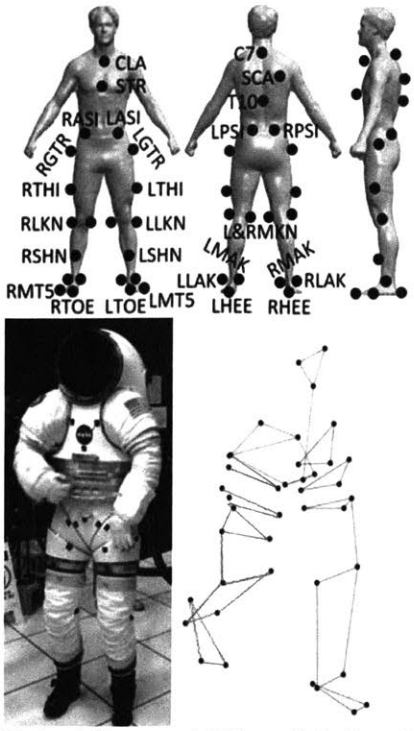

Figure 10: Unsuited (top) and Suited (bottom) Vicon Marker Placement. "L" and "R" denote Left and Right. Markers were placed on the Unsuited subject at the clavicle (CLA), sternum (STR), anterior superior iliac spines (ASI), greater trochanters (GTR), thigh (THI), medial knees (MKN), lateral knees (LKN), shins (SHN), medial ankle (MAK), lateral ankle (LAK), 5th metatarsals (MT5), big toes (TOE), heels (HEE), posterior superior iliac spines (PSI), 10th thoracic vertebrae (T10), 7th cervical vertebrae (C7), and scapula (SCA). When Suited, three markers were evenly spaced on each of the bearings. Two triads of markers were placed on the main brief section, one in the front and one in the rear. Another triad was placed on the hard upper torso (HUT). Other markers were chosen to replicate anatomical marker placements (MKN, LKN, MAK LAK, MT5, TOE, and HEE)

3.1.3 Procedure

For the Unsuited condition, passive reflective motion capture markers were placed at anatomical landmarks (Figure 10, top). The subject stood still to obtain a static pose, then performed trials that included walking forward (WF, 12 trials) and walking backward (WB, 6 trials) within the motion capture volume (10 m long by 1 m wide walkway). Following Unsuited operations, the subject donned the MkIII SSA, which was then pressurized. For the Suited configuration, the motion capture markers were placed external to the SSA (Figure 10, bottom). It can be difficult, or sometimes impossible, to identify anatomical landmarks to guide marker

placement, rather the placement was intended to highlight features of interest on the suit, especially on the HBA. While Suited, the static pose, as well as WF (10 trials) and WB (5 trials) were repeated.

3.1.4 Data Analysis

Logarithmic and Hyperbolic fit equations from Grasso et al.[26] were used to predict the Unsuited stride length and cadence, respectively. These predictions are useful to determine expected outcomes for dependent measures and to connect suit limitations to deviations from the predictions.

Logarithmic Equation for Stride Length (m), Walking Forward:

$$Stride = 1.28 + 0.41 \log(V) \qquad (3)$$

Logarithmic Equation for Stride Length (m), Walking Backward:

$$Stride = 1.21 + 0.36 \log(V) \qquad (4)$$

Hyperbolic Equation for Cadence (steps/min), Walking Forward:

$$Cadence = \frac{1}{0.54 + \frac{0.71}{V}} \qquad (5)$$

Hyperbolic Equation for Cadence (steps/min), Walking Backward:

$$Cadence = \frac{1}{0.53 + \frac{0.67}{V}} \qquad (6)$$

Where V is the average speed (m/s) of the subject, as calculated from the speed of a marker on the chest of the subject unsuited, and on the Hard Upper Torso (HUT) when suited. The hyperbolic equation was originally expressed for gait cycle (T), but here I take the inverse to predict cadence.

The rigid-body model, described in Chapter 2, was implemented here to predict functional motion envelopes. The position data (x,y,z) of the motion capture markers were used to calculate static and dynamic gait parameters for the subject while Suited and Unsuited. For the dynamic trials, the data sets were trimmed to include the steady state gait within the capture volume, which tended to include 2-3 strides.

The gait parameters examined for Hypothesis [1] were static base (m), dynamic base (m), step length (m), stride length (m), cadence (steps/min), center of mass speed (m/s), and foot clearance for the toe and heel (m). The static base was defined as the distance between the left and right heel markers when the subject was standing in a static pose. The HBA CAD model was also used to predict the minimum static base while suited by orienting the HBA to minimize the distance between the rolling convolute joints. Step length was defined as the parallel distance (along the walking axis) between two consecutive heel strikes of opposite feet, while stride length was defined as the distance between two consecutive heel strikes of the same foot (schematic shown in Figure 12). Cadence was defined as the step length divided by the time to complete that step. Speed was determined as a center of mass speed, and was calculated from a chest or HUT marker. The heel and toe clearance was defined as the vertical distance above the calibrated origin, where the calibrated origin was the height when the foot was in contact with the ground (a firm, wood surfaced platform). There were heels on the boots used, but the heel height was calculated as a difference in the heights when in stance vs. swing phase, so I was more concerned with a difference rather than total clearance height.

The parameter necessary for testing Hypothesis [2] was the waist bearing rotation (deg.), which was defined as the difference in motion between the HUT and main brief section. Normal vectors were calculated from the motion capture marker triads on both the front of the HUT and

HBA. For example, if the three markers in the triad were labelled A, B, and C, the normal vector could be calculated as $N = \overrightarrow{AB}\ X\ \overrightarrow{AC}$. With the two normal vectors (N1 and N2) calculated from each triad, the angle between the vectors was calculated as shown in equation (1). The difference between the maximum and minimum angles for each trial is the range that the waist bearing rotated during ambulation.

$$\theta = \cos^{-1}\left(\frac{N1 \cdot N2}{\|N1\|\|N2\|}\right) \qquad (7)$$

To test Hypothesis [3], the upper/mid bearing angular velocities (deg/s) are determined. The bearing angular velocities, $(\omega_x, \omega_y, \omega_z)$, were calculated with the system of equations

$$\frac{x_1(t+\Delta t)-x_1(t)}{\Delta t} - \frac{\bar{x}(t+\Delta t)-\bar{x}(t)}{\Delta t} = \omega_y(z_1 - \bar{z}) - \omega_z(y_1 - \bar{y}) \qquad (8)$$

$$-\left(\frac{y_1(t+\Delta t)-y_1(t)}{\Delta t} - \frac{\bar{y}(t+\Delta t)-\bar{y}(t)}{\Delta t}\right) = \omega_x(z_1 - \bar{z}) - \omega_z(y_1 - \bar{y}) \qquad (9)$$

$$\frac{z_1(t+\Delta t)-z_1(t)}{\Delta t} - \frac{\bar{z}(t+\Delta t)-\bar{z}(t)}{\Delta t} = \omega_x(z_1 - \bar{z}) - \omega_y(y_1 - \bar{y}) \qquad (10)$$

where (x_1, y_1, z_1) is the position of a single marker on a bearing and $(\bar{x}, \bar{y}, \bar{z})$ is the average of all three position markers, the centroid. Here, ω_x and ω_y represent angular velocities that result in pivoting out of plane, while ω_z is the bearing rotation and results in a change in the HBA shape. The estimated bearing torques to achieve the calculated angular velocities are then calculated using the parabolic fits from Chapter 2.1.1.

3.1.5 Statistical Analysis

A 95% confidence interval for the cadence and step length were constructed to assess the predicted values from Grasso et al.[26] An outlier analysis was performed to give statistical reasoning for removing any data points. An analysis of variance (ANOVA) was performed for each gait parameter to examine effects of task type (WF, WB) and suit configuration (Suited, Unsuited). Post-hoc comparisons were performed within each gait parameter between task types and suit configurations using a Tukey correction. Two-sample t-Tests were used to compare between left/right leg and Unsuited/Suited heel and toe height within the clearance analysis. Two sample t-Tests were also used to compare the bearing rotation and required torques between the upper and mid bearings on both the left and right side. A one-sample t-Test was used to test the null hypothesis that the mid bearing data when WB comes from a normal distribution with mean equal to zero.

3.2 Results

3.2.1 Unsuited Cadence and Stride Length Predictions

As this was a pilot study that contained only one subject, Unsuited stride length and cadence were compared with regressions from Grasso et al ($n = 7$).[26] The mean speed for both WF (1.12m/s) and WB (0.904m/s) were used as inputs to determine the predicted stride lengths (1.30m and 1.19m). These values were within the 95% confidence intervals of the stride lengths determined from the measured Grasso et al. data (1.31±0.03m and 1.20±0.03m). The predicted cadence for WF and WB (102 steps/min and 94.4steps/min) were outside the 95% confidence intervals (98.6±2 steps/min and 79.2±2 steps/min).

Table 2: Mean and standard deviation (SD) of dynamic gait parameters.

	Mean Step Length [m]	Mean Stride Length [m]	Mean Cadence [steps/min]	Mean Speed [m/s]	Mean Base [m]
Suited WF	0.595 (0.03)	1.24 (0.05)	88.8 (3)	1.06 (0.06)	0.190 (0.03)
Unsuited WF	0.631 (0.05)	1.31 (0.05)	98.7 (4)	1.12 (0.08)	0.0812 (0.02)
Suited WB	0.476 (0.04)	0.860 (0.09)	90.2 (5)	0.833 (0.08)	0.220 (0.04)
Unsuited WB	0.549 (0.07)	1.20 (0.06)	79.2 (5)	0.904 (0.1)	0.107 (0.03)

3.2.2 Effect of Suited Condition on Static Base

The static base (distance between the two heels) for Unsuited and Suited was 0.263m and 0.355m, respectively. Using the HBA CAD, the vertical distance, in the sagittal plane, from the rolling convolute medial edge to the center of the main brief section (hip joint center) was measured to be 0.219m. The horizontal distance, in the transverse plane, from the rolling convolute medial edge to the center of the HBA was measured to be 0.0412m. The minimum angle created by the brief at the hip joint is 10.65deg. The subject's leg length from the greater trochanter (GTR,) to the floor is 0.953m. Therefore, with the legs pressed against the medial edge of the rolling convolute joint, the predicted static base is 0.354m.

3.2.3 Effect of Suited Condition and Locomotion Task on Dynamic Gait Parameters

The outlier analysis found a single outlier for the Suited WF dynamic base (0.64m), which may have been the result of an abnormal step (i.e. stepping with a wider base than normal to catch oneself when off balance). This point was removed from the analysis, as it was not considered a steady state step. An ANOVA found a significant interaction effect of task (WF/WB) and configuration (Suited/Unsuited) for cadence and stride length ($p<0.005$) (Table 2). When contrasting the treatment conditions for stride length, there was a statistically significant difference between Suited and Unsuited for WF and WB ($p<0.05$). For stride length, there was no difference between WF and WB in the Suited configuration, but all other comparisons were different. An

ANOVA found an effect of configuration for step length, stride length, and speed ($p<0.005$). An ANOVA found an effect of Task for all gait parameters ($p<0.005$). An ANOVA for dynamic base showed an effect of configuration and task, with no interaction effects (Table 2).

3.2.4 Clearance Analysis

The clearance analysis results are shown in Figure 11. The ANOVA results showed that there was no effect of Leg (Right vs. Left) ($p=0.161$) on the maximum clearance height. However, there was an effect of anatomical landmark (Heel vs. Toe), suit configuration (Suited vs. Unsuited) and task (WF vs. WB) ($p<0.005$). Within each suit configuration and task combination, the maximum heel clearance was greater than the toe clearance ($p<0.005$). For both WF and WB, the maximum clearance for the Unsuited Heel and Toe was larger than when suited ($p<0.005$).

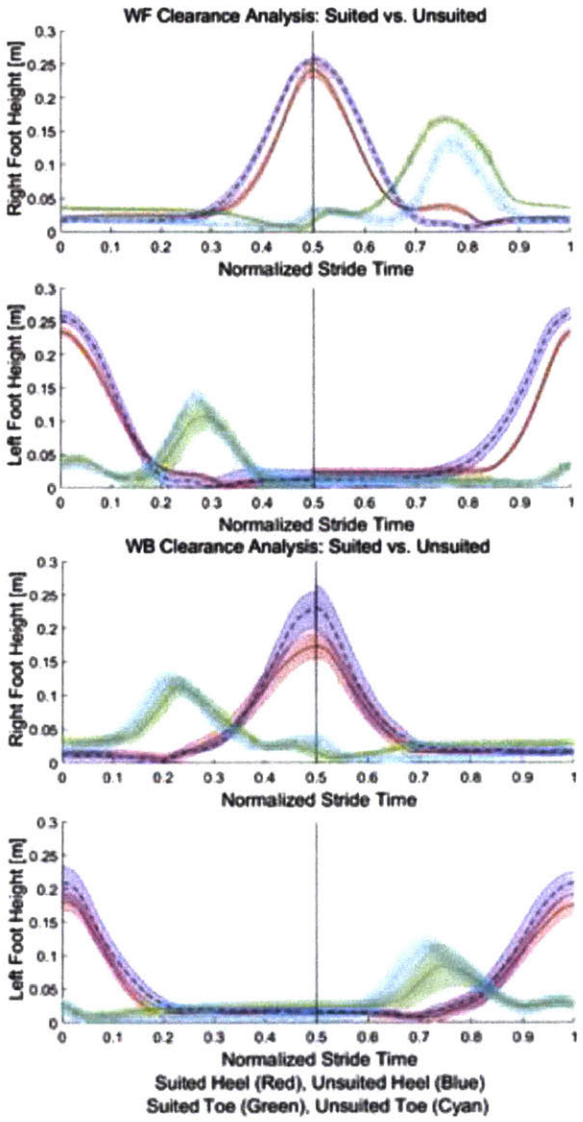

Figure 11: Clearance Analysis. The two top plots are the heel and toe clearances while WF, and the two bottom plots are while WB.

3.2.5 Waist Bearing Motion

The mean waist bearing rotations were 7.18deg and 7.23deg for WF and WB respectively, which were not significantly different (p=0.928).

3.2.6 Upper and Mid Hip Bearing Torque Analysis

The bearing analysis results are shown in Figure 12. When WF, the upper and mid hip bearings rotated in opposite directions simultaneously, allowing the HBA to change shape and

follow the subject's limb. However, the maximum rotation angle for the upper bearings were larger than the mid bearing ($p<0.005$). When WB, the upper bearings rotated, however the mid bearing had very little motion. For example, the maximum rotation in the right upper (23.1±3.97deg) and mid (2.11±2.93deg) bearing during the right swing phase while WB were different ($p<0.005$). The mean mid bearing torque when WB was not different from zero rotation ($p=0.111$). The angular velocities and torques are consistent with this motion profile. For example, when WF, the maximum torque in the right upper (15.6±1.35Nm) and mid (16.3±1.28Nm) bearings were not different ($p=0.1729$).

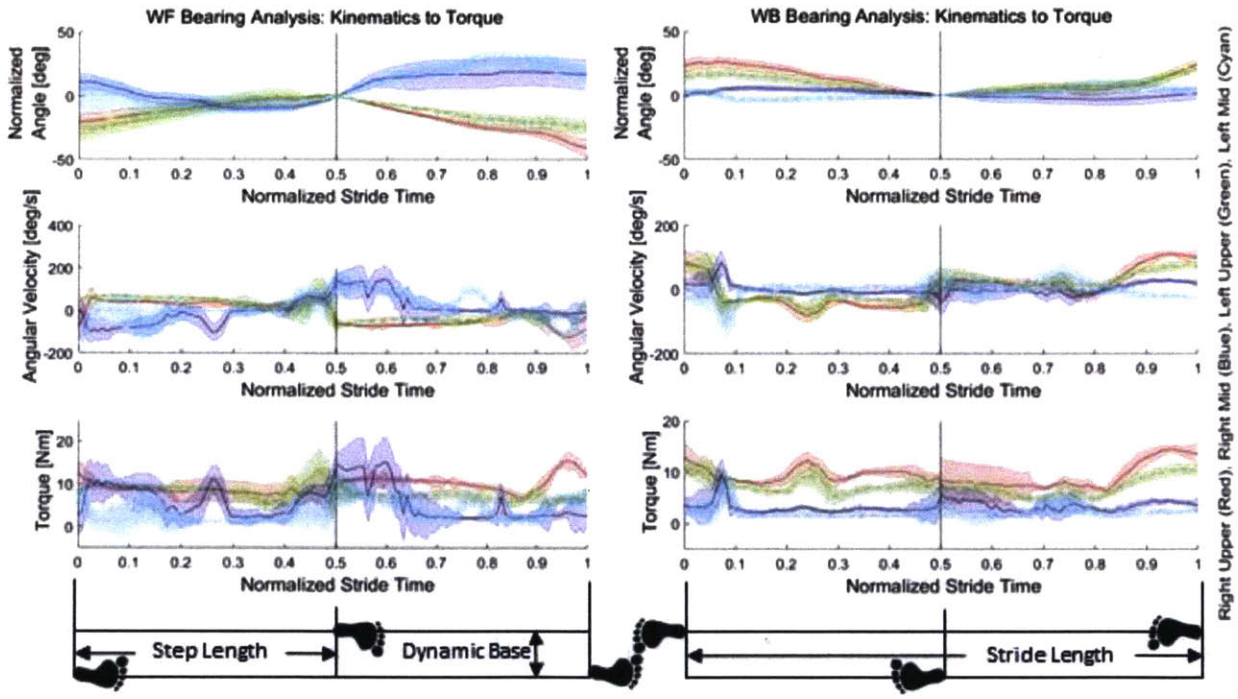

Figure 12: HBA Bearing Analysis. The left side of the figure represents WF data, while the right represents the WB data. The top plot on both sides represents the rotational displacement angle normalized to be zero during double stance (x=0.5 on the x-axis). The middle plots represent the calculated angular velocities that achieve the experimental displacements in the top plots. Finally, the bottom plots show the calculated torques required to achieve the angular velocities. The color-coded bearings, matched to the legend, are seen in Figure 1.

3.3 Discussion

This study aimed to relate the underlying suit component properties to the emergent biomechanics of the operator to describe how an operator's biomechanics are affected by the MkIII. Specifically, I hypothesize that [1] the MkIII HBA architecture has DOF limitations that restrict operator mobility and agility. The limitations will manifest in effects on both static and dynamic (WF and WB) gait parameters. [2] Based on subjective feedback from experienced suit testers, the waist bearing provides rotational motion in the transverse plane during ambulation, partially alleviating mobility restrictions introduced by the HBA. [3] Although the HBA volume does not change during hip joint motion, there is still a resistive speed-dependent torque associated with the rotating bearings. Those torques further diminish the mobility and agility of the operator, requiring increased hip joint torques along the limited rotational DOFs.

3.3.1 Hypothesis [1]

The Unsuited pilot data were first compared to the literature before comparing to the Suited data. Although the stride lengths were predicted accurately, the cadences were slower than predicted. Also, this subject had a lower Unsuited cadence and stride length when WB than WF, which is not consistent with previous studies that show an increase in cadence when WB to compensate for the decrease in stride length.[26,63] Here I observed that when Unsuited while WB, the subject had a wider dynamic base, smaller stride length, smaller step length, slower cadence, and slower speed, which all provide improved control of body mass over the supporting limb.[62] The selection of increased stability may be due to the experimental setup, which used an elevated walkway. The walkway may be easier to navigate when WF with visual cues, but more difficult when WB because it was narrow (1m), which could have led the subject to observe caution to avoid stepping off the side. This subject may have been more cautious than seen in the literature.

When Suited, an operator is not only manipulating the suit, but also carrying its weight. As mentioned previously, carrying a load on top of body mass decreases stride length while increasing cadence.[37] Our data show a decrease in stride length when Suited; however, the change in cadence is not consistent. When transitioning from Unsuited to Suited, cadence increases when WB, but decreases when WF. If the weight alone were altering gait, I would expect consistent change across WF and WB. This implies that the differences in the Unsuited and Suited gait may have additional factors.

The heel clearance analysis showed the suited condition resulted in lower clearance heights, which could be due to motion restrictions, or could be related to adapting the motion to minimize added torques due to the suit. The reduction in the maximum clearance heights of both heel and toe, for both WF and WB confirm that the operator mobility and agility is being restricted by the suit. The diminished mobility and agility, when compared to Unsuited, also manifested as a decrease in speed, stride length, and step length for both WF and WB. In addition to the added weight, these changes may be a result of the interaction and disparity between the natural hip biomechanics with the operational motion envelope of the HBA. The MkIII HBA has a smaller range of motion than the human hip as well as fewer DOFs. A human hip joint has three DOFs located within the single joint, whereas the HBA has a single degree of freedom per bearing and those are spread out distally from the hip. This is highlighted in the comparison of the Suited and Unsuited static bases.

Since a difference in static base exists, I examined if the architecture of the suit contributed to the wider base. The rigid-body SSA model of the HBA (Chapter 2) confirms the limitations in adduction and shows that the selected Suited static base was essentially the same as the minimum adduction permitted by the architecture. In this configuration, the medial thigh of the Suited

operator contacts the medial edge of the rolling convolute joint, which acts as a physical hard-stop. This architecture also restricted the dynamic base, but Hypothesis [2] explores how the waist bearing may provide additional motion to partially alleviate the restriction during dynamic task performance. When Unsuited, dynamic base was larger when WB than WF. However, when Suited, there was no difference in dynamic base. It was found that the Suited dynamic base (pooled, 0.200m) was larger than both Unsuited WF (0.081m) and WB (0.107m). This is consistent with the HBA limiting adduction as the minimum dynamic base was seen to have an adduction hard-stop while Suited that forced the dynamic base to be larger than the naturally selected dynamic base observed in the Unsuited case. In the CAD model, when manipulating the HBA into the double stance phase (when both feet are in contact with the ground), the dynamic base is predicted to increase (0.626m). Hypothesis [2] elaborates on why this prediction is not consistent with the data.

3.3.2 Hypothesis [2]

During ambulation, there was actually a reduction in base as compared to the static condition. I hypothesized that this can be attributed to the waist bearing, which rotates to allow further adduction of the compound hip assembly. The CAD model and static base show that the HBA is in its most adducted position when in the static pose. However, when walking, the HBA dynamically changes configuration as the operator drives the rotation of the bearings. Any rotation in the upper and mid bearings, away from their static pose locations, decreases the adduction ability of the operator because of the irregular geometry of the HBA sections between the bearings. However, the rotation of the waist bearing allows the operator to place his or her feet closer to their walking centerline and reduce their dynamic base. The waist bearing connects the HUT to the hips, transferring load while allowing for rotation along the bearing (Figure 1). Here I found

that the waist bearing rotations were not statistically different in the WF and WB tasks. Thus, it is consistent that the dynamic bases were not significantly different when WF and WB. The HBA design increased static base width, but the waist bearing provides transverse plane rotation to reduce that effect during dynamic motion. This is similar to the Unsuited case, where the rotation in the spine provides this same reduction in static vs. dynamic base.[68]

3.3.3 Hypothesis [3]

As hypothesized, the circumferential rotation of the bearings during Suited WF and WB created additional torques for the user to overcome. The motion of the bearings is not aligned with the natural desired joint trajectories because of DOF limitations inherent in the architecture, which produces programmed movements. The operator drives the HBA configuration through limb contact with the interior of the HBA as the hip is rotated. The limb, however, has to traverse the trajectories that the bearings and HBA geometry will allow, while exerting additional required torques to overcome the resistive bearing torques. To generate bearing rotation, the force has to be transferred from the operator's limb to the SSA distal to the bearings, increasing the moment arm of the applied force, and resulting in an increase in the required joint torques. As seen in the estimated torques, there was a difference between the bearing performance during WF and WB. When WF, the upper and mid bearings rotated in opposite directions. While WB, the upper bearing rotated while the mid bearing only rotated slightly or not at all. Thus, when WF, complementary motion occurred in both bearings, while when WB, only the upper bearing was necessary to achieve the foot placement observed. The bearing motion is consistent with the strategy measured through the dynamic gait parameters. The smaller step lengths when WB as compared to WF while Suited are associated with less hip extension (as compared to the greater hip flexion when WF) and thus less bearing rotation. This strategy may be an attempt to minimize energy expenditure as

proposed by Abe et al.[1] When WB, the overall speed and step length decrease from the Unsuited to Suited configuration, while the cadence increased. This shows that when WB, it may be more efficient to only force one bearing to spin and take smaller faster steps than it is to spin both bearings and take larger, slower steps while fighting the greater amount of resistive torque.

3.3.4 Limitations and Future Work

This pilot study only included one subject. Thus, conclusions and trends must be considered appropriately. The data show sufficient evidence to support the hypotheses and can be used to inform future studies with an increased sample size. An experimental limitation was the total distance that a subject could walk. It would be beneficial to have a larger track to walk on, allowing for more strides continuously in each trial. (The Grasso et al. study, used for comparisons, did not provide the walking distance). It may also be beneficial to remove the elevated walkway, and determine if that was truly the root cause of the need for increased control and stability when Unsuited and WB. In this study, the spacesuit added weight to the subject, and I examined the combined effect of the weight with the system architecture. In (Chapter5), a decomposition is performed, to determine how the distributed suit weight is applied to the operator inside and the effects of load transfer to the human operator in the human-SSA system.

3.3.5 Conclusion

In this chapter, I experimentally compared unsuited and suited (MkIII) gait parameters. Differences in performance were then examined using a Kinematic Rigid-Body Space Suit Assembly (SSA) Model (Chapter 2.1) of the Mark III (MkIII). The model of the MkIII SSA supported that the programmed motions lead to performance decrements. During those studies, the bearing angular velocities were also measured to understand the range of angular velocities experienced by each bearing during ambulation, an operationally relevant planetary task. Coupling

the bearing resistance data (Chapter 2.2.1) with the measured bearing kinematics (Chapter 3) can provide an improved understanding of the underlying programmed motions and an estimate of the required joint torque to operate the SSA.

In this chapter, I addressed Aim 1, showing the MkIII HBA has DOF limitations that restrict performance compared to unsuited. However, the DOF limitations do not explain all of the performance decrement. I was able to identify additional factors that could be contributing: increased hip joint torques associated with the bearing resistances, inertial effects of the SSA component masses, transfer of the distributed suit weight to the operator, and suit fit. Although I was unable to separate out their specific contributions to that performance decrement in Chapter 3 (Aim 1), it led us to our second and third research gaps. Chapters 4 (Aim 2) and 5 (Aim 3) both investigate specific contributions of the identified factors.

4. Decomposition of Required Hip Torque into Contributing Components

Research Gap: What is causing operators to experience increased joint torques when wearing an SSA?

Aim 2: To identify and quantify the MkIII HBA components that contribute to the increase in total hip joint torques required by the operators during ambulation.

Aim 2.1: To identify the contributing components of the SSA that resist motion and require operators to increase their joint torques compared to unsuited, and to measure the specific contributions of each to the overall increase in joint-torque. I specifically decompose the required HBA joint torques into specific component contributions, which an operator must overcome to achieve flexion/extension of the hip during ambulation.

Aim 2.2: To measure the sensitivity of hip joint torque and flexion / extension angle, to model input parameters. This research specifically examined two external forcing profiles, *fleet sizing* (a few discreet sizes to accommodate all users) of the boots, varied bearing resistances, and gravitational scenarios with multiple magnitude and direction configurations.

When evaluating an SSA, such as the MkIII, there are a number of experimental evaluation techniques that are used (Chapter 1.2.3), but those techniques are not always operationally equivalent. For example, an experiment conducted at Johnson Space Center (JSC) by Valish et al.[64], was designed to obtain SSA *joint torques*. However, the suit was empty (no human operator) and the applied torque was generated from an externally applied force with the suit strapped to a table. The applied torque, in reality, would have been generated by the human operator from the

inside of the suit and applied over a distributed area, rather than a single external point. In this chapter, I addressed Aim 2 by validating and then implementing the model (Chapter 2) to enable a simulation of the system dynamics with varied boundary conditions. The model was used to decompose the joint torques required by the operator to move the suit, to understand the contributing components to the overall torque. Then, changing the model inputs to match operational scenarios allowed for conclusions that are more relevant than conclusions based on experimental measures alone.

I specifically consider the decomposition of the required HBA joint torques that an operator must overcome to achieve flexion/extension of the hip. The decomposition permits the evaluation of the critical contributors to the required torques and the assessment of experimental evaluation methods for future SSA or other suit design and evaluation methods.

I use this model to investigate component level contributions to overall motion and torques. Then, I alter model inputs to detail the sensitivity of the system to those parameters. I specifically examined two external forcing profiles, fleet sizing (a few discreet sizes to accommodate all users) of the boots, varied bearing resistances, and gravitational scenarios with various magnitude and direction configurations.

4.1 Methods

4.1.1 Validation Procedure

After updating the kinematics model outlined in Chapter 2.1, the model was updated with mass/inertial properties as well as bearing resistances to allow for dynamics analyses. To ensure that the updates were implemented correctly, the model was validated against experimentally collected benchtop data.

The first validation was of the hip brief assembly (HBA) only, independent from the soft goods and boot, to verify the implementation of the bearing resistance definitions. Specifically, I wanted to check that both the magnitude and direction of the torque were correct and that the bearing was responding appropriately to external dynamics. The HBA model was oriented to match the experimental setup from Figure 5. Motion Analysis (MA), the dynamics solver in SolidWorks, was performed with the proximal bearing driven with a motor. A torque interrogator was used to record the torque necessary to achieve the prescribed constant angular velocity profile (a virtual dynamometer).

The lower body model with HBA, soft goods, and boot was then compared to the experimental data from Valish and Eversly [64]. The experimental study was performed on the MkIII SSA at NASA Johnson Space Center (JSC) by the Advanced Pressure Garment Development Lab. The experiments recorded the torques applied (collected at 2.9 Hz with a load cell) to manipulate each joint, as well as the joint angles (as estimated by an inertial measurement unit). Here, I specifically examined HBA flexion/extension. MA was performed with the model aligned to match the experimental setup in the NASA Johnson Space Center (JSC) experiments [64]. In both cases, it is important to remember that the suit was unmanned, and all forces were applied externally to the suit.

During the experimental flexion/extension tests, the right leg and waist bearing were strapped to the table, isolating the motion on the left side of the HBA and left leg. These boundary conditions were matched in the MA by removing the right limb and everything above the waist bearing, while locking the main hip brief in place (Figure 9). What remained was the HBA, and left rolling convolute joint, left lower-leg soft good, left ankle flange, and left boot. The suit model was orientated horizontal to the ground. The gravity level was nominally set to 1G and in the same

direction as the experiment. The gravity parameters were modified as part of the sensitivity analysis.

For this MA, the model was forced externally, just distal to the rolling convolute, the hip was allowed to rotate, and the hip flexion/extension angle was measured. The force was applied such that it was always orthogonal to the rolling convolute. The force direction was determined to mimic the experimental as closely as possible. The hip angle was calculated from vector formed from a virtual hip joint center (located at the centroid of the upper bearing) and the centroid of the rolling convolute at each time step. Since the programmed motion of the HBA forces the flexion/extension to have an out-of-plane component, the flexion/extension angle was taken as the projection of that motion on the sagittal plane.

During the experiment at JSC, the knee was not locked into a fixed position and was free to rotate in flexion/ extension. The orientation of the knee was not recorded and could not be used as an input to the model. Although the experimental setup allowed for knee motion, the dynamics model used a rigid body soft goods leg, which was segmented into two parts and an artificial knee joint added. The modeled knee joint was fixed during each MA. Based on observations of the experimental videos, a knee flexion angle of 45 degrees was nominally selected (Figure 9).

The model leg was also configured as a straight leg and with a 90-degree bend to examine the effect of the knee angle on the angle achieved for a given applied force. These two other configurations represented the extreme ranges of possible knee motion. The hip flexion/extension angles were calculated for each configuration to give a bound on the results.

4.1.2 Sensitivity Analyses Procedure

The Dynamics Rigid-Body MkIII SSA Model (Chapter 2.2) leverages SolidWorks' Motion Analysis (MA) capabilities and was used to determine the contributions to the hip joint torque, from each SSA component. Additionally, the sensitivity of the model to select input parameters was examined by altering the relevant model inputs. The inputs that were varied include the external forcing profile (nominal, and sinusoidal), fleet sizing (a few discreet sizes to accommodate all users) of the boots (small/nominal, medium, and large), and varied bearing resistances (0.5X, nominal, and 1.5X). To understand the effects of gravity on the system, I also evaluated alternate gravitational scenarios by changing the magnitude (Lunar, Martian, and Nominal/Earth gravity) and direction (nominal/transverse, and then axial). A better understanding of the dynamics under these varied input conditions can inform future SSA and exosuit design requirements.

One method to perform the aforementioned decomposition within the model is to turn the bearing resistances off, where the resulting required joint torques would be completely due to inertial effects associated with the moving mass of each component. Then, the mass of the SSA could be turned off by setting the densities to zero, and the resistance of each bearing, separately, can be added to determine the components of the overall torque due to each bearing. This method of selectively turning on and off different resistances and component masses while recalculating the hip angles should be accepted with caution as the recalculation would result in new and distinct kinematic motion profiles.

In an effort to avoid comparing required torques across different kinematic solutions, the bearing torques were calculated for a single solution using the absolute value of the angular velocity of each bearing during that solution and the polynomial fits (Torque vs. Angular Velocity) from the bearing characterizations (Chapter 2.3). The absolute value of the bearing torques were

used to avoid incorrectly summing the torques when moving in opposite directions, where "negative" torques would subtract from "positive" torques. However, in reality, any torque, irrespective of rotational direction, are additive. The difference between the total applied torque and the calculated summation of the bearing torques can be attributed to mass/inertial effects. The decomposition was performed using a sinusoidal forcing function with the nominal model configuration to remove the human-induced variability.

4.1.2 Data Analysis

The flexion/extension cycle was sectioned into two zones based on the cumulative bearing torques and the inertial/mass torques. Zone 1 is where the inertial/mass torques are larger than the bearing torques and Zone 2 is where the bearing torques are larger than the inertial/mass torques. In Zone 1, the percentage of the total applied torque were calculated for both the inertial/mass torque and the cumulative bearing torque, at each time step. Then, the percentages were averaged over the entire zone. Zone 2 was not included in the calculation because the dominating dynamics were different. There was very little applied torque in Zone 2, and the resistance torques were based on slowing the "coasting" inertia of the suit. Operationally, the human operator would not be fighting the resistance; therefore, it was not included in the decomposition.

The hysteresis plots (Hip Joint Torque vs. Hip Angle) for varied boot weight, knee angle, and bearing resistance were compared to the nominal hysteresis plot. Summarizing, I examined the sensitivity for three boot weights (Small - 2.10 lbs, Medium - 3.10 lbs, and Large - 3.46 lbs), three knee angles (Extended Knee - 0 degrees, Nominal Knee - 45 degrees, and a Flexed Knee - 90 degrees), two forcing functions (experimental and sinusoidal), three gravity magnitudes (Earth, Moon, Mars), and two gravity directions (transverse, axial). The sinusoidal forcing function frequency and amplitude were selected to match the experimental data peaks in an attempt to match the function closely, while eliminating variance. While examining the magnitude and direction of

gravity, the applied force was reduced such that the limb would not be driven outside its operational range in the lower gravity environments. A total of 16 cases were examined (Table 3).

4.1.3 Statistical Analysis

For each of the modified Cases, the mean flexion and mean extension angles were compared to the nominal model using 2-sample T-tests, while assuming different variations. Standard deviations of the flexion and extension angles were compared using an F-Test. The significance level used was 5% ($\alpha = 0.05$).

4.2 Results

4.2.1 Validation

The initial, HBA-only comparison verified that the bearing resistances were correctly captured in the model. The input angular velocities (Chapter 2.3.1) for the modeled bearing generated resistance torques aligned with the prescribed polynomial fits (Chapter 2.3.2), thus confirming that the fits were implemented appropriately with the reaction torques. (The output is not shown in the thesis because it was identical to the input, thus confirming the validation).

The experimental flexion/extension data and computational model results are shown in Figure 13 and summarized in Table 3. The nominal model (Case 2) under-estimated the experimental model (Case 1) hip angle during both peak flexion and extension. The differences between Cases 1 and 2 were significantly different ($p<0.005$).

Although there is a statistical difference in peak flexion and extension, operationally the model is a good approximation of the overall motion characteristics and response of the SSA to an external forcing. The model estimates about 75% of the mean hip angle range as compared to the experimental data and captures the hysteresis appropriately. Differences between the model

assumptions and experimental analysis that may yield the discrepancy are addressed in the limitations section (Chapter 2.2.4).

The MA model was able to capture the hysteresis and slopes observed in the experimental data, although the peak flexion and extension angle was not captured (Figure 13, Table 3). The model does accurately estimate about 75% of the mean hip angle range as compared to the experimental data. There are a few contributing factors that may have led to the discrepancy between the MA and experimental results, including the manner in which the angles were estimated and the assumptions made within the model. For example, we assume that the experimental operator was only contacting the suit at the point of applied torque, but in reality, their contralateral hand was supporting the boot and applying an additional torque. All Cases, each with a varied model input, are defined and the respective results collated in Table 4.

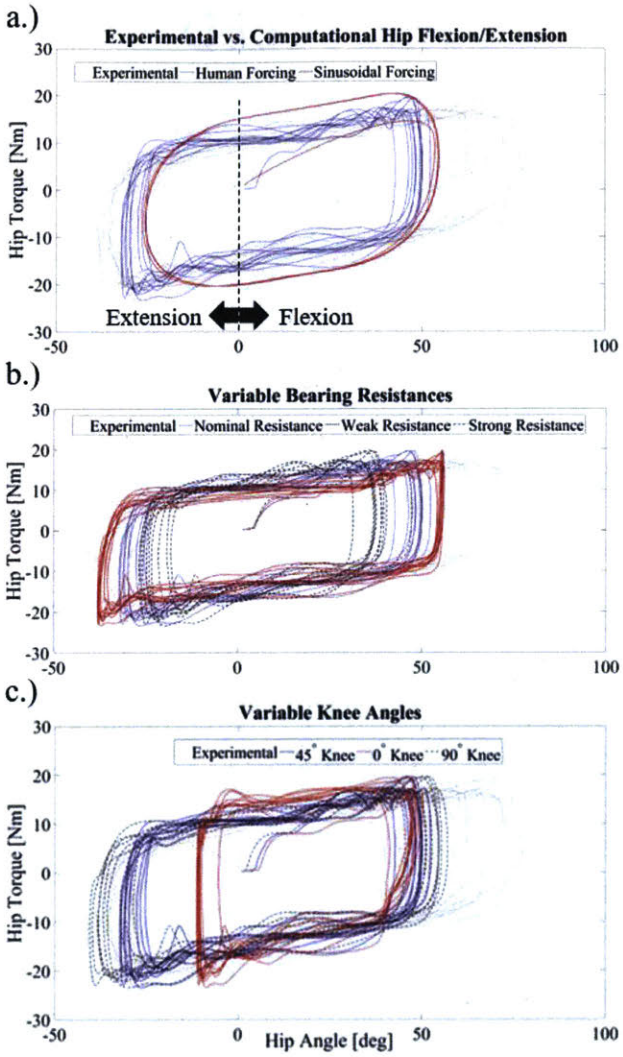

Figure 13: Hysteresis comparisons. (a) Comparison between the experimental data (Case 1), the nominal model (Case 2), and an alternate forcing function (Case 3). The hip torque was applied and the hip angle was measured for the experimental case and estimated for the computational case. (b) Comparison between the nominal model and variable bearing resistances (Case 8 & 9). (c) Comparison between the nominal model and variable knee angles (Case 6 & 7). Cases are defined in Table 3.

Table 3: Collated computational model inputs and outputs as well as the experimental independent and dependent variables.

Case	Bearing Resistances	Boot Size	Knee Orientation (Degrees)	Forcing Function	Gravity Level (Planetary Body)	Gravity Direction (Transverse or Axial)	Peak Flexion Angle (8 cycles)					Peak Extension Angle (7 cycles)				
							Maximum (Degrees)	Minimum (Degrees)	Mean (Degrees)	Standard Deviation (Degrees)	p-Value	Maximum (Degrees)	Minimum (Degrees)	Mean (Degrees)	Standard Deviation (Degrees)	p-Value
1	Exp. (Nominal)	Small (2.10 lbs)	Exp. (Variable)	Experimental	Earth	Transverse	77.70	58.88	69.46	6.82	<0.005	-41.96	-30.26	-35.54	4.07	<0.005
2	Nominal	Small (2.10 lbs)	45	Experimental	Earth	Transverse	50.11	46.37	48.72	1.37	-	-32.13	-25.40	-29.84	2.48	-
3	Nominal	Small (2.10 lbs)	45	Sinusoidal	Earth	Transverse	54.58	54.41	54.43	0.06	<0.005	-25.59	-25.52	-25.58	0.03	<0.005
4	Nominal	Medium (3.10 lbs)	45	Experimental	Earth	Transverse	50.96	47.59	49.70	1.25	0.160	-30.88	-24.34	-28.69	2.42	0.397
5	Nominal	Large (3.46 lbs)	45	Experimental	Earth	Transverse	51.37	47.99	50.10	1.25	0.055	-30.39	-23.91	-28.22	2.24	0.237
6	Nominal	Small (2.10 lbs)	0	Experimental	Earth	Transverse	50.26	46.98	48.10	1.12	0.337	-11.27	-9.96	-10.77	0.48	<0.005
7	Nominal	Small (2.10 lbs)	90	Experimental	Earth	Transverse	55.26	**49.94**	53.00	2.04	<0.005	-40.46	-28.69	-36.15	4.31	<0.05
8	Weak (0.5X)	Small (2.10 lbs)	45	Experimental	Earth	Transverse	56.01	55.34	55.64	0.22	<0.005	-38.10	-35.38	-37.27	1.04	<0.005
9	Strong (1.5X)	Small (2.10 lbs)	45	Experimental	Earth	Transverse	40.38	36.78	38.33	1.36	<0.005	-26.75	-19.27	-23.97	2.74	<0.005
10	Nominal	Small (2.10 lbs)	45	Experimental	Earth	Axial	30.53	22.89	25.29	2.43	<0.005	-20.76	-13.61	-17.46	2.83	<0.005
11	Nominal	Small (2.10 lbs)	45	(3/8)*Sinusoidal	Earth	Transverse	23.05	23.00	23.02	0.02	-	-14.10	-14.04	-14.08	0.02	-
12	Nominal	Small (2.10 lbs)	45	(3/8)*Sinusoidal	Mars	Transverse	30.17	27.96	29.65	0.81	<0.005	-13.04	-11.13	-11.61	0.69	<0.005
13	Nominal	Small (2.10 lbs)	45	(3/8)*Sinusoidal	Moon	Transverse	31.73	22.21	28.57	3.38	<0.005	-22.41	-13.79	-16.91	2.99	<0.05
14	Nominal	Small (2.10 lbs)	45	(3/8)*Sinusoidal	Earth	Axial	16.71	16.71	16.71	0.00	-	-14.28	-14.28	-14.28	0.00	-
15	Nominal	Small (2.10 lbs)	45	(3/8)*Sinusoidal	Mars	Axial	22.54	21.30	22.16	0.46	<0.005	-19.61	-19.45	-19.49	0.06	<0.005
16	Nominal	Small (2.10 lbs)	45	(3/8)*Sinusoidal	Moon	Axial	24.87	20.72	23.47	1.51	<0.005	-22.09	-19.97	-20.53	0.72	<0.005

The case numbers down the far left column indicate different configurations. Case 1 represents the results from experimental analysis. Case 2 through 16 are the SolidWorks Motion Analysis model results for each given input configuration. Case 2 (shaded) is the nominal case, where I attempted to match Case 1 inputs to make a direct comparison between experimental and model results. The three bold horizontal lines separate sections within which statistical analyses were conducted and each Case was compared with the gray row in that section (Case 2 or 11 or 14). The p-values correspond to 2-way T-tests comparing each Case to the nominal model, assuming different variances for each Case. Cases that are not statistically different (P>0.05) are shaded for ease of visualization (Case 4, 5, 6, 12, and 13).

4.2.2 Sensitivity to Fleet Sizing of Boots

There was not a significant effect of changing the boot masses (Cases 4 and 5) from the nominal configuration (Case 2). While the nominal model as well as the experimental data used a small boot (2.10 lbs), Case 4 implemented a medium boot (3.10 lbs) while Case 5 implemented a large boot (3.46 lbs).

4.2.3 Sensitivity to Forcing Function

Since the forcing function for both the experimental testing (Case 1) and nominal model (Case 2) was performed by a human, there was natural variability within a cycle and across cycles in terms of both the magnitude of the applied force and the direction. In the operational setting, a crewmember inside the suit would force the suit with similar variability expected from a human operator. In Case 3, the model was configured nominally, but the external forcing function was changed to a sinusoidal force, reducing variability of the peak flexion and extension (Figure 13a, in red). When comparing the variability, the sinusoidal forcing function input results in smaller standard deviations for both flexion ($F(7,7) = 533.3$, $p<0.005$) and extension ($F(6,6) = 8814$, $p<0.005$).

4.2.4 Sensitivity to Knee Angle

Variations in knee angle (Cases 6, and 7 in Figure 13c) and bearing resistance (Cases 8, and 9 in Figure 13b) resulted in differences when compared to the nominal model (Case 2). Increasing knee flexion results in an increase in hip flexion and extension while decreasing knee flexion results in a decrease in hip flexion and extension. Increasing the bearing resistances results in a decrease in hip flexion and extension while decreasing the bearing resistances results in an increase in hip flexion and extension.

4.2.5 Sensitivity to Gravity Direction and Magnitude

When the direction of gravity is in the axial direction, the hip flexion and extension angles are reduced compared to the transverse (nominal) direction, (Figure 14a). In Figure 14b and Figure 14c, reducing gravity results in increases in hip flexion and extension angles. A reduction in gravity simulates planetary exploration of another planet.

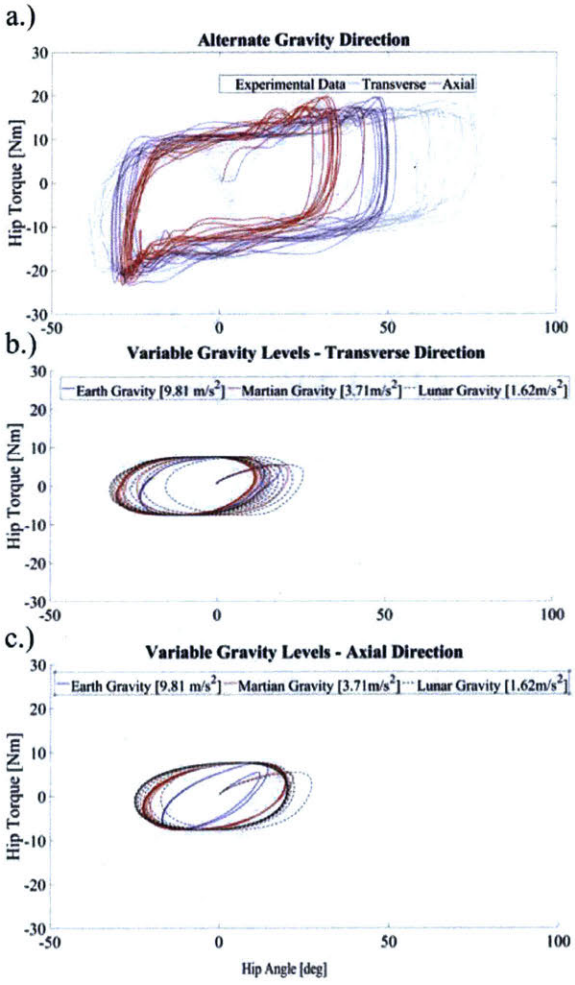

Figure 14: Hysteresis Comparisons with Variable Gravity. (a) Comparison between the experimental data (Case 1), the nominal model with the transversely applied gravity direction (Case 2), and the model with an axially applied gravity direction (Case 10). (b) Comparison between the three gravity levels when gravity is applied in the transverse direction (Cases 11, 12, and 13). For these cases, the forcing function was 3/8ths of the sinusoidal forcing function. (c) Comparison between the three gravity levels when gravity is applied in the axial direction (Cases 14, 15, and 16). For these cases, the forcing function was also 3/8ths of the sinusoidal forcing function.

4.2.6 Underlying Bearing Motion

Using the sinusoidal input and model configuration from Case 3, the underlying bearing motion relative to the hip flexion/extension motion is presented for two flexion/extension cycles (Figure 15). The proximal bearing is rotating more than the distal bearing during hip flexion, but the distal bearing is rotating more in hip extension (Figure 15a). There are also times when the bearings are moving in opposite directions (Figure 15b). The proximal bearing is moving throughout the flexion extension motion, however the distal bearing has periods where it is not rotating (Figure 15a and Figure 15b).

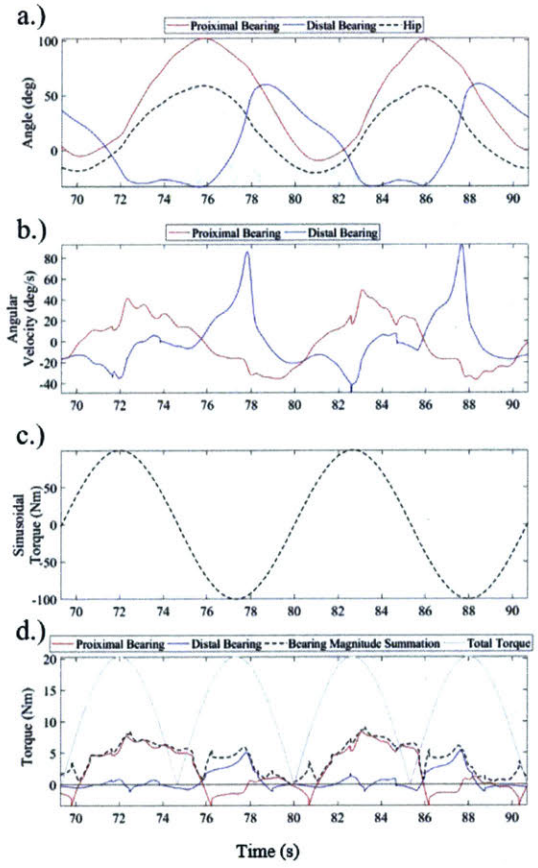

Figure 15: (a) The angular position of each bearing and the hip (in the 2D sagittal plane). (b) The bearing angular velocities. (c) An example of an external sinusoidal forcing function. (d) The individual bearing torques, the summation of their absolute values, and the absolute value of the externally applied torque (the amplitude of the applied torque was 20 Nm, which is smaller than the example applied torque in 15d).

The hysteresis observed in Figure 13 and Figure 14 stems from a phase shift between the applied force and the motion of the system as highlighted in Figure 15. The hip angle (Figure 15a) is not aligned with the sinusoidal torque (Figure 15c). This is easily visible as shown for Case 3, which has a small variability in estimated motion. However, the same trends are apparent in the other cases.

4.2.7 Required Torque Decomposition

When decomposing the torques (Figure 16), it is evident that over the flexion/extension cycle, the major contributor to the overall hip torque is the inertial component, which is due to moving the mass of the SSA components. On average, the inertia contributes about 76% (SD = 11%) of the total hip torque to drive the motion of the suit within Zone 1. The remaining 24% is produced by the resistive torques associated with the spinning bearings. In Zone 2, there is very little applied force and yet there is still torque being realized in the bearings since an angular velocity still exists as the suit continues to "coast" (continue rotating due to momentum, even with little or no applied torque).

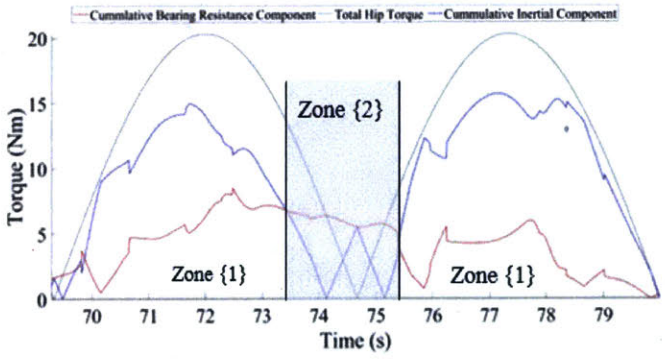

Figure 16: The black line shows the absolute value of the sinusoidal forcing function input for Case 3. The green line shows the summation of the absolute values of the proximal and distal bearing torques. The cyan line represents the absolute value of the difference between the two curves, which is also the absolute value of the inertial torque component.

4.3 Discussion

In this chapter, I implemented a dynamic Rigid-Body Space Suit Assembly (SSA) Model (Chapter2.2), leveraging SolidWorks and a built-in Motion Analysis (MA) tool. The MA model was used to decompose the required HBA joint torques that an operator must overcome to achieve flexion and extension of their hip. The decomposition permits the evaluation of the critical contributors (mass/inertia and bearing resistances) to the required torques. I specifically examined two external forcing profiles, fleet sizing (a few discreet sizes to accommodate all users) of the boots, varied bearing resistances, and gravitational scenarios with multiple magnitude and direction configurations. The analysis is capable of informing future SSA and exosuit design and evaluation methods.

4.3.1 Mark III (MkIII) Hip Brief Assembly (HBA) Hysteresis

The model appropriately captures the hysteretic behavior of torque vs. angle plots, but it was not clear, a priori, what was driving the presence of the hysteresis. The dynamics model approach enabled examining the physics causing the hysteresis, which was found to result from a phase shift between the applied force and the motion of the system. For example, the peak force applied in flexion is not aligned with peak flexion angle. That phase shift is due to energy lost in the system because of a number of factors including bearing resistances (speed dependent as shown in Chapter 2.3), component mass inertia effects (speed dependent as shown in Chapter 2.2), heat, sound, friction, soft-goods fibers rubbing on each other, the magnitude of gravity, and the direction of gravity.

The hysteresis observed in soft-goods only joints has the added effect of a "stable location", which is the orientation the joint adopts when there are no forces acting on it. When deviated from that stable location, the joint has a torque acting to return it to that position. However, with the

MIII hip, the bearings provide mobility, and do not have any "stable" orientation, but are equally stable in any orientation. The soft-goods suit is only speed dependent based on the component mass inertia effects, but the MIII also has the speed dependent effects of the bearings.

4.3.2 Space Suit Assembly (SSA) Mass Effects

Another interesting finding, as seen in Table 3 and Figure 13b, was that as knee flexion increases (0, 45, 90 deg.), hip extension angle increases while flexion did not significantly change. This is most likely because there is a period in every cycle where the force applied is low, but the inertia carries the suit into flexion. When the knee flexion angle increases, the distributed mass of the leg acts over a shorter moment arm at the hip. With the smaller moment arm, the suit does not carry itself up into flexion as far, and the user has to input more force to accommodate. It is interesting because in certain configurations, it can be useful to have extra weight. Operators must learn to let the suit work for them and put energy in at the correct time, like when children swings their legs at just the right moment on a swing.

In Figure 16, there is an interplay between the inertia of the SSA components that are continuing to move and the bearings resisting that motion. In Zone 2, there is minimal externally applied hip torque, but the interaction between the inertia and bearing resistances give insight into their roles during the flexion/extension motion. The bearing torques remain high as they dissipate residual energy, although they are not necessarily enacting that force on the human operator. The human operator, attempting to manipulate the suit efficiently, can move at the same rate as the suit in this region, avoiding incurring additional torques. The operator can allow the bearing torques to act against the mass/inertial torques, directly on the SSA components alone and slow the suit motion.

When gravity is axially applied, the flexion and extension angles both increase while the gravity level decreases. The increase in hip flexion and extension angles are due to a greater dependence on suit mass with axially applied gravity. In that direction, the externally applied force must lift the leg in both directions. When gravity is transversely applied, the externally applied force only has to push the inertial components of the suit mass along a supported surface and not fight the weight of the limb as well. This is confirmed when comparing mean flexion and extension angles between the transversely applied gravity cases and the axially applied gravity cases. The axially applied gravity cases have lower hip flexion, but larger hip extension angles. The suit geometry causes the suit to generate out-of-plane motion when moving the hip in extension, with the out-of-plane motion against gravity. However, when axially applied, the out-of-plane motion is not aligned with gravity and has less influence.

Shorter et al.[60] showed that a ROM limitation had a compensatory increase in stride length, while an SSA operator was observed to have a reduction in step length.[15] The resistive, speed-dependent joint torque associated with the spinning bearings and moving suit mass creates additional constraints on the operator that diminishes the mobility and agility of the operator. The dynamics modeling tool (Chapter 2.2) enabled the decomposition in the increased required joint torques into its contributing constituents, permitting further understanding of the designed system limitations.

4.3.3 Limitations and Future Work

The model can be improved to reduce the differences between the experimental and computational results. For example, it would be useful to change the direction of the applied force vector in addition to the current capability to change the force magnitude. Instead of a knee modeled with a few discrete and set angles, it would be beneficial to have an "active" knee model

that would be subject to a prescribed kinematic profile (knee angle vs. time) or have defined properties that allow it to behave like a spacesuit knee. The active knee would be dynamic during the MA, and allow the model would be capable of calculating the knee joint torques throughout hip flexion/extension.

Another useful feature would be an estimate of the normal forces of contact between the supported boot and the boot itself to obtain more data for Cases 4 and 5 (see table I). Additionally, a normal force could be applied to the boot, which can be varied over time, to mimic the experimental boundary condition where the boot was supported.

Additionally, the bearing resistance expressions used in the model can be extended to account for off-axis loads. The bearing analyses were obtained assuming only normal forces applied along the axis of rotation (held perpendicular to gravity, Chapter 2.2.1). However, operationally, the bearings are at angles relative to gravity and experience loads off the axis of rotation. To obtain the experimental bearing characterizations with off-axis loads, which can be implemented in the model, the bearings will have to be forced by a dynamometer to achieve a range of angular velocities while applying various off-axis loads using cantilevered masses. Another update for the bearing resistances could be the effects of lifecycle, maintenance schedules, and exposure to Lunar or Martian regolith.

It is important to note that in this study, there was no human in the suit. The validation of the model was compared to an external forcing of the suit. The next steps include using the validated model with a human operator modeled to manipulate the suit internally. A first step could be to use the experimental kinematic data (joint angles) from the JSC study[64] to define the kinematic motion of a motor that drives the human hip model (HHM) to contact and force the

HBA/SSA lower-limb model. Similar to the validation comparisons, there would be a torque interrogator, recording the torque required by an actuator to achieve the kinematic input.

4.3.4 Conclusion

In this chapter, I addressed Aim 2, successfully decomposing the required joint torques into the contributing components, to understand the contributing components to the overall torque. Then, changing the model inputs to match operational scenarios allowed for conclusions that are more relevant.

I specifically considered the decomposition of the required HBA joint torques that an operator must overcome to achieve flexion/extension of the hip. The decomposition permits the evaluation of the critical contributors to the required torques and the assessment of experimental evaluation methods for future SSA or other suit design and evaluation methods.

I used this model to investigate component level contributions to overall motion and torques. Then, I altered model inputs to detail the sensitivity of the system to those parameters. I specifically examined two external forcing profiles, fleet sizing (a few discreet sizes to accommodate all users) of the boots, varied bearing resistances, and gravitational scenarios with various magnitude and direction configurations.

5. Effects of Suit Weight and Suit Fit on Operator Performance

Research Gap: How does the distributed weight of an SSA, transferred to the operator, affect performance?

Aim 3: To quantify the magnitude of the distributed MkIII SSA weight transferred to the operator at the shoulder straps and measure the changes in stability associated with changes in suit fit, or how tightly-coupled the system is.

Aim 3.1: To test the hypothesis that the MkIII SSA self-supports part of its own weight, which increases in double stance (DS) as compared to single stance.

Aim 3.2: To test the hypothesis that operators lose postural stability when suited as compared to unsuited, and as they become more tightly-coupled with the suit.

The weight of the suit can first be broken into two components: the weight transferred to the operator and the self-supported weight. Self-support is the fraction of total suit weight that is transferred directly to the ground without requiring the operator's support. The weight transferred to the operator can be split into two components as well: the weight that is transferred through the designed interaction locations (which in the case of the MkIII SSA, are shoulder straps) and the weight transferred through other non-designed locations (such as the operator's arm contacting the inside of the suit[5.4]). The operator must continually support that fraction of the suit weight as well as overcome the inertial effects associated with the moving mass during dynamic tasks.[24,47] In this chapter, I consider static tasks and examine how the fraction of weight transferred to the operator affects stability. Suited operation requires load carriage as the operator will support a portion of the space suit weight.

Indexing, or strategically placed padding between the suit and operator, can be used to adjust suit fit.[27] The thickness and location of that padding can be increased or decreased to make

the human-SSA system more or less tightly-coupled, respectively. For example, the suit can become more tightly–coupled with the operator by increasing the thickness of the padding, essentially reducing the gap between the operator and the suit. As discussed, the MkIII drives programmed motions through mobility restrictions, forcing operators to move within a limited motion envelope. Increasing coupling through indexing may force operators to adhere even closer to the mobility limitations inherent in the MkIII architecture, affecting postural control.

5.1 Methods

5.1.1 Subjects

This study was performed by four male subjects that fall within the range of astronaut characteristics. The subjects were 31, 25, 25, and 27 years old and 71, 66, 68, and 67 inches tall, respectively (Table 4). Although two of the subjects fall a year short of the astronaut selection criteria for age (26-46 years old), all were within the criteria for height (62-75 in) of astronaut candidates. All subjects passed a class I medical and were self-reported as physically fit with no active injuries. While two subjects were just outside the required age range, the four subjects fit well within astronaut selection criteria. Three of the subjects were novice users of the space suit (Subjects 2, 3, and 4) and one was expertly trained (Subject 1). Each novice subject conducted one fit-check session in the MkIII SSA, to familiarize himself with the suit and to achieve the proper baseline fit. Subject 2 completed his fit-check two months before testing. Subject 3 completed his fit-check three weeks before testing. Subject 4 completed his fit-check one week before testing. The fit-checks were performed without the use of any extra padding, to leave space for the padding used in the experiment for changing the indexing. The study protocol was approved by the NASA Johnson Space Center IRB and MIT Committee on the Use of Humans as Experimental Subjects. Subjects provided written informed consent prior to participation.

Table 4: Relevant subject anthropometric data including height, crotch height, knee height, hip breadth and thigh circumference. Thigh circumference was used to calculate the thigh diameter and determine the gap between the outside of the subject's thigh and the inside of the hip brief assembly (HBA). Indexing thicknesses were determined based on getting as close as possible to filling 50% of that gap with Configuration 1 and 100% of that gap with Configuration 2. Configuration 0 is not listed here, as it was 0% fill (no padding) for all subjects.

								Indexing Thickness (in)	
Subject	Age	Height (in)	Shoe Size (US)	Crotch Height (in)	Knee Height (in)	Hip Breadth (in)	Thigh Circumference (in)	1	2
1	31	71	10	32.5	18	14.5	22.5	0.375	0.75
2	25	66	8.5	29	18.5	14.5	22	0.375	0.75
3	25	68	11	31	19.5	14.5	22.5	0.375	0.75
4	27	67	8.5	32	20	16	23	0.25	0.5

5.1.2 Equipment

The study was performed in the Anthropometrics and Biomechanics facility (ABF) at the NASA Johnson Space Center in normal Earth gravity. A number of sensor systems were used, including external force plates to measure ground reaction forces, in-sole sensors to collect ground reaction forces at the operator's foot, and load cells to measure tension force in the SSA shoulder straps. Additional sensor systems were used during the experiments, but the data were not used in this chapter. The excluded sensors including a set of 20 single distributed pressure sensors to measure interactions between the operator and SSA at the hip, and inertial measurement units that were used to measure both the operator and suit kinematics. Those systems were collecting data, useful in measuring dependent measures, for investigating dynamic ambulation. That analysis is part of future work.

Ground reaction forces at the base of the unsuited operator's foot and the suited operator's boot were collected using four Advanced Mechanical Technologies Inc. (AMTI) OR6-7-2000 force plates (Figure 17, Left), recording at 1000 Hz, with date and times stamps for each frame. The external force plate data were collected in discrete files; one for each trial. The four force plates were each labeled with large Roman numerals (I-IV) to identify them and setup adjacent to each other, forming a single larger square.

Pressure data under the feet were collected using two Novel Pedar In-Sole sensors (Figure 17, Right) recording at 50 Hz. The insole sensor data were collected in discrete files; one for each trial. The pressure data across the surface of the insole sensors were used to calculate the ground reaction forces at the base of the operator's foot in both unsuited and suited trials. The insole sensor and distributed sensor data were streamed live via Bluetooth to a nearby computer, but were also recorded locally, which was used in the analysis to eliminate the potential for lost data from Bluetooth dropout.

The tension force in the SSA shoulder straps, when suited, were collected using four Omega LC201-100 Sub Mini Load Cells at 10 Hz. The load cells were each integrated into the shoulder straps that were designed into the MkIII SSA as the primary location for the transfer of suit weight to the operator. Custom brackets were fabricated to allow the load cells to be positioned in line with the straps as well as route the power/data cables out to the Omega OM-DAQXL-1-NA data acquisition box. The MkIII SSA is a rear-entry suit, meaning there is a large hatch in the rear of the suit where operators enter and exit to don and doff the suit. The data acquisition box for the load cells was mounted directly on the exterior of the hatch door, and the power/data cables were run to each load cell through a suit port. The box displayed the force of each load cell, in real time, and the force was locally recorded as well. Date and times were recorded, but were based on an internal clock that was manually set. Therefore, the date and time data had a time shift from the force plate data. The load cell data were collected in a few continuous files, with each file containing multiple trials.

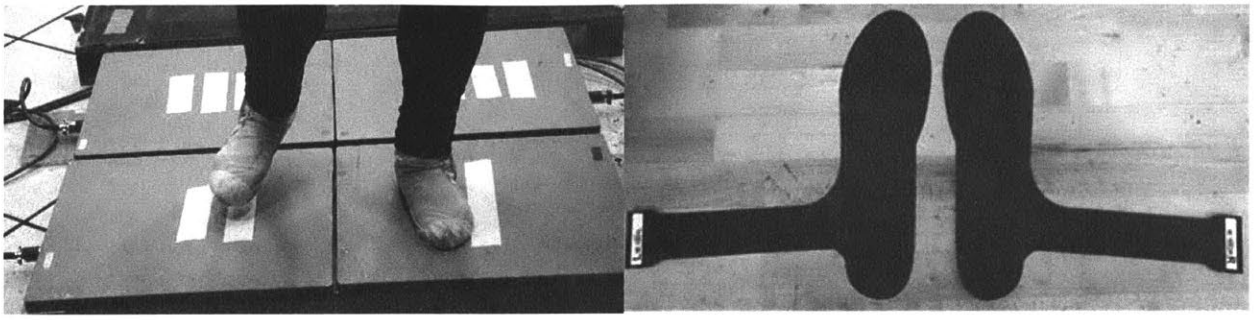

Figure 17: (Left): Force plate sensors used to measure total ground reaction forces, labelled with Roman Numerals I through IV. The subject in the image is performing a single stance trial, standing on their left foot on force plate I. (Right): In-Sole sensors used to measure the ground reaction forces at the operator's feet, located inside of the liquid cooling ventilation garment (LCVG) booties.

When suited, the MkIII was pressurized to nominal suit pressure (4.3 psi) in a tethered configuration (i.e., not with the closed-loop portable life support system (PLSS)). The MkIII in the tethered configuration weighs around 59 kg.[2,65] In our study, the MkIII had an average weight of 61.5 kg across all configurations and subjects. The difference in weight was because of different suit components (Table 4), the added mass of the sensor systems, data acquisition equipment, and foam used for indexing. While unsuited, the subject wore a compression shirt and pants with the liquid cooled ventilation garment (LCVG) that was also worn while in the suit. While suited and unsuited, the Novel Pedar sensors were integrated into the booties of the LCVG, which maintained their position underneath the subject's feet during unsuited and suited trials. While suited, the multiple indexing configurations (Configuration 0, 1, and 2) were achieved using Viton Fluororoelastomer Foam sheets. They were fastened to the LCVG in the desired locations using mesh sleeves that were custom made to stretch to accommodate padding of varying thickness around the circumference of both the hips and thighs. The subject was in configuration 0 during the unsuited tasks, with no foam in their mesh sleeves.

5.1.3 Procedure

While unsuited, the subject stood still with each foot resting on an independent external force plate to obtain static double stance (DS) data. The subject held the DS pose for 30 seconds at a time for a single trial and then repeated the pose for 6 trials. The subject relaxed and stepped away from the force plates between each trial, returning to the force plates before the next trial began. After the DS trials, the subject performed single stance trials where they initially stood in DS and then transitioned to single stance. In single stance, the foot in contact with the ground was located over only one force plate. The single stance pose was repeated for each foot for a total of 6 trials per foot. Thus, for the Unsuited configuration, there were 6 DS, 6 Single Stance Left (SSL), and 6 Single Stance Right (SSR). If the subject was unable to maintain SSL/SSR for the full 30 seconds, the trial was terminated when the contralateral foot touched down. Following unsuited operations, the subject donned the MkIII SSA, which was then pressurized following nominal pressurization procedures and safety protocols.

While suited, the DS and SSL/SSR poses were repeated for multiple indexing configurations, where the suit fit was adjusted using padding. There were three separate suited indexing configurations; (1) no added padding, (2) padding was sized to fill 50% of the gap between the subject and the internal surfaces of the suit, and (3) padding was sized to fill 100% of the gap (Table 5). The padding thickness was selected on a subject-by-subject basis based on their anthropometric data (Table 5). Starting with thigh circumference, thigh diameter was calculated. Thigh diameter was subtracted from the smallest diameter inside the HBA (8 in, as measured with the model developed in Chapter 2) to determine the gap between the human and suit at the thigh. Padding was then rounded to the nearest 0.125 in because that was the minimum padding thickness. The padding was placed circumferentially around the hips as well as the thighs (Figure 18). Since anthropometric data from each subject is required, I would suggest that all potential

subjects or crewmembers have 3D laser scans completed, from which all required anthropometric measures can be extracted.

Table 5: Relevant subject suit sizing parameters including the boots, arm soft-goods, leg sizing rings, leg soft-good, waist sizing rings, liquid cooling ventilation garment, shoulder strap length, and total average suit weight across all trials for that subject. The suit weights could change based on the component sizing, indexing, and data acquisition equipment inside the suit.

Subject	MIII Boot (US)	Arm Soft-Good	Leg Sizing Ring (in)	Leg Soft-Good	Waist Bearing Sizing Ring (in)	LCVG	Shoulder Strap Length	Avg. Suit Weight [kg (lbs)]
1	David Clark 11	Extra-Short	0.604	Large-Exra-Long	0.75	Large Long	8	62.6 (138.0)
2	David Clark 11	Extra-Short	None	Large Short	None	Medium Short	9.5	61.3 (135.2)
3	David Clark 13	Short	None	Large Medium	None	Large	10	62.4 (137.6)
4	David Clark 11	Extra-Short	0.304	Large Long	None	Large	8.5	60.4 (133.2)

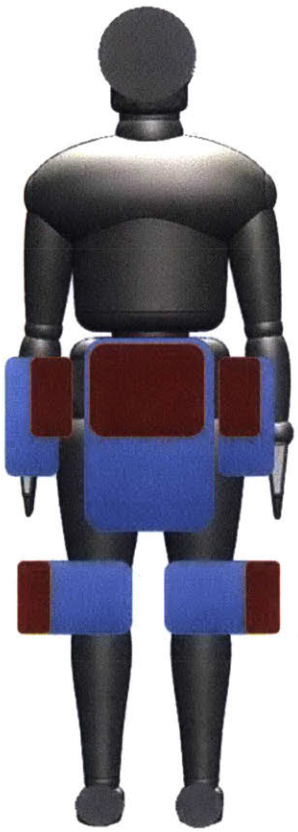

Figure 18: Padding placement used for indexing subjects in the suit. The blue (Configuration 1) represents a single layer closing 50% of the gap between the subject and the inside of the suit. The red (Configuration 2) represents a second layer of padding to fill 100% of the gap.

At the start of every trial, the subject would rise up onto their toes and then drop back onto their heels three times as a way to synchronize all of the data from each sensor system in post processing. Following the static tasks, the subjects also performed a dynamic ambulation task. The subjects walked across a 10 m long by 1 m wide walkway. The ambulation task was repeated for a total of 12 trials. The ambulation data was not used in this thesis as the analysis that I performed was specifically looking at suit fit and load transfer statically. Similar analyses for dynamic tasks are considered for future work.

5.1.4 Data Analysis

In all but three suited cases, the Novel in-sole sensors curled inside the LCVG booties, which caused spikes or time-out errors in the measured pressure in those locations (resulting in over estimation, or under estimation of force respectively). Therefore, a correction was attempted. When the subject was unsuited, the external force plate and insole sensors should record the same force, equal to the weight of the subject in that configuration. Therefore, the difference of the insole sensor average from the external force plate average was found for each of the unsuited configurations and subtracted from the in-sole sensor average for each of the corresponding suited configurations. However, the corrections were unreliable as the curling and timeouts were not consistent across configuration, thus the correction factor was not always appropriate. Without a way to ensure an appropriate correction for each trial, the insole sensor data was determined to be unreliable; therefore, the data was not used here.

The initial step in the data analysis was to synchronize the load cell and force plate data for each trial (Figure 19). The load cell data were added to a single file, sorted by date/time for each datum, with the time shift errors manually corrected based on comparisons with the force plate data.

Segmentation of the steady state data was performed manually from the synchronized data sets, where the best start and end time were selected. The manual selection allowed for optimal selection of the steady state sections within each trial, after the heel-ups and before the trial ended. This procedure was easy for the DS trials (Figure 19), but in SSLR/SSR was more nuanced. In these cases, attention was given to the individual force plate data (each representing a single foot) to see when the contralateral foot contacted the ground, indicating that the subject was unable to maintain single stance. Single stance trials where the operator could not maintain the stance for the entire 30 seconds resulted in shorter regions of steady state. An inability to maintain single SSL/SSR represents a loss of postural stability, therefore, steady state time (s) was used as a dependent variable to analyze postural stability. Postural stability was also estimated with the variance in both x and y position of the center of pressure (COP), and the variance in the vertical ground reaction force (F_z, or VGRF).

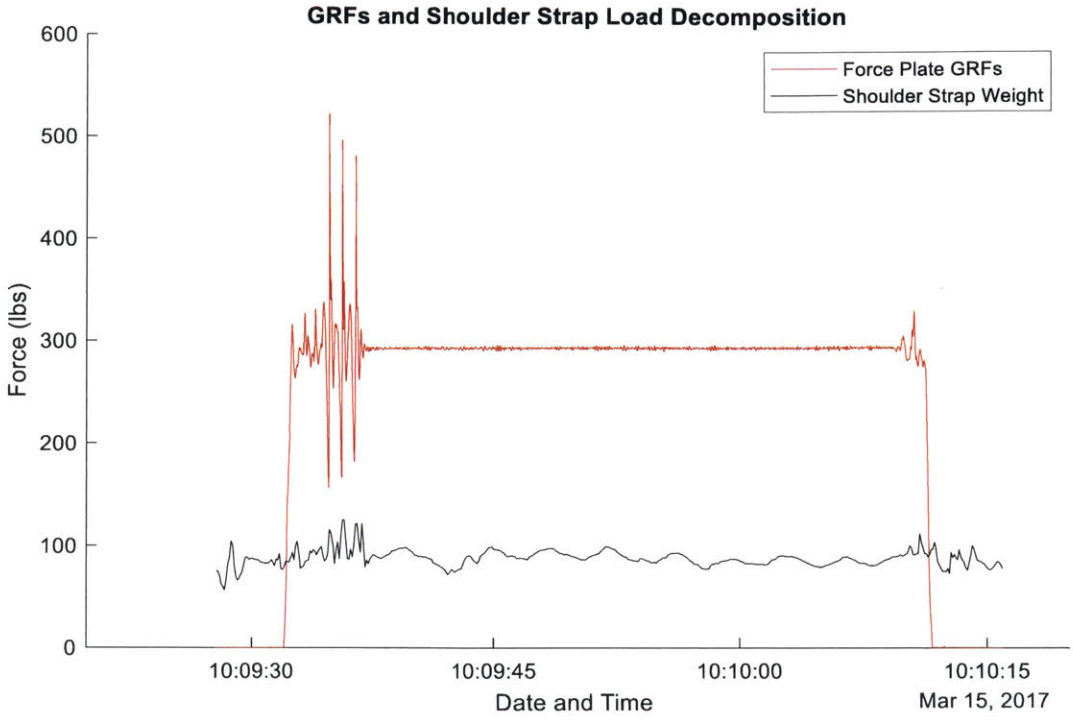

Figure 19: Example synchronized data and overlaid segmented data prior to segmenting the steady state region. This figure represents a single trial, in this case: subject 2, suited, double stance, and no padding. The three spikes at the beginning reflect heel lifts that were performed at the start of each trial to aid in aligning the multiple data streams.

Center of pressure information was calculated using the external force plates as it was the most reliable, accurate, and complete source of data. When performing static tasks, only two plates were activated (Fig. 2, Left). The COP for each plate (plates I and II) was calculated using the following equations:[70]

$$COPx_i = -\frac{M_{y_i} + F_{x_i} * d_z}{F_z} \qquad (11)$$

$$COPy_i = \frac{M_{x_i} + F_{y_i} * d_z}{F_z} \qquad (12)$$

Where i is 1 or 2 (force plate I or II), M_x, and M_y are the moments in X and Y, and F_x, F_y, and F_z are the ground reaction forces in X, Y, and Z. d_z is the plate thickness of 82.5 mm. After calculating the COP for each individual force plate, they were combined to give the global COP, as if the force plates acted as a single large force plate, and providing a single measure for COP_x and COP_y at each time point. The global COP was calculated as a weighted average (normal force on the plate divided by the total normal force on both plates) of the individual COPs for each plate, as shown below.[18]

$$COP_x = COP_{x_1}\left(\frac{F_{z_1}}{F_{z_1}+F_{z_2}}\right) + COP_{x_2}\left(\frac{F_{z_2}}{F_{z_1}+F_{z_2}}\right) \qquad (13)$$

$$COP_Y = COP_{y_1}\left(\frac{F_{z_1}}{F_{z_1}+F_{z_2}}\right) + COP_{y_2}\left(\frac{F_{z_2}}{F_{z_1}+F_{z_2}}\right) \qquad (14)$$

The variance for COP_x and COP_y and VGRF were estimated for the DS and SSL/SSR trials. VGRF was an output of the force plate sensors.

With the data synchronized and segmented for each trial, the force plate and load cell data were averaged across trial (Table 6). The shoulder strap and external force plate data was used to calculate the percent of total suit weight that was applied to the operator at the shoulder straps, Percent Shoulder (PS).

$$Percent\ Shoulder = \frac{Average\ Weight\ on\ Shoulder\ Straps}{Average\ Suited\ Trial\ Weight - Average\ Unsuited\ Trial\ Weight} \qquad (15)$$

The suit weight was calculated by taking the difference between the suited trial total weight (measured by the force plates) and the unsuited trial weight (Subject weight, also measured with the force plate). The total weight at the shoulder straps was calculated per strap, and then added together. Each strap contained two load cells. The load for an individual strap was determined by multiplying the lesser of the two load cells by two, as the difference in the front and rear load cell on a given strap would be the shear force applied to the shoulder. Taking the minimum of the two load cells and multiplying by two gives the total vertical force at the shoulders.

5.1.5 Statistical Analysis

A Kruskal-Wallis test was performed across subjects to compare groups (Figure 20) for each dependent measure in the postural stability analysis (Chapter 5.2.2). Each group is a different combination of the independent variables; configuration and task (Figure 20). The test determines if any of the groups are different by comparing the medians. In Appendix B., additional Kruskal-Wallis tests were performed within each subject for percent shoulder (PS). Post-hoc Wilcoxon rank sum tests were used to compare each group to determine which were different. The dependent measures tested were PS, variance in COP_x, variance in COP_y, variance in F_z (VGRF), and time (length of trial). Since this is a conservative test, post-hoc corrections were not used on the p-values ($\alpha = 0.05$).

Group	Configuration	Task
1	0	DS
2	0	SSL
3	0	SSR
4	1	DS
5	1	SSL
6	1	SSR
7	2	DS
8	2	SSL
9	2	SSR
10	3	DS
11	3	SSL
12	3	SSR

Figure 20: Configuration and Task combinations for each comparison group. Configuration 0 is Unsuited, Configuration 1 is Suited with no added padding, Configuration 2 is Suited with 50% gap filled padding, and Configuration 3 is Suited with 100% gap filled padding. DS stands for double stance, SSL is single stance left, and SSR is single stance right.

5.2 Results

In this chapter, I address two hypotheses: **[1]** the MkIII SSA self-supports part of its own weight, which increases in DS as compared to SSL/SSR; and **[2]** operators lose postural stability when suited as compared to unsuited and as they become more tightly-coupled with the suit.

5.2.1 Suit Weight Distribution

Table 6 presents the mean and standard deviation of the ground reaction forces measured by the force plates, and the shoulder strap weight measured by the load cells. Additionally, the table presents the average percentage of suit weight transferred to the operator at the shoulder straps (PS), for each configuration. The data in Table 6, along with the statistical analysis of PS are useful in addressing hypotheses [1]. When comparing PS, the Kruskal-Wallis tests showed that not all groups are equal for both pooled and within subjects comparisons ($p<0.005$).

Subject 1 did not complete any suited tasks with the shoulder straps in place, therefore; the analysis was not performed on Subject 1. However, Subject 2, 3, and 4 did produce PS data. When all subjects are pooled, PS is not different between SSL and SSR in all suited configurations ($Z=1.69$, $p=0.0905$, $Z=1.93$, $p=0.0531$, $Z=0.491$, $p=0.6236$ for Configurations 1, 2, and 3, respectively). When comparing single to double stance, SSL/SSR is greater than DS across all suited Configurations ($Z=-4.34$, $p<0.005$, $Z=-3.97$, $p<0.005$, $Z=-3.79$, $p<0.005$ for Configurations 1, 2, and 3, between DS and SSL, respectively). PS is not different between any Configurations within double stance or within single stance, showing that indexing does not affect PS. Therefore, the pooled analysis supports an effect of task, but not configuration on PS.

Since this is a small subject pool (n=3), variation within subjects was also considered, and shown in Appendix B. In agreement with the pooled analysis, Subjects 2, 3, and 4 all showed increased PS in SSL/SSR as compared to DS for all configurations. There were other differences within subject, and those are presented in the Appendix B.

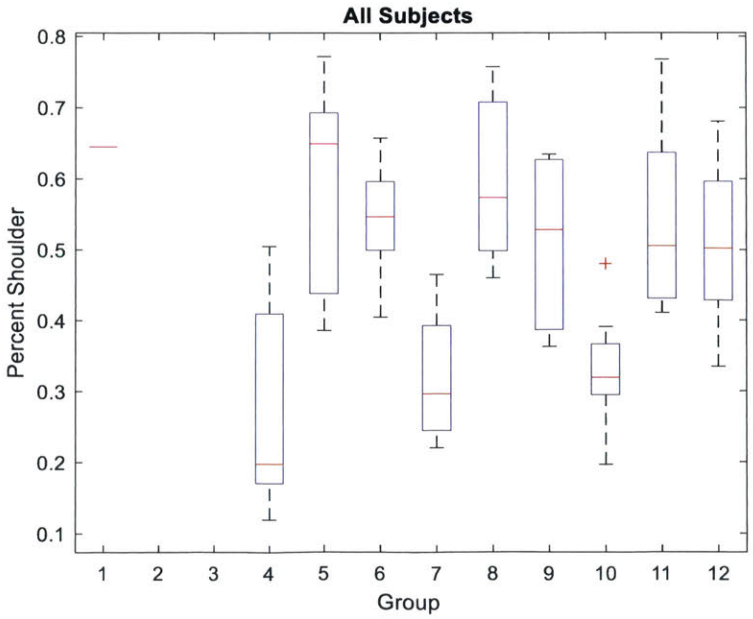

Figure 21: Percent Shoulder, All Subjects

Table 6: Mean and standard deviations of both the external force plate GRFs and the fraction of the total suit weight supported at the shoulder straps. The percentage of suit weight that is transferred to the operator through the shoulder straps is calculated and presented as mean percent shoulder and the lower and upper bounds on the 95% confidence interval. (mean [lower bound, upper bound]).

				Subject							
				1		2		3		4	
				Mean (lbs)	SD (lbs)	Mean (lbs)	SD (lbs)	Mean (lbs)	SD (lbs)	Mean (lbs)	SD (lbs)
Double Stance	Unsuited		External Force Plates	183.3	0.26	157.5	0.16	177.4	0.37	195.2	0.88
	Suited	Configuration 0	External Force Plates	321.4	0.42	293.5	0.85	315.1	1.38	328.9	1.20
			Shoulder Straps	-	-	66.5	6.72	22.5	7.14	27.4	6.98
			Percent Shoulder	-		49.0% [40.0%, 58.0%]		16.3% [13.0%, 19.6%]		20.4% [16.6%, 24.1%]	
		Configuration 1	External Force Plates	-	-	294.6	0.83	317.1	1.41	330.4	1.68
			Shoulder Straps	-	-	56.5	6.52	35.3	7.05	-	-
			Percent Shoulder	-		40.9% [35.7%, 46.1%]		25.8% [21.9%, 29.7%]		-	
		Configuration 2	External Force Plates	-	-	295.2	0.89	320.2	1.20	330.3	1.63
			Shoulder Straps	-	-	41.1	7.70	50.5	7.60	-	-
			Percent Shoulder	-		30% [22.1%, 37.8%]		35.4% [28.3%, 42.5%]		-	
Single Stance Left	Unsuited		External Force Plates	182.6	1.30	156.5	1.94	176.9	3.26	194.8	3.35
	Suited	Configuration 0	External Force Plates	319.0	3.67	289.8	3.45	311.3467259	4.1	326.7	3.99
			Shoulder Straps	-	-	95.0	9.42	88.3	5.83	55.7	5.44
			Percent Shoulder	-		70.7% [64.5%, 77.0%]		65.7% [62.2%, 69.3%]		42.3% [40.1%, 44.5%]	
		Configuration 1	External Force Plates	-	-	291.7	3.60	312.4	4.60	327.5	4.72
			Shoulder Straps	-	-	67.6	3.77	92.9	5.46	-	-
			Percent Shoulder	-		49.1% [47.0%, 51.2%]		70.4% [65.6%, 75.2%]		-	
		Configuration 2	External Force Plates	-	-	291.3	3.72	315.1	5.47	328.2	5.05
			Shoulder Straps	-	-	58.9	3.20	89.9	8.26	-	-
			Percent Shoulder	-		43.5% [41.6%, 45.4%]		64.4% [57.0%, 71.9%]		-	
Single Stance Right	Unsuited		External Force Plates	182.7	1.25	156.6	1.77	176.2	5.26	194.2	1.82
	Suited	Configuration 0	External Force Plates	319.1	2.90	289.8	3.78	311.0	3.84	326.6	3.17
			Shoulder Straps	-	-	73.7	5.93	81.2	7.58	60.1	4.02
			Percent Shoulder	-		56.5% [52.2%, 60.9%]		60.2% [55.8%, 64.7%]		46.1% [41.4%, 50.8%]	
		Configuration 1	External Force Plates	-	-	291.4	3.25	312.5	4.83	327.6	4.94
			Shoulder Straps	-	-	55.5	7.81	83.8	9.13	-	-
			Percent Shoulder	-		40.3% [35.8%, 44.8%]		62.0% [59.8%, 64.2%]		-	
		Configuration 2	External Force Plates	-	-	291.2	3.98	315.2	4.52	328.3	4.24
			Shoulder Straps	-	-	55.3	9.20	84.9	6.39	-	-
			Percent Shoulder	-		42.3% [34.3%, 50.2%]		59.0% [51.9%, 66.1%]		-	

5.2.2 Postural Stability

Hypothesis [3], interrogating changes in postural stability, was analyzed with four separate dependent variables: variance in COP_x (Figure 22), variance in COP_y (Figure 23), variance in VGRF (Figure 24), and Time (Figure 25). The boxplot results of each dependent variable and subject are presented in the Appendix C.

COP_x: When pooling all subjects, the variance in COP_x showed no significant difference between SSL and SSR for any Configuration. DS is different from SSL and SSR for all configurations. In DS, the variance in COP_x is greater in the Suited Configuration than Unsuited

(Z=-2.37, p=0.0179, Z=-3.55, p<0.005, Z=-2.94, p<0.005 for Configuration 1, 2, and 3 as compared to Configuration 0, respectively). For both SSL and SSR, there is no effect of Configuration.

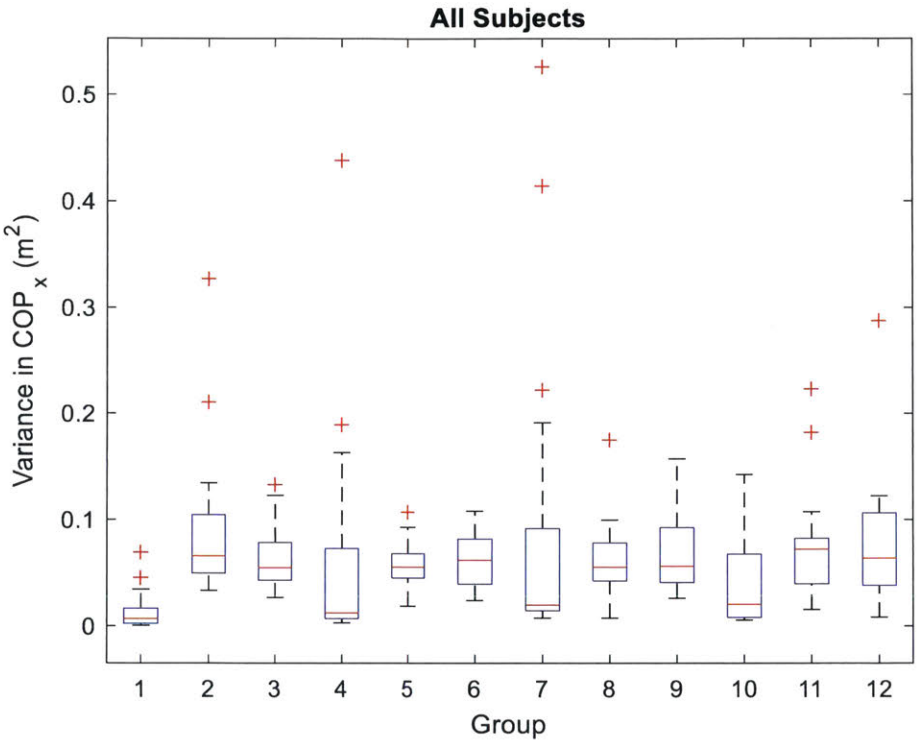

Figure 22: Variance in Center of Pressure in X, All Subjects

COP_y: When pooling all subjects, the median variance in COP_y was lower in SSR than SSL, but was only significantly lower in Configuration 2 (Z=2.00, p=0.0452). In DS, the variance in COP_y is greater when Suited than Unsuited (Z=-2.72, p<0.005, Z=-3.22, p<0.005, Z=-2.72, p=0.006 for Configuration 1, 2, and 3 as compared to Configuration 0, respectively). For both SSL and SSR, there is no effect of Configuration.

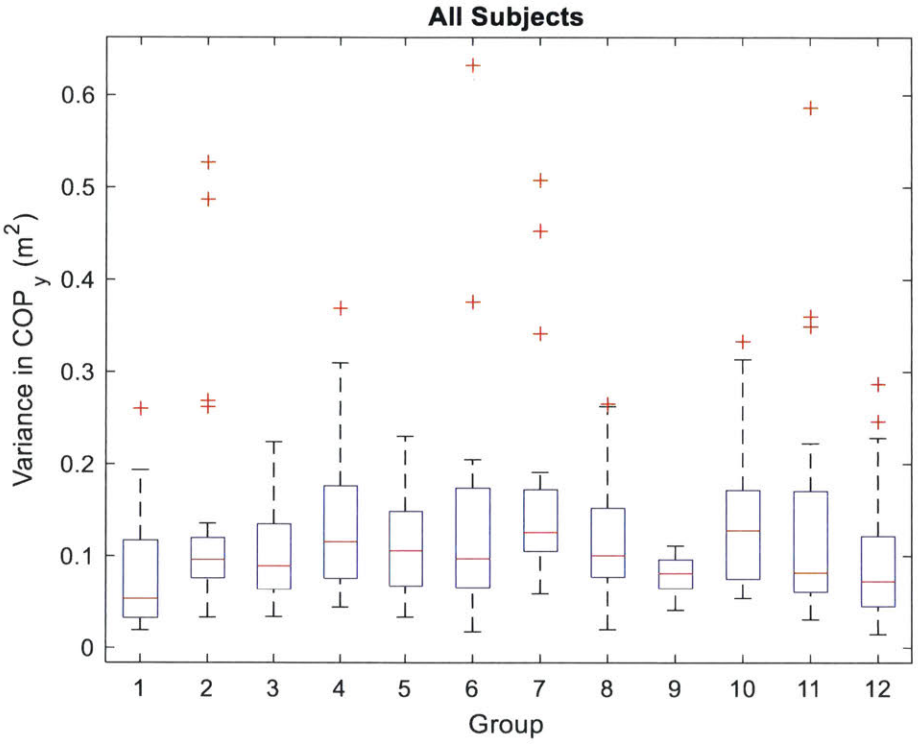

Figure 23: Variance in Center of Pressure in Y, All Subjects

Variance in VGRF: When comparing the variance in VGRF for groups across all subjects, using Post-hoc Wilcoxon rank sum tests, SSL/SSR is statistically larger than DS, but there are no differences in SSL and SSR ($Z=1.23$, $p=0.217$, $Z=1.68$, $p=0.0929$, $Z=0.541$, $p=0.589$, $Z=0.0791$, $p=0.937$ for Configurations 0, 1, 2, and 3, respectively). When comparing DS, Suited variance was greater than Unsuited ($Z=-4.64$, $p<0.005$, $Z=-4.86$, $p<0.005$, $Z=-5.09$, $p=<0.005$ for Configuration 1, 2, and 3 as compared to Configuration 0, respectively). When comparing SSL/SSR, Suited variance was also greater than Unsuited. When comparing Suited Configurations for single stance (SSL/SSR), the two indexed Configurations (2 and 3) both had greater variance than Configuration 1, except for SSL between Configuration 1 and 3 ($Z=-1.13$, $p=0.258$). In DS, there was no effect of indexing.

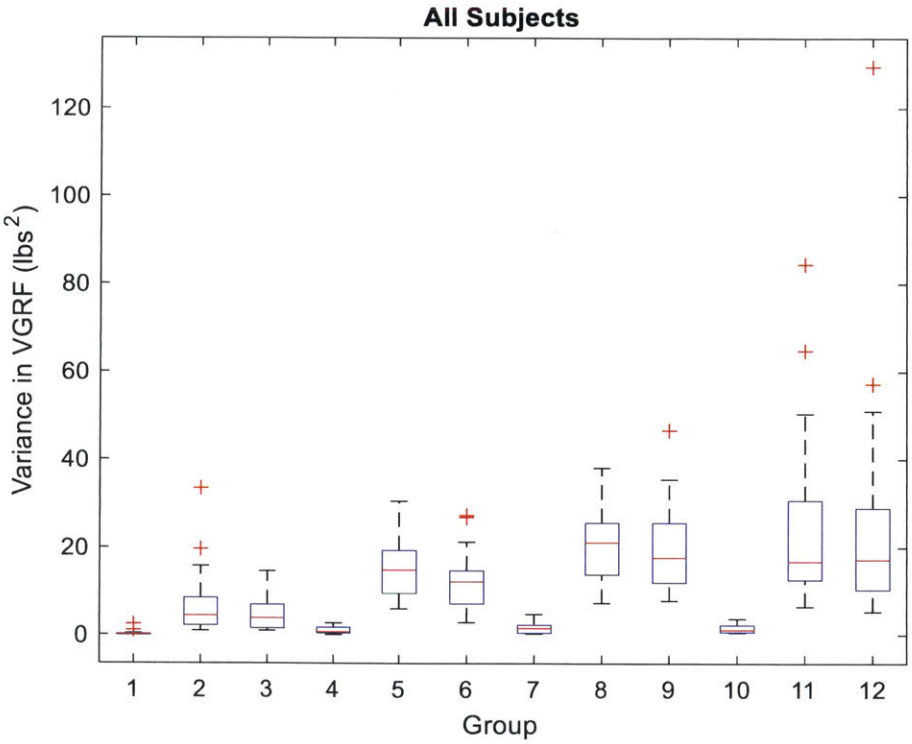

Figure 24: Variance in VGRF, All Subjects

Time: When comparing the time of the trials, DS was different from SSL/SSR. Comparisons between DS were not considered because full-length DS trials were achieved in every configuration, as expected. For single stance, within each Configuration, SSL and SSR are not statistically different (Z=0.825, p=0.410, Z=-0.526, p=0.599, Z=-0.819, p=0.413, Z=0.902, p=0.367 for Configurations 0, 1, 2, and 3, respectively). When Suited and performing SSL, there is no difference in indexing configuration (1, 2, and 3). However, when Suited and performing SSR, Configuration 3 is significantly smaller than Configuration 1 (Z=2.22, p=0.0262) and 2 (Z=2.39, p=0.0169), which are not different from each other (Z=0.216, p=0.829).

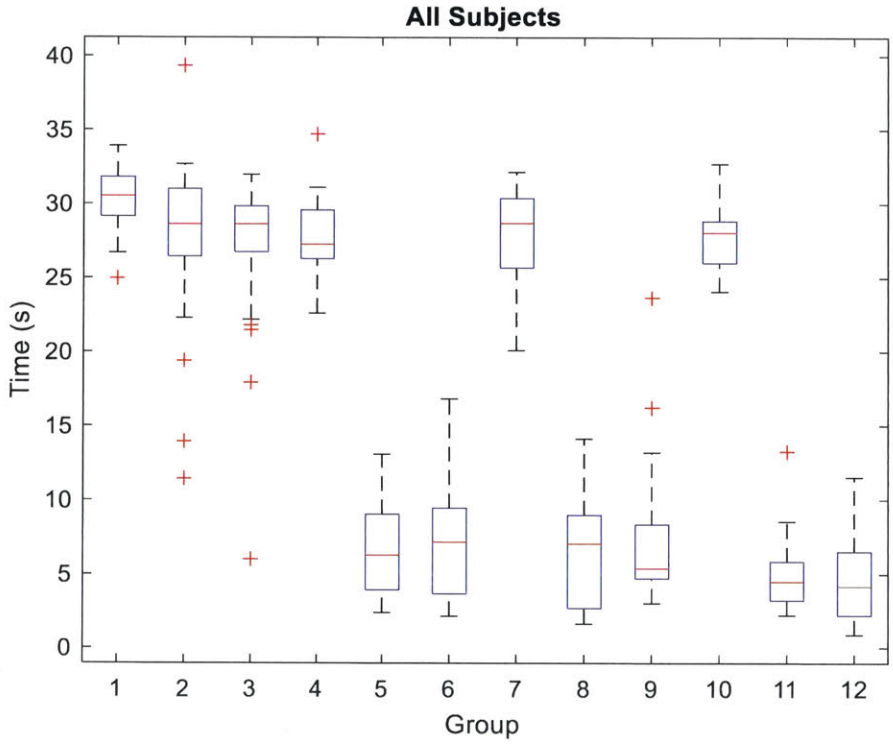

Figure 25: Time, All Subjects

5.3 Discussion

This study aimed to interrogate the distribution of suit weight and the effects of indexing configuration on postural stability. The loading on the shoulder straps were measured to understand the weight distribution across indexing configuration. Additionally, an analysis was performed to understand how that distributed weight of the suit effects postural stability. Specifically, I hypothesized that **[1]** the MkIII SSA self-supports part of its own weight, which increases in DS as compared to single stance; **[2]** operators lose postural stability when suited as compared to unsuited and when they become more tightly-coupled with the suit.

5.3.1 Suit Weight Distribution

The weight of the suit can first be broken into two components: the weight transferred to the operator and the self-supported weight. The weight transferred to the operator can be split into two components as well: the weight that is transferred through the designed interaction locations

(which, in the case of the MkIII SSA, are shoulder straps) and the weight transferred through other non-designed locations (such as the operator's arm contacting the inside of the suit).

Since the in-sole sensor data was non-usable, I was unable to measure the self-support percentage directly, but I could measure the loading on the designed loading location, the shoulder straps (Table 6). In all trials, the force applied to the shoulder straps was lower than the total suit weight; therefore, not all of the suit weight was being directly applied to the shoulder straps. If it is assumed that there is a small percentage of the suit weight transferred to the operator through interaction locations, besides the shoulder straps, then the remainder of the suit weight is self-supported. This is a reasonable assumption since the tasks were both static tasks and the suit does not have any other location with expected significant vertical forces.

Therefore, since the percent of the suit weight transferred to the operator through the shoulder straps increases during single stance (both SSL/SSR) as compared to DS stance, then it can be inferred that self-support decreases. Hypothesis [1] is supported: the MkIII does self-support and it decreases during SSL/SSR as compared to DS. In SSL/SSR, the suit has only one column of support (pressurized leg soft-goods) versus two; therefore buckling under less force, and driving the operator to carry a larger load at their shoulders.

5.3.2 Postural Stability

Postural stability was estimated with the variance in both x and y position of the center of pressure (COP), the variance in the vertical ground reaction force (F_z, or VGRF), and the length of time of each trial. Variance in COP_x and COP_y both show that stability decreases in SSL/SSR as compared to DS, but there was no clear difference in indexing detected by either variable. However, the literature predicted that variance in VGRF has an improved sensitivity, over variance

in COP, to detect small differences in stability from changes in Configuration during static standing tasks.[25,32,54]

The variance in VGRFs also increases when suited as compared to unsuited (Configuration 0 vs Configurations 1, 2, 3). In addition, for all tasks, Configuration 1 is statistically smaller than Configuration 2 and 3. However, Configuration 2 and 3 are not statistically different for DS, SSL, or SSR. Therefore, variance in VGRF supports a decrease in stability with indexing, but that decrease is not linear since Configurations 2 and 3 are not different.

The length of time of each trial also confirms that stability decreased in the suited compared to the unsuited Configuration. In double stance, there is sufficient support to maintain stability throughout a trial, regardless of indexing. However, in single stance, increased indexing leads to a decrease in the mean trial time for right stance. Thus, the time for SSR shows that the most indexed configuration leads to the most unstable posture. When combining the results from Variance in VGRF and time, there is mixed support for the hypothesis that increased indexing results in decreased postural stability. The indexing was only located at the hips; therefore, at all levels of indexing, operators maintain the same ability to make postural corrections at the ankle. If indexing was located at the hip and ankle, there may be more of an effect on postural stability.

It would be expected that the increased indexing would increase coupling between the human and suit. Increased human-SSA coupling restricts the operator's motion to remain within the motion envelope of the suit. Therefore, when operating the suit, any perturbation in the human-SSA system center of mass (COM) must be corrected by programmed motions. In contrast, when the subject is less indexed their motion envelope is less coupled with the suit, permitting small postural adjustments within the suit.

5.3.3 Limitations and Future Work

The Novel pressure sensors were highly variable and were prone to giving time-out errors because of bending in the sensors near the edge where the sensors contacted the LCVG boots. A more robust in-sole sensor system would have allowed for a direct measuring of self-support percentage.

The load cells were only collecting data at 10 frames per second because of limitations in the mobile data acquisitions system. Since the system necessitated portability, the sampling rate capability was sacrificed. A more capable data acquisition system would provide higher frame rates, and could allow a comparison between the variance in VGRF and the variance in PS, which I would expect to be correlated since the component of VGRF attributed to suit weight is transferred to the operator at the shoulder straps.

Increasing the number of trials for each subject would have increased statistical power and could have enabled more sensitivity to changes in indexing. However, it is unclear when a difference in postural stability is operationally relevant. A follow-on analysis that would be beneficial would be an understanding the effects of the external loads that human operators experience when wearing a spacesuit in different configurations and tasks. Specifically, it would be interesting to see the effects of shoulder strap loading on spinal curvature, spinal loading, and erector muscle activations. Additionally, it would be interesting to conduct the study again with highly trained users to see how their strategies for operating the suit change dependent measures. Finally, future work should extend the analysis capabilities from finding differences to translating those differences to operational consequences.

5.3.4 Conclusion

The load decomposition and stability analysis performed here provide a deeper understanding of the complex human-SSA interactions, with respect to the distributed loading.

Specifically, I showed that **[1]** the MkIII SSA self-supports part of its own weight, which is greater in DS than in SSL/SSR; **[2]** showed mixed support that operators lose postural stability when suited as compared to unsuited and when they become more tightly-coupled with the suit.

Based on improved understanding of the human-SSA interactions, it would be beneficial to design future suits with variable indexing, such as inflatable bladders so that operators could alter their level of coupling with the suit in different scenarios to continually optimize their postural stability when operating the suit. For example, it may be beneficial to have tightly-coupled boots/feet, but less coupling at the hip. Adaptable indexing may allow subjects of varying control strategies and anthropometrics to find a more optimal level of coupling in different phases. For example, in static stance, the coupling should be decreased to improve stability. However, in ambulation, the coupling should be increased to minimize relative motion (associated with overcoming larger inertial components) between the suit and operator.

When considering stability in an SSA compared to unsuited, consider two extreme cases. The first case would be an un-coupled case where there is sufficient space between the inside of the suit and the human (consider a bubble or ball shaped suit). In this case, the operator maintains all of the stability they had when unsuited, but would lose the ability to complete any planetary tasks such as picking up a rock. However, now consider a completely-coupled case, where the operator cannot move unless the suit moves. In this case the mobility of the operator will be restricted, matching human and SSA DOFs and motion envelopes. Restricting the operator mobility, results in a decrement in stability for the current suit architecture. Suits should be designed to consider an optimization in coupling to allow the tightly-coupled human suit system to achieve planetary mission tasks, while minimizing the effort to maintain stability for a reduction in injury potential. Additionally, it would be beneficial for future planetary exploration suits to

actively adjust self-support dynamically. In the current configuration, the weight transferred to the human at the shoulder straps can vary depending on task.

6. Conclusions

6.1 Kinematic Comparisons

The torque required to rotate the Hip Brief Assembly (HBA) upper and mid bearings (Figure 1) was characterized in Chapter 2.1.1. Coupling these data with measured kinematics lead to an improved understanding of the underlying programmed motions to provide future design guidelines for wearable systems. In this thesis, I presented the results of a pilot study of locomotion while Unsuited and Suited with the MkIII SSA. The study described, aimed to integrate underlying suit component characteristics with the emergent biomechanics of the operator to investigate how an operator's biomechanics are affected by the MkIII, specifically how the HBA architecture effects hip motion. These data are relevant for improving future SSA architectures through design requirements development and evaluation methods.

I hypothesized that [1] the MkIII HBA architecture has DOF limitations that restrict operator mobility and agility. The limitations manifest in effects to both static and dynamic (WF and WB) gait parameters. [2] Based on subjective feedback from experienced suit testers, the waist bearing provides rotational motion in the transverse plane during ambulation, partially alleviating mobility restrictions introduced by the HBA. [3] Although the HBA volume does not change during hip joint motion, there is still a resistive speed-dependent torque associated with the spinning bearings. Those torques further diminish the mobility and agility of the operator.

I showed that [1] the MkIII HBA architecture has DOF limitations that restrict operator mobility and agility. The limitations manifest in effects to both static and dynamic (WF and WB) gait parameters. [2] The waist bearing provides rotational motion in the transverse plane during ambulation, partially alleviating mobility restrictions introduced by the HBA. [3] Although the HBA volume does not change during hip joint motion, there is still a resistive speed-dependent

torque associated with the spinning bearings. Those torques further diminish the mobility and agility of the operator, requiring increased hip joint torques along the limited rotational DOFs and reducing ground clearance.

The results of this study are beneficial in informing and evaluating future SSA design requirements, as well as those for other wearable systems. For example, the results of Hypothesis [1], showed altered gait because of the SSA architecture. Design requirements on certain static and dynamic gait parameters (e.g., step length or dynamic base) could be created to inform maximum allowable percent deviations from nominal kinematics. For example, a requirement could be imposed that the dynamic base must permit a certain tolerance from the Unsuited mean. Requirements can also be generated for specific suit components, such as the HBA bearings or waist bearings, requiring a minimum performance, or a maximum allowable added torque for relevant angular velocities. Future studies can also inform design requirements based on energy expenditure differences between the Unsuited and Suited condition, supplementing the biomechanical analyses with metabolic analyses.

6.2 Decomposition of Required Hip Torque into Contributing Components

The results of the kinematics analysis showed a reduction in performance when suited, pointing to both a DOF/ROM discrepancy as well as inherent resistances within the SSA that require the operator to input additional joint torques. However, both the kinematics modeling and experimental analysis is inadequate in determining the specific SSA components contributing to the required torques. A dynamics model was developed and implemented to look at hip flexion and extension associated with ambulation.

I implemented a dynamic Rigid-Body Space Suit Assembly (SSA) Model (Chapter 2.2), leveraging SolidWorks and a built-in Motion Analysis (MA) tool. The MA model was used to

decompose the required HBA joint torques that an operator must overcome to achieve flexion and extension of their hip. The decomposition permits the evaluation of the critical contributors (mass/inertia and bearing resistances) to the required torques.

Validated models allow engineers to predict human-suit interactions before a prototype is manufactured. The predictions can be used to make design changes prior to fabrication, which can reduce costs. The dynamics model is also useful for supplementing experimental suit analyses and can allow for more operationally relevant analyses than are possible experimentally. The model used here enabled a decomposition of the underlying torque profiles, showing that the main contributor is the mass distribution. The dynamics model could accurately reproduce hysteretic behavior seen in suit joints as well as perform sensitivity analyses that provide unique insight into the human-suit interactions.

Future suit evaluations should consider operationally relevant scenarios or couple computational modeling to explore the design space further. The exosuit designs should strategically minimize weight, and optimize the bearing placement through modeling. The human-suit system is a complex interactive relationship. The operator adds energy to the suit, and therefore the suit moves. However, when the operator is no longer adding energy to the suit, it continues to move, only slowing from inherent resistances such as those of the bearings. Unfortunately, if operators want to move in another direction, they have to overcome the energy that they previously put into the system while simultaneously overcoming the inherent resistance again. Minimizing mass will reduce this effect. However, the suit can be implemented such that the mass can help the operator, which is probably why experienced operators emerge after optimizing their interaction with the suit over many hours of training. The present analysis highlights that the suit can be improved through a strategic reorganization of the bearings for accommodation of natural

biomechanics and a reduction in mass. These design changes may lead to a reduction in learning and adaptation time and possibly injury reduction. The model can also be used to examine programmed motion strategies to inform operators. Leveraging the outputs, operators may be able to efficiently manipulate the suit in difficult operational environments or orientations.

6.3 Effects of Suit Weight and Suit Fit on Operator Performance

Most of the control necessary to maintain a postural stability are fine motor controls to make small changes in body position and to dampen vertical oscillations.[35] However, those small motions take advantage of the many extra DOFs that the SSA does not have. In Chapter 5, I show mixed support for the hypothesis that increased indexing decreases postural stability. Specifically, I showed that the reduction in postural stability was evident in VGRF and time, but was not a linear relationship for either dependent measure. Indexing at the ankle along with indexing at the hip may magnify the effect of indexing such that differences in configuration can be detected by the dependent measures investigated.

When indexing is lower, the human operator is able to continue to make small motions inside of the suit, within the open space between themselves and the inner surface of the suit. Although, once indexing is increased, there is no longer any open space and any small movement take the suit and all its weight along for the ride. The corrective actions become limited, as they must conform to the motions the suit can make. Essentially, increased coupling between the human-SSA system does not provide the operator with improved postural stability. Increased coupling can be harmful to postural stability as it drives operator motions into the motion envelope of the suit and resulting in a need for more programmed motions.

It can make more sense to have reduced coupling to operate a suit more efficiently, especially when completing static tasks. However, as coupling continues to decrease, it would be

expected that eventually control of the suit would become impossible, as a lack of interactions would occur. At one extreme, no coupling would essentially be a spacecraft, where the operator can freely move around inside the architecture. At the other extreme, a completely-coupled suit would essentially be skin. However, if skin had DOF and ROM limitations, it would be quite detrimental to the operator. Therefore, based on the analysis, tightly-coupled wearables with unmatched motion envelopes from their operators have a region of optimal coupling that allows acceptable performance. In that region, the operator would have enough interaction with the suit to facilitate forcing the suit to achieve mission tasks, but not so many interactions that they lose the required mobility to achieve mission tasks. Additionally, it would be beneficial to adjust indexing at the hip and ankle simultaneously to optimize overall performance. Human operators can learn to adapt to a given SSA that they are operating, but engineers have the ability improve the human-SSA system from the beginning by leveraging existing tools and data.

6.4 Contributions

The analyses completed as part of this thesis have answered existing research gaps in the field of human-SSA systems. Specifically, the resulting contributions are as follows:

1. Developed high-fidelity SolidWorks model of the Mark III (MkIII) Planetary Technology Demonstrator, including matched kinematics.
2. Showed that the MkIII HBA architecture has DOF limitations that restrict operator mobility and agility. The waist bearing provides rotational motion in the transverse plane during ambulation, partially alleviating mobility restrictions introduced by the HBA. Although the HBA volume does not change during hip joint motion, there is still a resistive speed-dependent torque associated with the spinning bearings.

3. Showed that the required torques further diminish the mobility and agility of the operator, requiring increased hip joint torques along the limited rotational DOFs.
4. Showed that the SSA reduced ground clearance. A reduction in ground clearance could lead to increased chances of trips or falls and inhibit planetary exploration capabilities by reducing the acceptable suitable terrain conditions.
5. Measured the speed dependent bearing resistances of the integrated HBA bearings. The result can be used to set tolerances, guide proper orientations, provide lifetime analyses, and improve computational models of bearings in SSAs. The bearing torque required generally increases with speed. Operators should consider agility, not simply mobility. The faster an operator drives the suit, the more resistance they will incur from bearings alone. Inertial effects increase with speed as well. There is a difference in bearing resistance for each bearing. Setting tolerances for contractors to require similar performance in each rotation sense can minimize injury risk and asymmetries in motion. Additionally, for a given speed and direction, the required torque varies and the regions where the required torque is above the mean torque, and are consistent across trial, representing "sticking points."
6. Developed a Dynamic Rigid-Body MkIII SSA Model, leveraging SolidWorks and a built-in Motion Analysis (MA) tool. The MA model was used to decompose the required HBA joint torques that an operator must overcome to achieve flexion and extension of their hip. The decomposition permits the evaluation of the critical contributors (mass/inertia and bearing resistances) to the required torques. A human operator, attempting to manipulate the suit efficiently, could move at the same rate as the suit, and avoid incurring additional

torques. The operator can allow the bearing torques to act against the mass/inertial torques, directly on the SSA components alone and slow the suit motion.

7. Showed that the dynamic model appropriately captures the hysteretic behavior of torque vs. angle plots. The dynamics model approach enabled examining the physics causing the hysteresis, which was shown to stem from a phase shift between the applied force and the motion of the system.
8. Showed that when gravity is axially applied, the flexion and extension angles both increase while the gravity level decreases. The increase in hip flexion and extension angles are due to a greater dependence on suit mass with axially applied gravity. In that direction, the externally applied force must lift the leg in both directions. When gravity is transversely applied, the externally applied force only has to push the inertial components of the suit mass along a supported surface and not fight the weight of the limb as well. This is confirmed when comparing mean flexion and extension angles between the transversely applied gravity cases and the axially applied gravity cases.
9. Showed that the MkIII partially self-supports its own weight, and that amount of self-support changes as task changes. This is useful in setting suit requirements for self-support, especially in passive architectures where any weight that is not self-supported is directly applied to the operator.
10. Measured changes in postural stability associated with wearing the MkIII in comparison to the unsuited condition. Postural stability, as measured by the variance in vertical ground reaction force and length of trial (time) showed a decrease in postural stability associated with wearing a suit, and mixed support for increased indexing.

6.5 Future Work

The modeling tool developed as part of this research will be useful in addressing additional questions. For example, the model can be used to determine the effects of suit fit or fleet sizing on the required joint torques. The geometric parts could be used in more advanced models that go beyond rigid-body representations such as a finite element analysis (FEA) model. In that scenario, the rigid-body components could be represented with the part geometries defined in chapter 2, while the soft-goods are allowed to deform as they would in an operational setting. Additionally, follow-on experiments could be performed to measure the difference in bearing resistances when experiencing and off-axis load, as they do operationally.

The load cell data obtained and analyzed in Chapter 5 can be implemented in musculoskeletal modeling to determine the differences in spinal loading and erector muscle activations between the unsuited and suited configurations. It would also be useful in determining the differences across task such as Double Stance, or Left/Right Single Stance.

Spacesuits provide life support for human operators while they explore other planets, but should also allow the operator to achieve mission tasks as effectively as possible. Experimental and modeling analyses should be used to set design requirements to drive optimizations for efficient human-SSA interactions.

Bibliography

1. Abe D, Yanagawa K, Niihata S. Effects of load carriage, load position, and walking speed on energy cost of walking. Appl Ergon [Internet]. 2004 Jul [cited 2016 Mar 22];35(4):329–35. Available from: http://www.sciencedirect.com/science/article/pii/S0003687004000572
2. Abramov I, Moiseyev N, Stoklitsky A. Concept of space suit enclosure for planetary exploration. SAE Conf [Internet]. 2001 [cited 2014 Mar 18]; Available from: http://spacecraft.ssl.umd.edu/design_lib/ICES01-2168.suit_enclosure.pdf
3. Anderson A. Understanding Human-Space Suit Interaction to Prevent Injury During Extravehicular Activity. Massachusetts Institute of Technology; 2014.
4. Anderson A, Hilbert A, Bertrand P, Mcfarland S, Newman DJ, Facility B, et al. In-Suit Sensor Systems for Characterizing Human-Space Suit Interaction. In: International Conference on Environmental Systems. 2014. p. 1–15.
5. Anderson A, Mengüç Y, Wood RJ, Newman DJ. Development of the polipo pressure sensing system for dynamic space-suited motion. IEEE Sensors [Internet]. [cited 2018 Apr 29]; Available from: http://ieeexplore.ieee.org/abstract/document/7132689/
6. Appell HJ. Muscular atrophy following immobilisation. A review. Sport Med. Adis International; 1990;10(1):42–58.
7. Atwell B, Boeder P, Ross A. Space Radiation Analysis for the Mark III Spacesuit. 2013 [cited 2014 Mar 18]; Available from: http://arc.aiaa.org/doi/pdf/10.2514/6.2013-3381
8. Blaya JA, Herr H. Adaptive control of a variable-impedance ankle-foot orthosis to assist drop-foot gait. IEEE Trans Neural Syst Rehabil Eng. IEEE; 2004;12(1):24–31.
9. Bleex EE, Zoss AB, Kazerooni H, Chu A. Biomechanical Design of the Berkeley Lower. 2006;11(2):128–38.
10. Carr CE, McGee J. The Apollo Number: space suits, self-support, and the walk-run transition. PLoS One [Internet]. Public Library of Science; 2009 Jan 12 [cited 2015 Dec 29];4(8):e6614. Available from: http://journals.plos.org/plosone/article?id=10.1371/journal.pone.0006614
11. Carr CE, Newman DJ. Space suit bioenergetics: framework and analysis of unsuited and suited activity. Aviat Space Environ Med [Internet]. 2007 Nov [cited 2015 Dec 29];78(11):1013–22. Available from: http://www.ncbi.nlm.nih.gov/pubmed/18018432
12. Carr CE, Newman DJ. Space Suit Bioenergetics: Framework and Analysis of Unsuited and Suited Activity. Aviat Space Environ Med. 2007 Nov;78(11):1013–22.
13. Cheng-Wu F, Hao-Shen Z, Ming-Qing C, Pang Y, Liu X, Guanghui X. Extravehicular Space Suit Bearing Technology Development Research. [cited 2018 Apr 29]; Available from: http://iopscience.iop.org/article/10.1088/1757-899X/187/1/012014/pdf
14. Cowley MS, Margerum S, Hharvill L, Rajulu S. Model for Predicting the Performance of Planetary Suit Hip Bearing Designs. 2012 Jul 21 [cited 2016 May 4]; Available from: http://ntrs.nasa.gov/search.jsp?R=20130000596
15. Cullinane CR, Rhodes RA, Stirling LA. Mobility and Agility During Locomotion in the Mark III Space Suit. Aerosp Med Hum Perform [Internet]. 2017 Jun 1 [cited 2017 Aug 2];88(6):589–96. Available from: http://www.ncbi.nlm.nih.gov/pubmed/28539149
16. Cullinane CR, Rhodes RA, Stirling LA. Hip Torque Decomposition with a Computational Mark III Space Suit Model [Submitted, In Review]. Comput Methods Biomech Biomed Engin.
17. Diaz A, Newman D. Musculoskeletal Human-Spacesuit Interaction Model. [cited 2018

Apr 14]; Available from: https://pdfs.semanticscholar.org/d5d1/628fabba60c1ab210b7d47263621b97ec373.pdf
18. Exell T, Kerwin D, Irwin G, Gittoes M. Calculating Centre of Pressure from Multiple Force PLates for Kinetic Analyses of Sprint Running. Biomech Sport Port J Sport Sci [Internet]. [cited 2018 Apr 12];29(11). Available from: https://ojs.ub.uni-konstanz.de/cpa/article/viewFile/4973/4615
19. Ferris DP, Czerniecki JM, Hannaford B. An ankle-foot orthosis powered by artificial pneumatic muscles. J Appl Biomech. NIH Public Access; 2005;21(2):189–97.
20. Gast MA, Moore SK. A glimpse from the inside of a space suit: What is it really like to train for an EVA? Acta Astronaut [Internet]. 2011 Jan [cited 2016 Feb 29];68(1–2):316–25. Available from: http://www.sciencedirect.com/science/article/pii/S0094576510003036
21. Geboers JF, Drost MR, Spaans F, Kuipers H, Seelen HA. Immediate and long-term effects of ankle-foot orthosis on muscle activity during walking: a randomized study of patients with unilateral foot drop. Arch Phys Med Rehabil. 2002;83(2):240–5.
22. Geboers JF, Van Tuijl JH, Seelen HA, Drost MR. Effect of immobilization on ankle dorsiflexion strength. Scand J Rehabil Med. 2000;32(2):66–71.
23. Gernhardt M, Jones J, Scheuring R, Abercromby F, Tuxhorn J, Norcross J. Risk of Compromised EVA Performance and Crew Health Due to Inadequate EVA Suit Systems. In: McMurphee J, Charles J, editors. Human Health and Performance Risks of Space Exploration Missions. NASA SSP-2009-3405; 2009.
24. Gernhardt ML, Jones JA, Scheuring RA, Abercromby AF, Tuxhorn JA, Norcross JR. Risk of Compromised EVA Performance and Crew Health Due to Inadequate EVA Suit Systems. Hum Res Progr. 2009;333–58.
25. Goldie PA, Bach TM, Evans OM. Force platform measures for evaluating postural control: reliability and validity. Arch Phys Med Rehabil [Internet]. 1989 Jul [cited 2018 Apr 11];70(7):510–7. Available from: http://www.ncbi.nlm.nih.gov/pubmed/2742465
26. Grasso R, Bianchi L, Lacquaniti F. Motor patterns for human gait: backward versus forward locomotion. J Neurophysiol [Internet]. 1998 [cited 2016 Mar 21];80(4):1868–85. Available from: http://jn.physiology.org/content/80/4/1868.short
27. Graziosi D, Ferl J, Splawn K. Evaluation of a Rear Entry System for an Advanced Spacesuit. Evaluation [Internet]. 2005 [cited 2014 Apr 1]; Available from: https://imageserv5.team-logic.com/mediaLibrary/93/Evaluation_of_a_Rear_Entry_System_for_an_Advanced_Spacesuit.pdf
28. Griffin B, Howard R, Rajulu S, Smitherman D. Creating a Lunar EVA Work Envelope. SAE Int J Aerosp [Internet]. 2009 [cited 2018 Apr 29]; Available from: http://papers.sae.org/2009-01-2569/
29. Guizzo E, Goldstein H. The rise of the body bots. Spectrum, IEEE. 2005;42(10):50–6.
30. Hesse S, Werner C, Matthias K, Stephen K, Berteanu M. Ankle-Foot Orthosis on Gait and Lower Limb Muscle Activity of Hemiparetic Subjects With an Equinovarus Deformity. Stroke. 1999;30:1855–61.
31. Hitt J, Oymagil AM, Sugar T, Hollander K, Boehler A, Fleeger J. Dynamically Controlled Ankle-Foot Orthosis (DCO) with Regenerative Kintetics: Incrementally Attaining User Portability. In: IEEE International Conference on Robotics and Automation. Roma, Italy; 2007. p. 10–4.
32. Hong C-Y, Guo L-Y, Song R, Nagurka ML, Sung J-L, Yen C-W. Assessing postural

stability via the correlation patterns of vertical ground reaction force components. Biomed Eng Online [Internet]. BioMed Central; 2016 Dec 2 [cited 2018 Apr 11];15(1):90. Available from: http://biomedical-engineering-online.biomedcentral.com/articles/10.1186/s12938-016-0212-z
33. Jaramillo MA, Angermiller BL, Morency RM, Rajululu SL. Refinement of Optimal Work Envelope for Extra-Vehicular Activity (EVA) Suit Operations. 2008 Sep 1 [cited 2018 Apr 29]; Available from: https://ntrs.nasa.gov/search.jsp?R=20080042401
34. Karlsson A, Frykberg G. Correlations between force plate measures for assessment of balance. Clin Biomech [Internet]. Elsevier; 2000 Jun 1 [cited 2018 Apr 11];15(5):365–9. Available from: http://linkinghub.elsevier.com/retrieve/pii/S0268003399000960
35. Karlsson A, Frykberg G. Correlations between force plate measures for assessment of balance. Clin Biomech (Bristol, Avon) [Internet]. 2000 Jun [cited 2018 Apr 11];15(5):365–9. Available from: http://www.ncbi.nlm.nih.gov/pubmed/10758298
36. Kawamoto H, Lee S, Kanbe S, Sankai Y. Power Assist Method for HAL-3 using EMG-based Feedback Controller *. In: IEEE International Conference on Systems, Man and Cybernetics. 2003. p. 1648–53.
37. LaFiandra M, Wagenaar RC, Holt KG, Obusek JP. How do load carriage and walking speed influence trunk coordination and stride parameters? J Biomech [Internet]. 2003 Jan [cited 2016 Mar 22];36(1):87–95. Available from: http://www.sciencedirect.com/science/article/pii/S0021929002002439
38. LaGoy AD, Johnson CD, Allison KF, Flanagan SD, Lovalekar MT, Nagai T, et al. Impact of Increased Load Carriage Magnitude on the Dynamic Postural Stability of Men and Women. 2018 Jan 10 [cited 2018 Apr 11]; Available from: http://d-scholarship.pitt.edu/33340/
39. Li J, Ye Q, Ding L, Liao Q. Modeling and dynamic simulation of astronaut's upper limb motions considering counter torques generated by the space suit Modeling and dynamic simulation of astronaut's upper limb motions considering counter torques generated by the space suit. Comput Methods Biomech Biomed Engin [Internet]. 2017 [cited 2018 Apr 14];20(9):929–40. Available from: http://www.tandfonline.com/action/journalInformation?journalCode=gcmb20
40. Matty J, Aitchison L. A method for and issues associated with the determination of space suit joint requirements. 2009 [cited 2018 Apr 29]; Available from: http://papers.sae.org/2009-01-2537/
41. Meyen F, Holschuh B, Kobrick R, Jacobs S, Newman D. Robotic Joint Torque Testing: A Critical Tool in the Development of Pressure Suit Mobility Elements. In: 41st International Conference on Environmental Systems [Internet]. Reston, Virigina: American Institute of Aeronautics and Astronautics; 2011 [cited 2018 Apr 29]. Available from: http://arc.aiaa.org/doi/10.2514/6.2011-5105
42. Mitchell K, Ross A, Blanco R, Wood A. Hazard Analysis for the Mark III Space Suit Assembly (SSA) Used in One-g Operations. 2012 [cited 2014 Mar 18]; Available from: http://ntrs.nasa.gov/search.jsp?R=20120017944
43. Morgan DA, Wilmington RP. Comparison of Extravehicular Mobility Unit (EMU) Suited and Unsuited Isolated Joint Strength Measurements. NASA/TP. 1996;(June).
44. Nelson AJ. The functional ambulation performance of elderly fallers and non-fallers walking at their preferred velocity. NeuroRehabilitation. 1999;13(3).
45. Newman D, Barratt M. Life Support and Performance Issues for Extravehicular Activity

(EVA). In: Churchill S, editor. Fundamentals of Space Life Sciences. Melbourne, FLorida: Krieger Publishing Co.; 1997.
46. Newman DJ, Schmid PB, Rahn D, Badler N, Metaxas D. Modeling the Extravehicular Mobility Unit (EMU) Space Suit : Physiological Implications for Extravehicular Activity (EVA). Soc Automot Eng Inc. 2000;(724).
47. Norcross J, Clowers K. Metabolic Costs and Biomechanics of Level Ambulation in a Planetary Suit. Tech Rep [Internet]. 2010 [cited 2014 Apr 1];NASA/TP-20. Available from: http://ston.jsc.nasa.gov/collections/trs/_techrep/TP-2010-216115.pdf
48. Opperman R a., Waldie JM a., Natapoff A, Newman DJ, Jones J a. Probability of Spacesuit-Induced Fingernail Trauma Is Associated with Hand Circumference. Aviat Space Environ Med [Internet]. 2010 Oct 1 [cited 2014 Mar 31];81(10):907–13. Available from: http://openurl.ingenta.com/content/xref?genre=article&issn=0095-6562&volume=81&issue=10&spage=907
49. Palmieri RM, Ingersoll CD, Stone MB, Krause BA. Center-of-Pressure Parameters Used in the Assessment of Postural Control. J Sport Rehabil [Internet]. 2002 [cited 2018 Apr 11];11:51–66. Available from: https://journals.humankinetics.com/doi/pdf/10.1123/jsr.11.1.51
50. Park Y-L, Chen B, Perez-Arancibia N, Young D, Stirling L, Wood R, et al. Design and control of a bio-inspired soft wearable robotic device for ankle-foot rehabilitation. Bioinspiration and Biomimetics. 2014;16007.
51. Park Y-L, Chen B, Young D, Stirling L, Wood RJ, Goldfield E, et al. Bio-inspired active soft orthotic device for ankle foot pathologies. In: 2011 IEEE/RSJ International Conference on Intelligent Robots and Systems [Internet]. IEEE; 2011 [cited 2018 Apr 10]. p. 4488–95. Available from: http://ieeexplore.ieee.org/document/6094933/
52. Parry D, Jr LC, Hanson D, Towle G. A study of techniques and equipment for the evaluation of extravehicular protective garments. 1966 [cited 2018 Apr 29]; Available from: http://www.dtic.mil/docs/citations/AD0635206
53. Powers CM. The influence of abnormal hip mechanics on knee injury: a biomechanical perspective. J Orthop Sports Phys Ther. 2010;40(2):42–51.
54. Prieto TE, Myklebust JB, Hoffmann RG, Lovett EG, Myklebust BM. Measures of Postural Steadiness: Differences Between Healthy Young and Elderly Adults. IEEE Trans Biomed Eng [Internet]. 1996 [cited 2018 Apr 12];43(9). Available from: https://pdfs.semanticscholar.org/0919/729b995eb61d231a40191a65e8a933ed3837.pdf
55. Reinhardt A, Magistad J. AX-5 space suit reliability model. 1990 [cited 2018 Apr 29]; Available from: http://papers.sae.org/901361/
56. Ross A, Rhodes R, Dover ILC. Z-2 Prototype Space Suit Development. 44th Int Conf Environ Syst. 2014;(July):1–11.
57. Scheuring R a., Mathers CH, Jones J a., Wear ML. Musculoskeletal Injuries and Minor Trauma in Space: Incidence and Injury Mechanisms in U.S. Astronauts. Aviat Space Environ Med [Internet]. 2009 Feb 1 [cited 2014 Mar 31];80(2):117–24. Available from: http://openurl.ingenta.com/content/xref?genre=article&issn=0095-6562&volume=80&issue=2&spage=117
58. Schmidt PB, Newman DJ, Hodgson E. Modeling Space Suit Mobility: Applications to Design and Operations. Int Conf Environ Syst [Internet]. 2001 Jul;(1). Available from: http://www.sae.org/technical/papers/2001-01-2162
59. Schmidt PB, Newman DJ, Hodgson E. Modeling Space Suit Mobility: Applications to

Design and Operations. [cited 2018 Apr 14]; Available from: http://spacecraft.ssl.umd.edu/design_lib/ICES01-2162.suit_mobility.pdf
60. Shorter KA, Wu AR, Kuo AD. The high cost of swing leg circumduction during human walking. Gait Posture [Internet]. 2017 [cited 2017 Aug 23];54:265–70. Available from: http://ac.els-cdn.com/S0966636217300942/1-s2.0-S0966636217300942-main.pdf?_tid=26108838-8856-11e7-a33e-00000aab0f26&acdnat=1503529104_4019715b95c12ae942d2630804e0a868
61. Strube EM, Sumner A, Kollock R, Games KE, Lackamp MA, Mizutani M, et al. The Effect of Military Load Carriage on Postural Sway, Forward Trunk Lean, and Pelvic Girdle Motion. Int J Exerc Sci [Internet]. Western Kentucky University; 2017 [cited 2018 Apr 11];10(1):25–36. Available from: http://www.ncbi.nlm.nih.gov/pubmed/28479946
62. Sutherland D. The development of mature gait. Gait Posture [Internet]. 1997 Oct [cited 2016 Mar 9];6(2):163–70. Available from: http://www.sciencedirect.com/science/article/pii/S0966636297000295
63. Thorstensson A. How is the normal locomotor program modified to produce backward walking? Exp Brain Res [Internet]. 1986 Feb [cited 2016 Mar 21];61(3):664–8. Available from: http://link.springer.com/10.1007/BF00237595
64. Valish D, Eversley K. Space Suit Joint Torque Measurement Method Validation. Int Conf Environ Syst. 2012;1–14.
65. Wade M. NASA Mark III [Internet]. Encyclopedia Astronautica. [cited 2015 Dec 13]. Available from: http://www.astronautix.com/craft/nasrkiii.htm
66. Walsh CJ, Endo K, Herr H. A Quasi-Passive Leg Exoskeleton for Load-Carrying Augmentation. Int J Humanoid Robot. 2007 Sep;4(3):487–506.
67. Wehner M, Quinlivan B, Aubin PM, Martinez-Villalpando E, Baumann M, Stirling L, et al. A lightweight soft exosuit for gait assistance. In: IEEE International Conference on Robotics and Automation (ICRA). 2013. p. 3362–9.
68. Whittle MW, Levine D. Three-dimensional relationships between the movements of the pelvis and lumbar spine during normal gait. Hum Mov Sci [Internet]. 1999 Oct [cited 2016 Mar 7];18(5):681–92. Available from: http://www.sciencedirect.com/science/article/pii/S0167945799000329
69. Yamamoto T, Smith CE, Suzuki Y, Kiyono K, Tanahashi T, Sakoda S, et al. Universal and individual characteristics of postural sway during quiet standing in healthy young adults. Physiol Rep [Internet]. Wiley-Blackwell; 2015 Mar [cited 2018 Apr 11];3(3). Available from: http://www.ncbi.nlm.nih.gov/pubmed/25780094
70. AMTI Force Platform Calculations [Internet]. [cited 2018 Apr 12]. Available from: http://health.uottawa.ca/biomech/courses/apa6903/amticalc.pdf

Appendix

A. Additional Bearing Analysis

A.1.1 One Additional Timepoint Analysis

The HBA bearing torque profiles were obtained using a dynamometer (Figure 26) at nominal suit pressure (4.3 psi) with the bearings *in situ*. The upper and mid hip bearings were each assessed individually by locking out the other. For each bearing, the suit was oriented to align the axis of rotation with the dynamometer while holding the bearing parallel to the ground (Figure 27). I developed the bearing test rig to allow the dynamometer to be directly connected to the bearing, while matching their axis of rotation, and without damaging either the suit or dynamometer.

The torques required to maintain constant rotation rates of 10, 20, and 30 deg/s were measured by the dynamometer attached to the bearing test rig for both the clockwise and counterclockwise sense. These angular velocities were chosen based on the assumed operational angular velocity of the hip motion during ambulation. Each trial is defined as 360 deg rotation. For a given speed, the bearing was rotated 3 times in one sense (CW), then the other (CCW). This was repeated, yielding 6 trials. For each set, the first trial includes a run-up region (Trials 1, 4) and the third trial includes a run-down region (Trials 3, 6).

The results show that the torque required increases with speed (Figure 28, Figure 29). The dashed black lines represent the average of the trials for a given bearing, speed, and direction. For a given speed and direction, the torque profiles oscillated, and the regions where the required torque is above average are consistent across trial, representing "sticking points". A least squares linear regression of trial set (2 sets of 3 rotations) and trial order (1st, 2nd, or 3rd rotation) were not significant ($p=0.172$ and $p=0.510$, respectively) which permits averaging across trials in the analysis.

Figure 26: Dynamometer (PrimusRSTM) by BTE

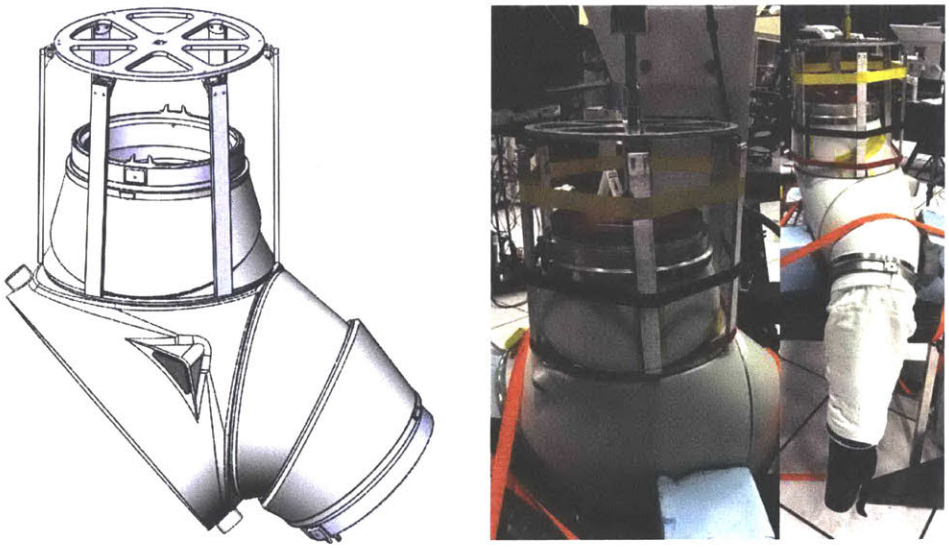

Figure 27: Bearing test rig and hip brief assembly (HBA) orientation (Left). Images of the experimental test setup (Right). In both the left and right images, the setup is shown for the proximal (upper) bearing. The suit was reoriented to accommodate the distal (mid) bearing after, while locking the upper bearing rotation. In the images on the right, the suit has one leg attached, while the other leg was replaced with a stopper. The waist bearing and upper body was replaced with another stopper that had a hosing attachment to pressurize the remaining components to nominal suit pressure.

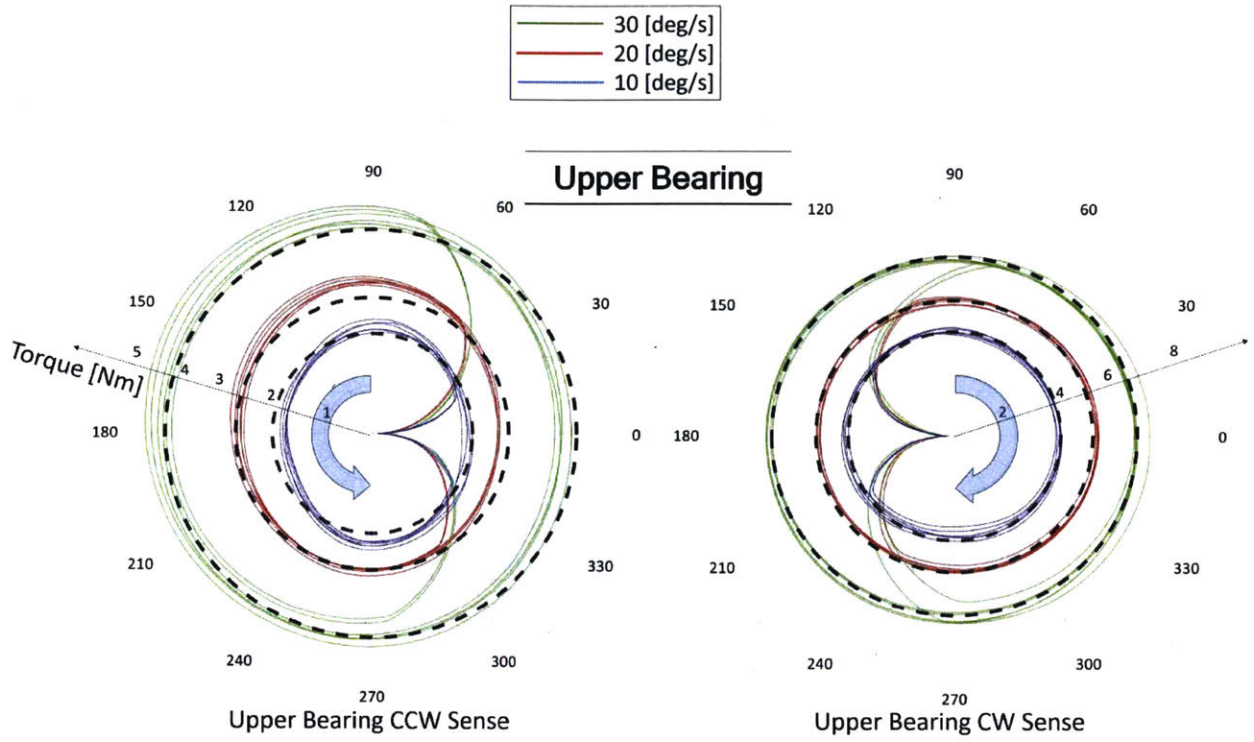

Figure 28: Upper Bearing Counter Clockwise (Left) and Clockwise (Left) Data Polar Plots

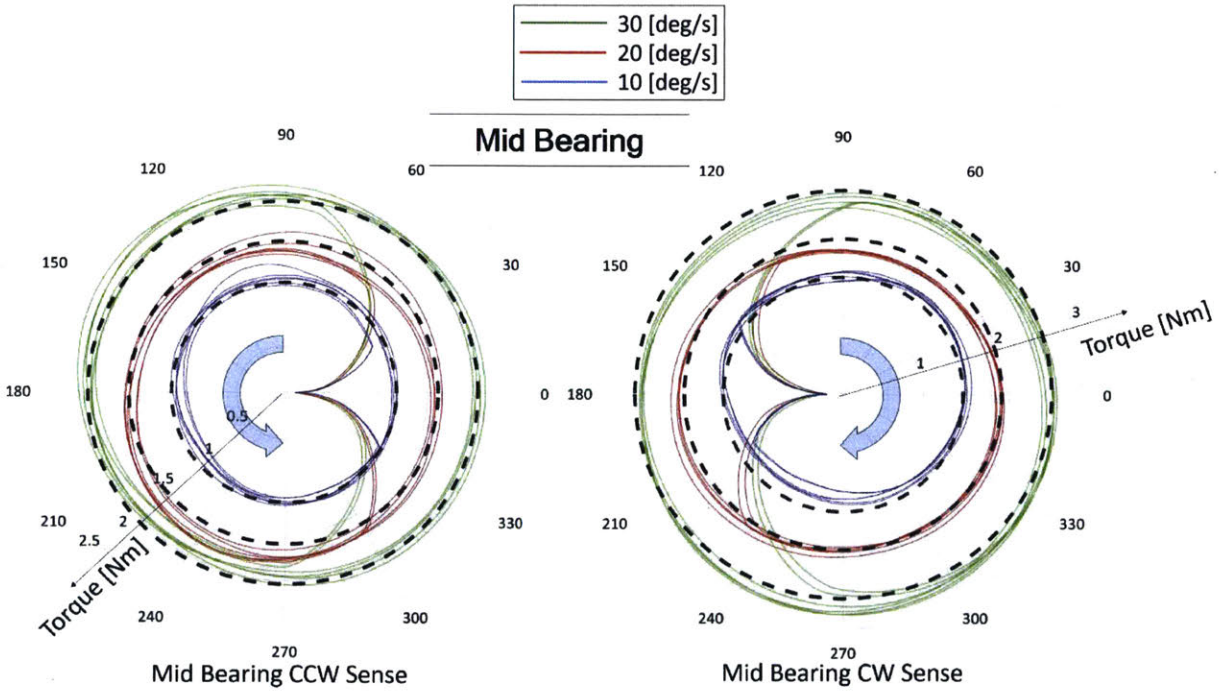

Figure 29: Mid Bearing Counter Clockwise (Left side) and Clockwise (Left side) Data Polar Plots

Table 7: Mean required torque averaged over trial.

Bearing	Rotation Sense	Speed [deg/s]	Mean Torque [Nm]	Standard Deviation [Nm]
Upper	CW	10	3.452	0.208
		20	4.541	0.209
		30	6.004	0.261
	CCW	10	2.072	0.239
		20	2.878	0.268
		30	4.296	0.358
Mid	CW	10	1.470	0.196
		20	1.963	0.191
		30	2.575	0.234
	CCW	10	1.155	0.170
		20	1.618	0.192
		30	2.015	0.214

A least squares linear regression of the averaged trials against speed and rotational sense yielded a statistically significant effect of speed ($p<0.0005$) and rotational sense ($p<0.0005$) within each bearing. For example, the upper bearing required torques of 3.45±0.21, and 2.07±0.24 Nm when rotated at 10 deg/s clockwise and counterclockwise respectively, which are significantly different for this and all other speeds (Table 7).

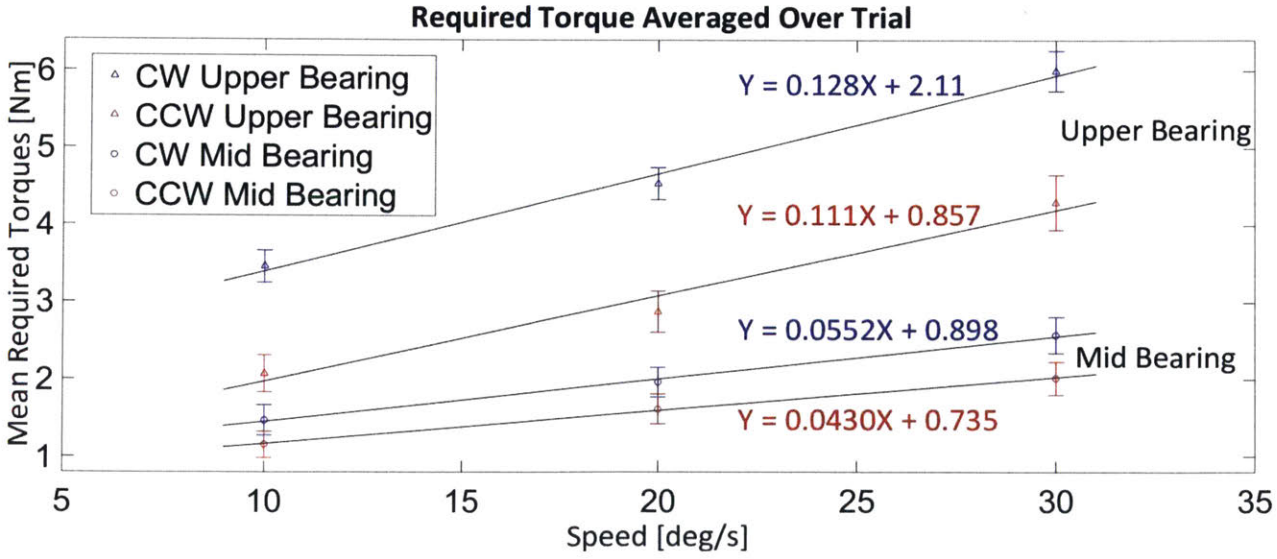

Figure 30: Mean required torque averaged over trial.

The significant effects of rotational sense and speed were greater for the upper bearing than for the lower bearing. The difference in the LS-means (mean after controlling for trial and trial order) for rotational sense (CW vs. CCW) are 1.52 and 0.368 Nm for the Upper and Mid bearings respectively. The difference in the LS-means for speed (20 vs. 30, 10 vs. 20) are 1.44, 0.948 and 0.505, 0.478 for the Upper and Mid bearings respectively. In Figure 8, the data is represented well by a linear fit (coefficient of determination, $R^2 \geq 0.975$). The slopes show the bearing damping coefficient ($\beta = 0.128, 0.112, 0.0552, 0.0430$ Nm/Deg/s), or the resistance to motion. The upper bearing is more resistive to motion ($\beta_U > \beta_M$).

While this original characterization of the angular velocities of the bearings would extended to 30 deg/s, the bearing angular velocities were measured during a suited gait study (Chapter 3) to reach over 150 deg/s during normal ambulation. To achieve an operationally relevant comparison, thc bearings were characterized again, to evaluate the required operator dynamics during nominal ambulation, but this time up to 180 deg/s, providing data below and above the normal operating range of the bearing during typical planetary tasks.

A.1.2 Auditory Signal Comparison

During the updated testing, the left distal bearing began to make a clicking noise. The suit technicians stated that this clicking has happened previously during suited operations. They have previously taken the bearing apart and found no evident cause for the clicking noise. To determine if whatever was causing the clicking had any effect on the bearing resistance, the range of angular velocities were performed again to compare the torques between when the bearing is making the clicking noise to when it is not.

The torques required when the bearing is making noise and when the bearing is not making noise are not different. Results show that the clicking was not changing the required torques and therefore, when hearing clicking during suited operations, the experiments can proceed as normal.

A.1.3 Pressurization Comparison

Another point of interest for the suit technicians and operators is the difference between pressurized and unpressurized performance. The left proximal bearing was evaluated again for the same ranges of angular velocities, in the unpressurized condition. When comparing the unpressurized to the pressurized condition, the unpressurized required less torque. Therefore, the suit team was informed that unpressurized operations were not completely capturing the needed effort to operate the bearings. This analysis confirmed predictions already in place by the suit team.

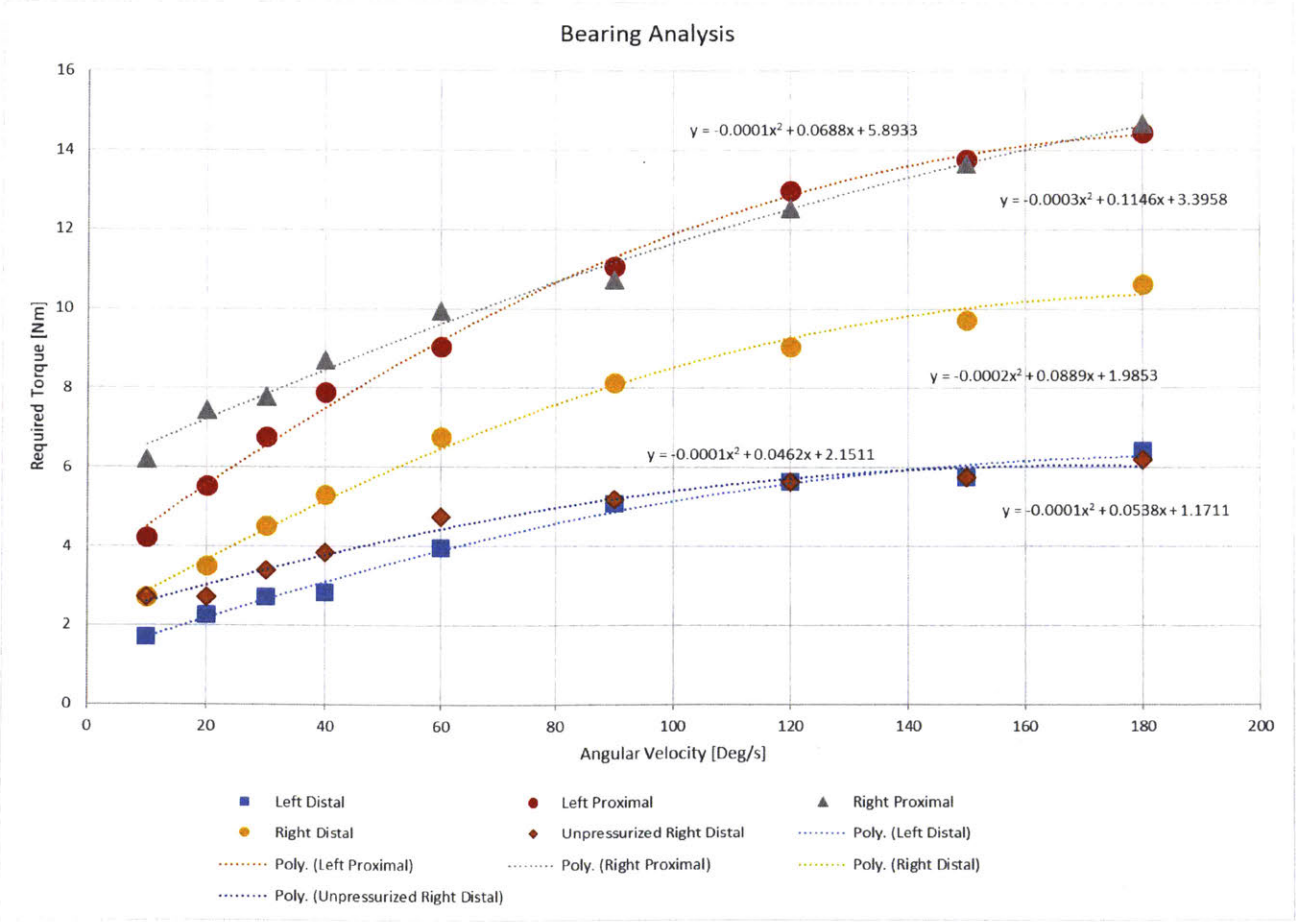

B. Within Subjects Percent Shoulder (PS) Comparisons

Subject 4 had limited data, so trends were not seen, but it adds to what we observe in Subjects 2, and 3. Subject 2 and Subject 3 had full data sets. Subject 2 showed a decrease in the load transferred to the shoulder as indexing or coupling increased. When in DS (Groups, 4, 7, and 10), PS trended down. Configuration 3 is significantly lower than Configuration 1 and 2 ($p<0.005$, $p=0.030$ respectively). However, Configuration 2 is not significantly different from Configuration 1 ($p=0.151$).

Furthermore, for Subject 2, PS was higher during SSL than during SSR for both Configurations 1 and 2. However, PS was not different between SSL and SSR for configuration 3. PS during SSR and DS is not different. Within SSL, PS in Configuration 2 and 3 were less than Configuration 1 ($p<0.005$), but Configurations 2 and 3 were not different ($p=0.2857$).

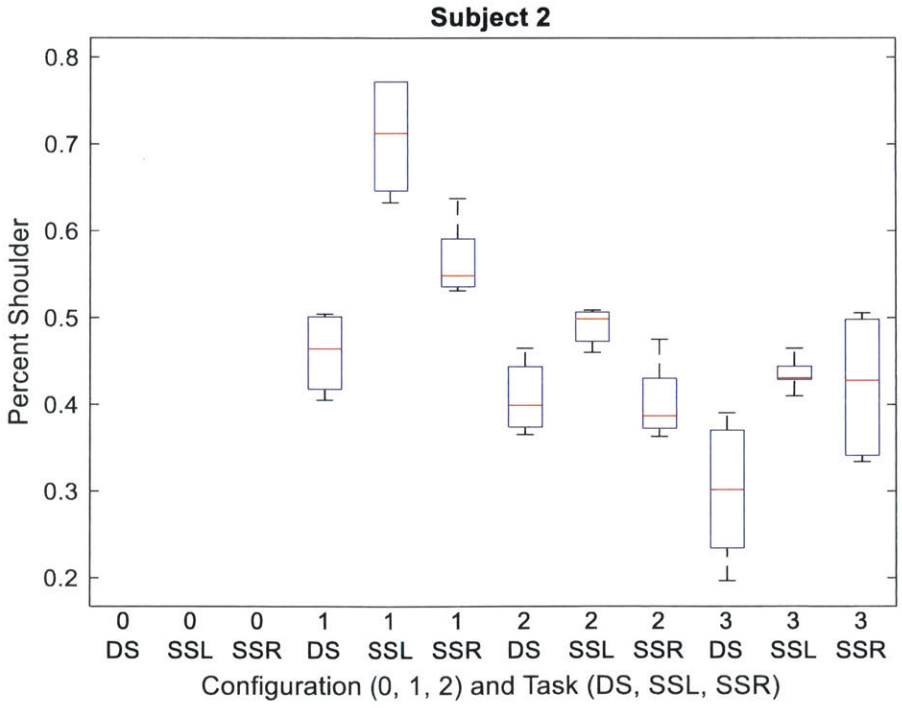

Figure 31: Percent Shoulder, Subject 2

Subject 3 showed an increase in the load transferred to the shoulder as indexing or coupling increased. When in DS (Groups, 4, 7, and 10), PS trended up. Configuration 3 is significantly higher than Configuration 1 and 2 ($p<0.005$, $p=0.009$ respectively). Additionally, Configuration 2 is greater than Configuration 1 ($p=0.151$).

Furthermore, for Subject 3, PS was greater during SSL than during SSR for both Configurations 1 ($p=0.041$) and 2 ($p<0.005$). However, PS was not different between SSL and SSR for configuration 3 ($p=0.24$). Within SSL, Configurations 1 and 2, 2 and 3, and 1 and 3 are not different ($p=0.240$, $p=0.0931$, $p=0.132$, respectively).Within SSR, PS in Configuration 2 and 3 were less than Configuration 1 ($p=0.041$), but Configurations 2 and 3 were not different ($p=0.589$).

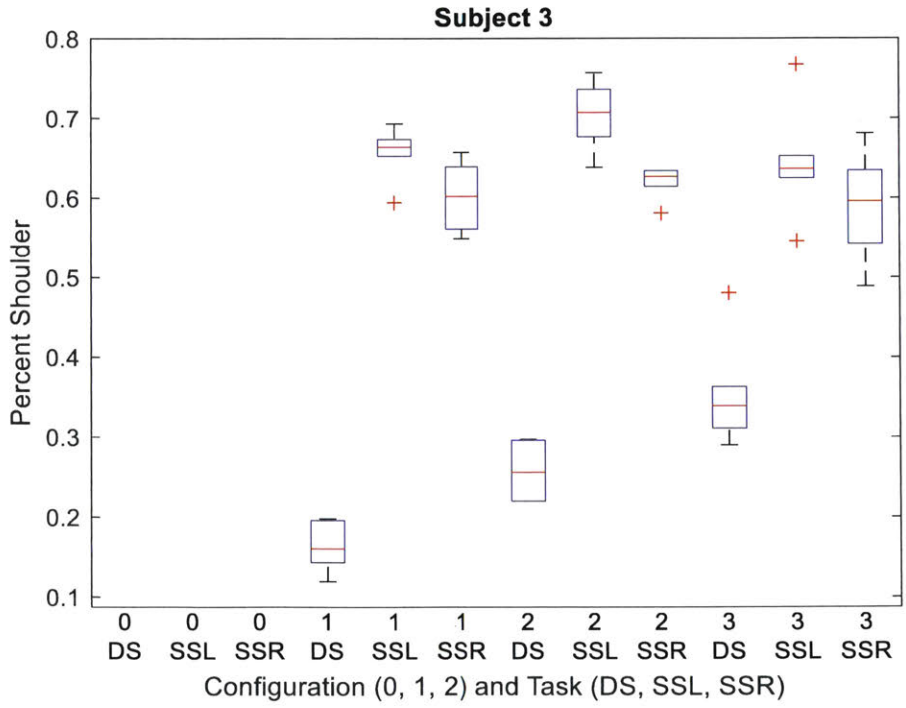

Figure 32: Percent Shoulder, Subject 3

Subject 4 has an increase in PS when in SSL/SSR as compared to DS ($p<0.005$). However, PS in SSL and SSR, for subject 4, are not different ($p=0.240$).

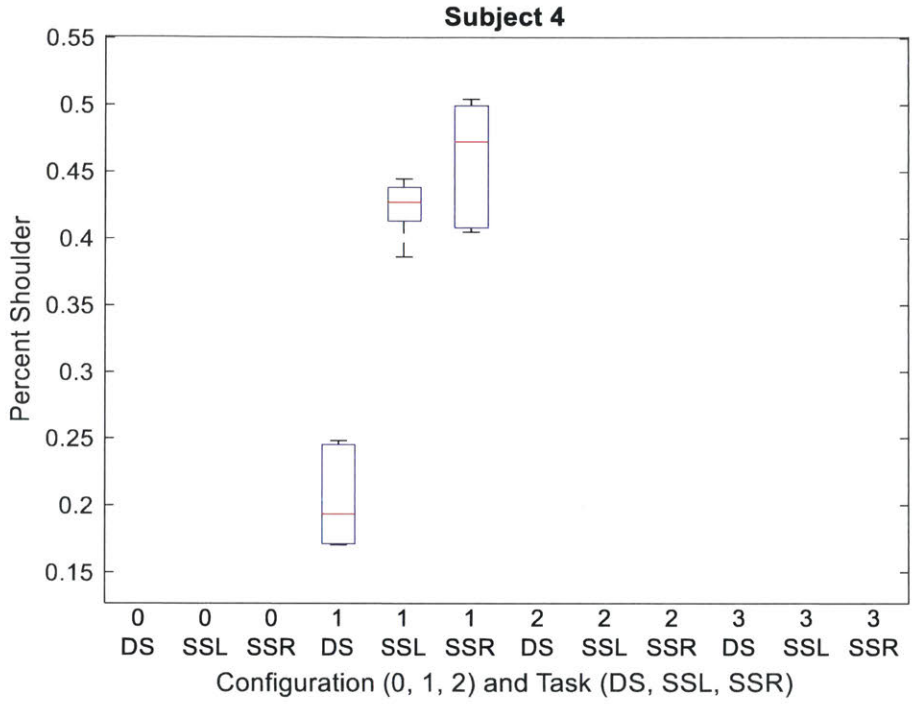

Figure 33: Percent Shoulder, Subject 4

C. Boxplots Postural Stability Dependent Measures

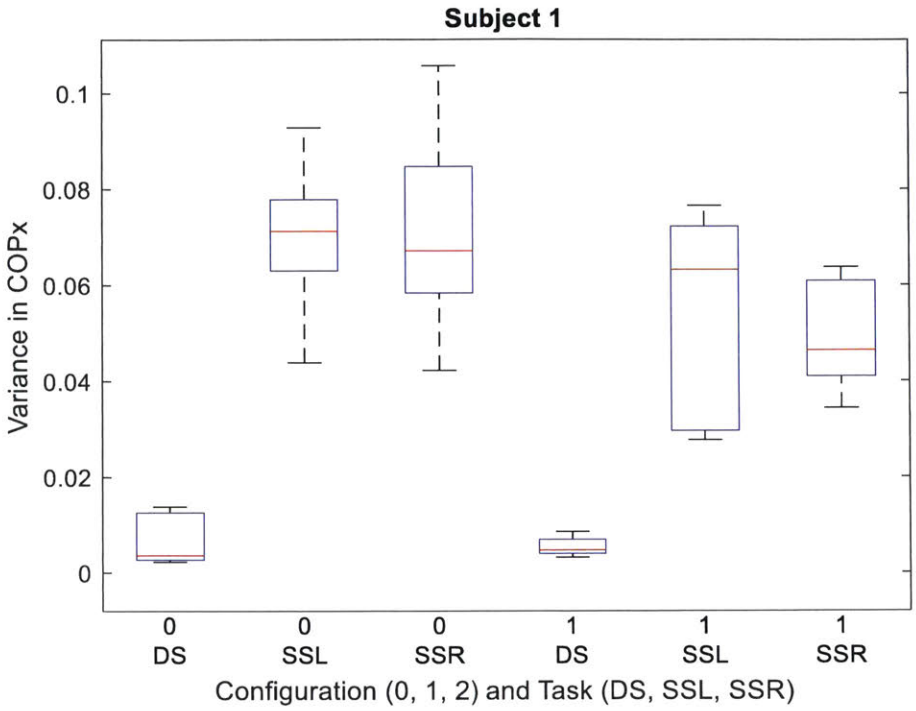

Figure 34: Variance in COP_x , Subject 1

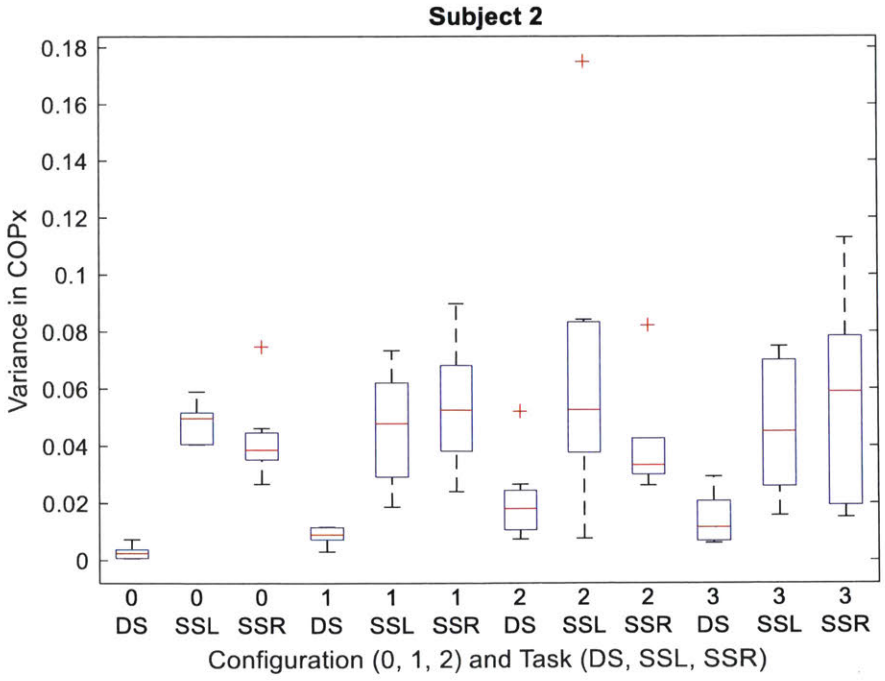

Figure 35: Variance in COP_x , Subject 2

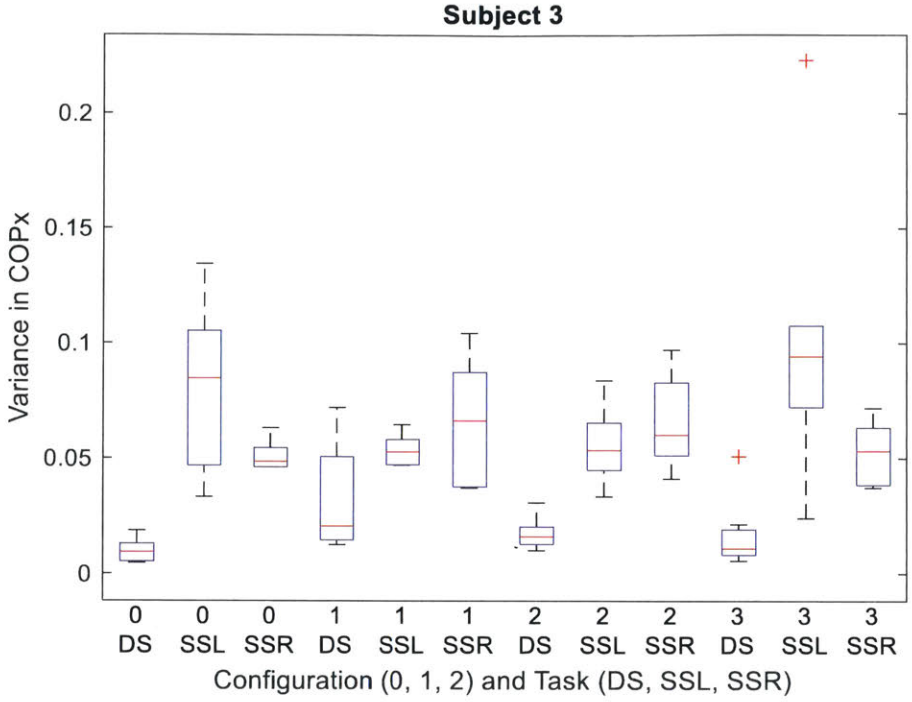

Figure 36: Variance in COP_x , Subject 3

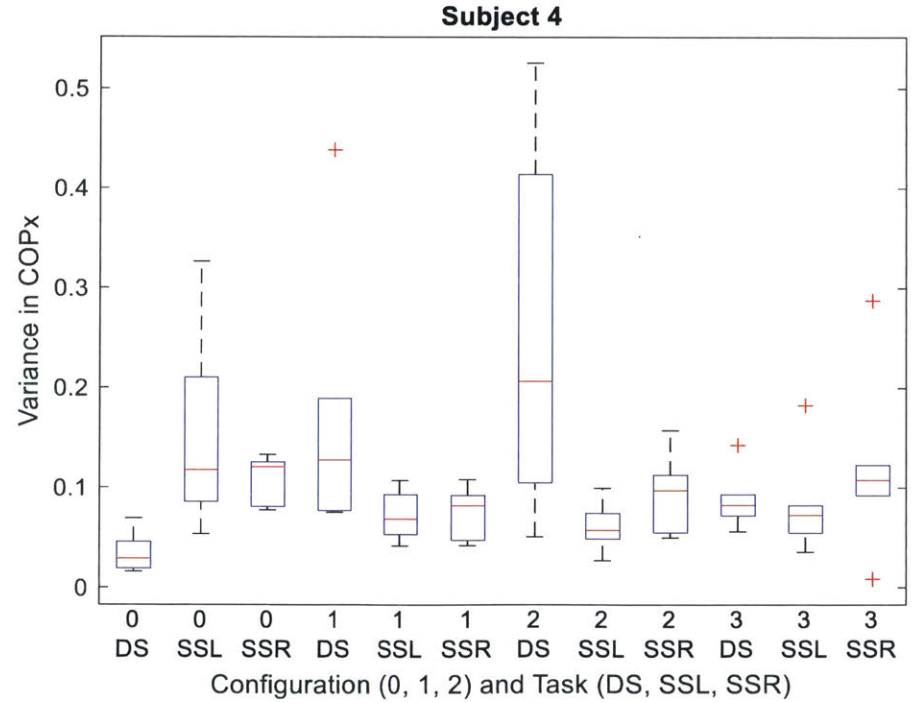

Figure 37: Variance in COP_x , Subject 4

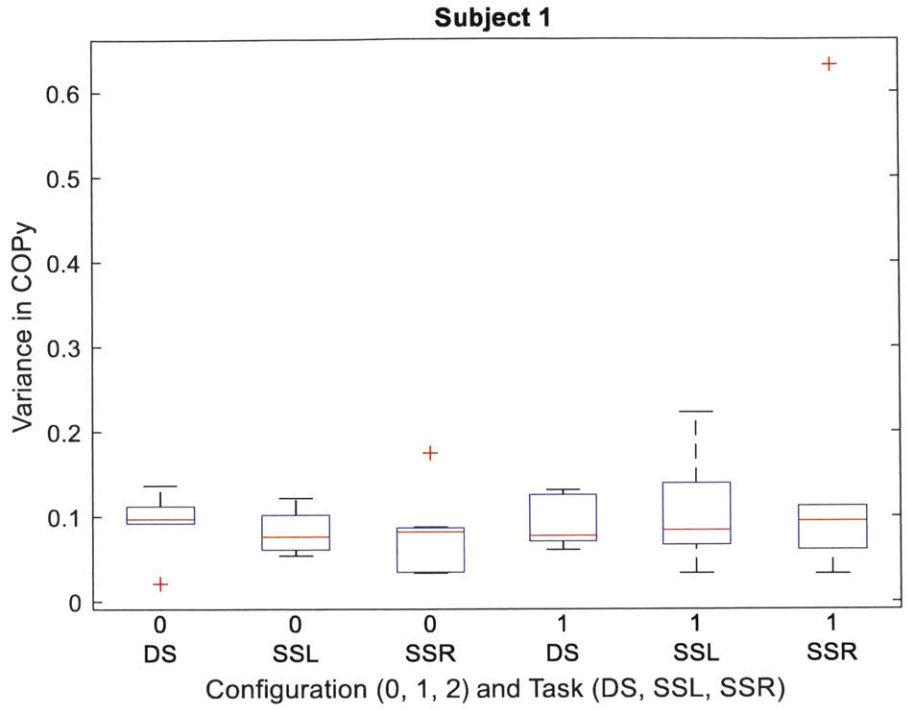

Figure 38: Variance in COP_y , Subject 1

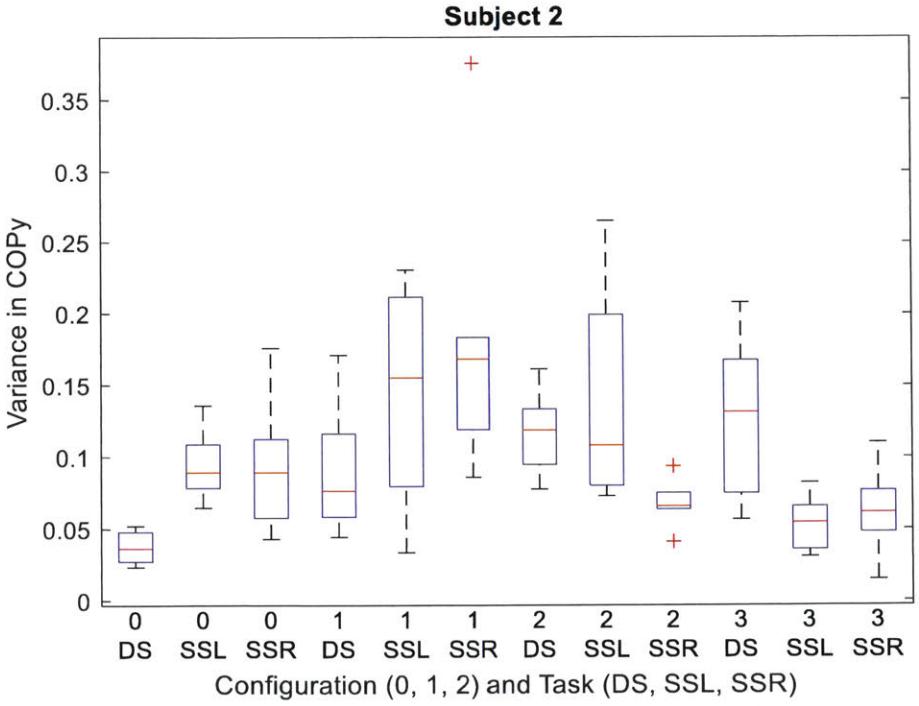

Figure 39: Variance in OP_y , Subject 2

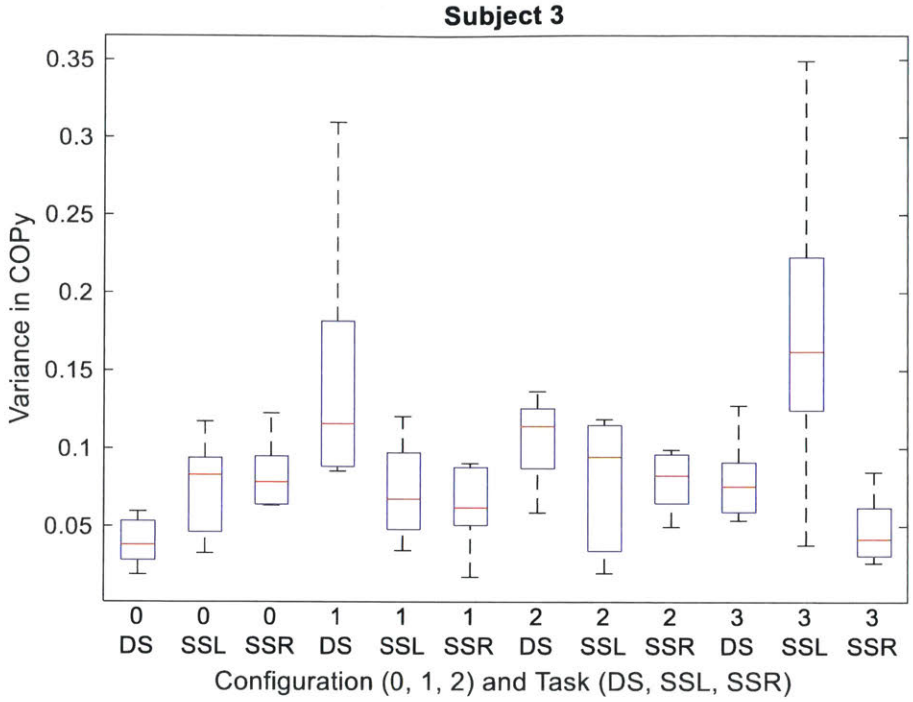

Figure 40: Variance in COP_y , Subject 3

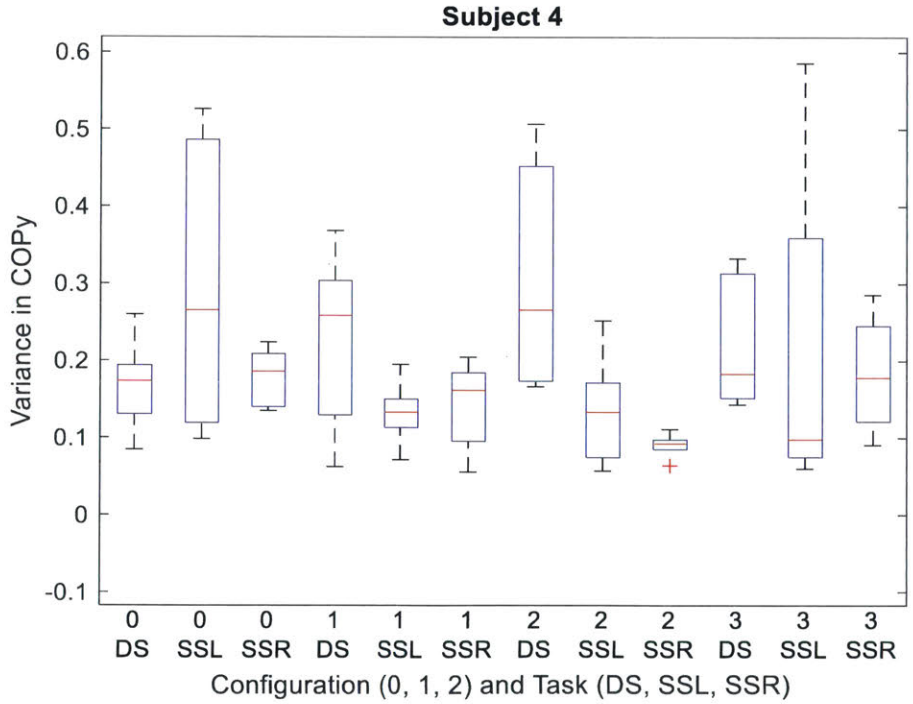

Figure 41: Variance in COP_y , Subject 4

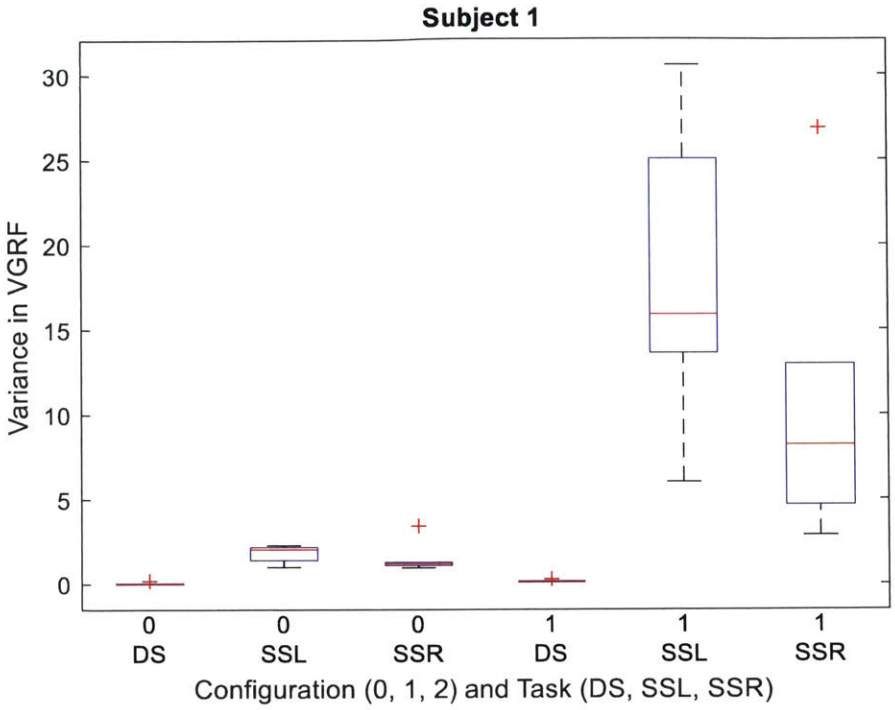

Figure 42: Variance in VGRF, Subject 1

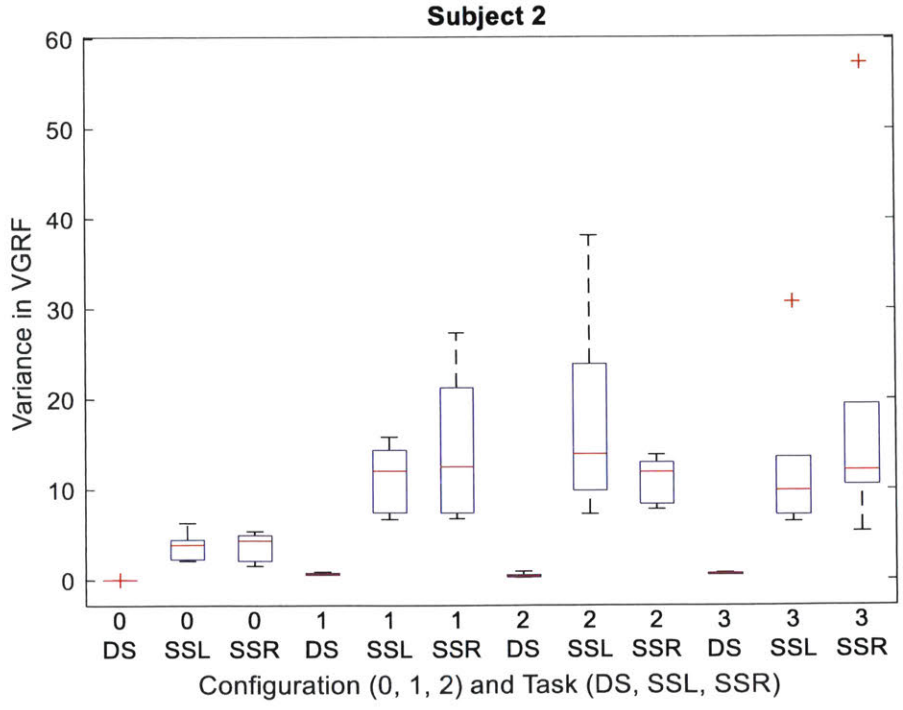

Figure 43: Variance in VGRF, Subject 2

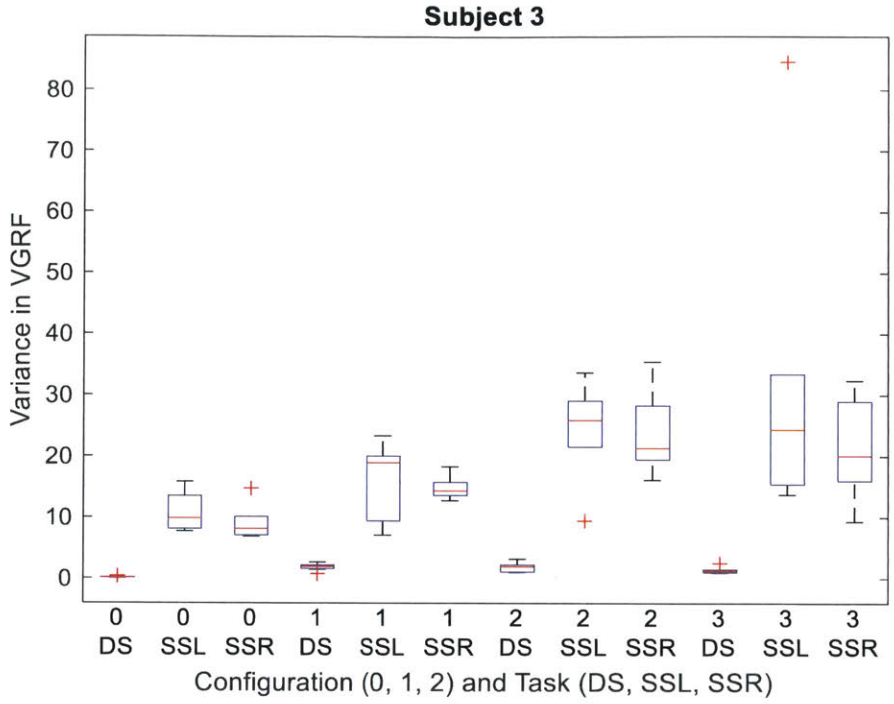

Figure 44: Variance in VGRF, Subject 3

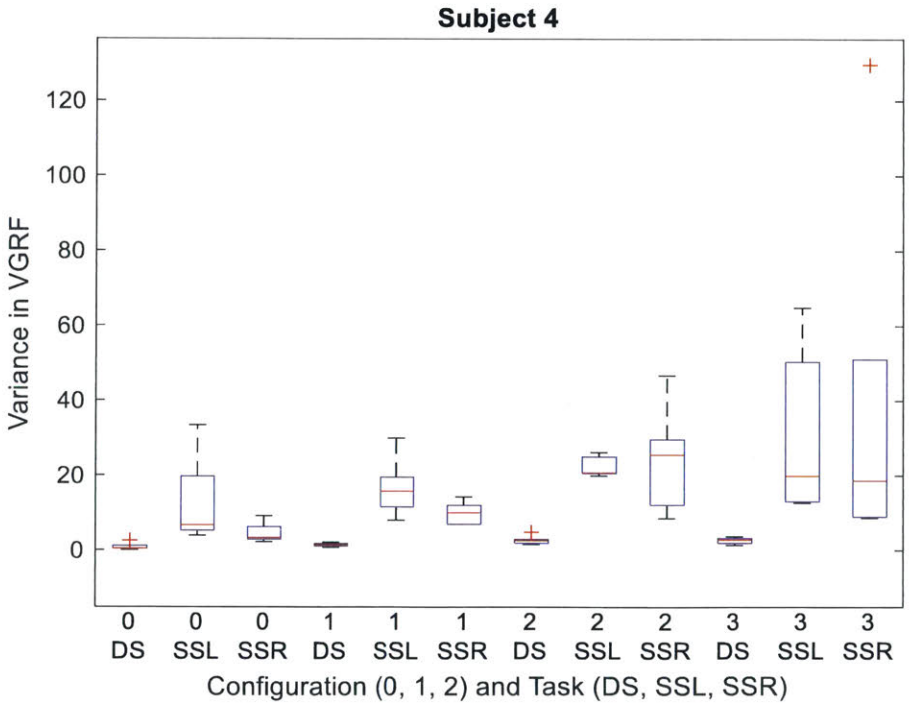

Figure 45: Variance in VGRF, Subject 4

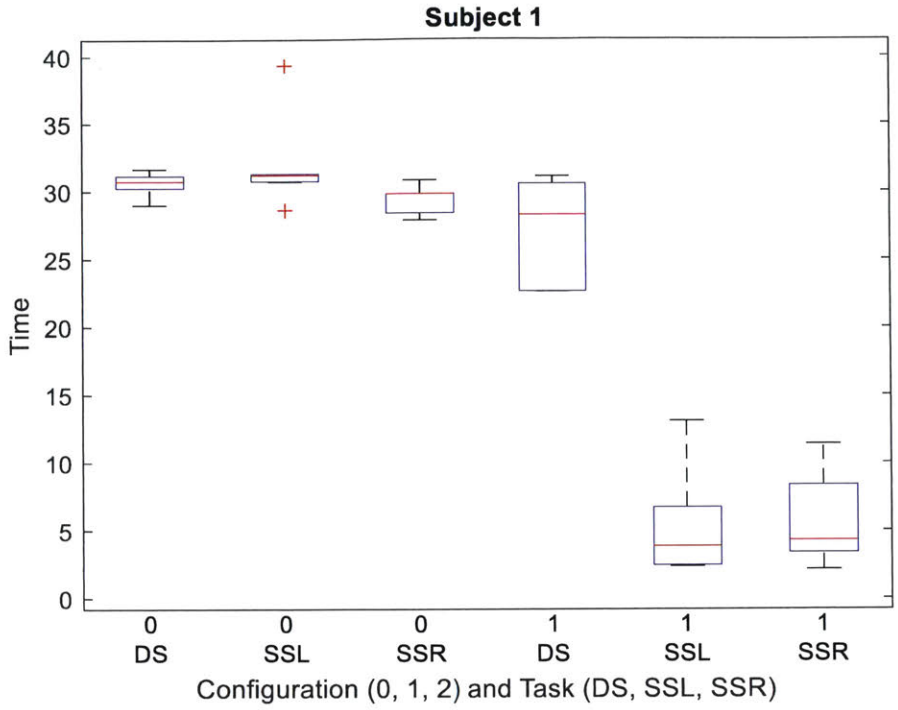

Figure 46: Time, Subject 1

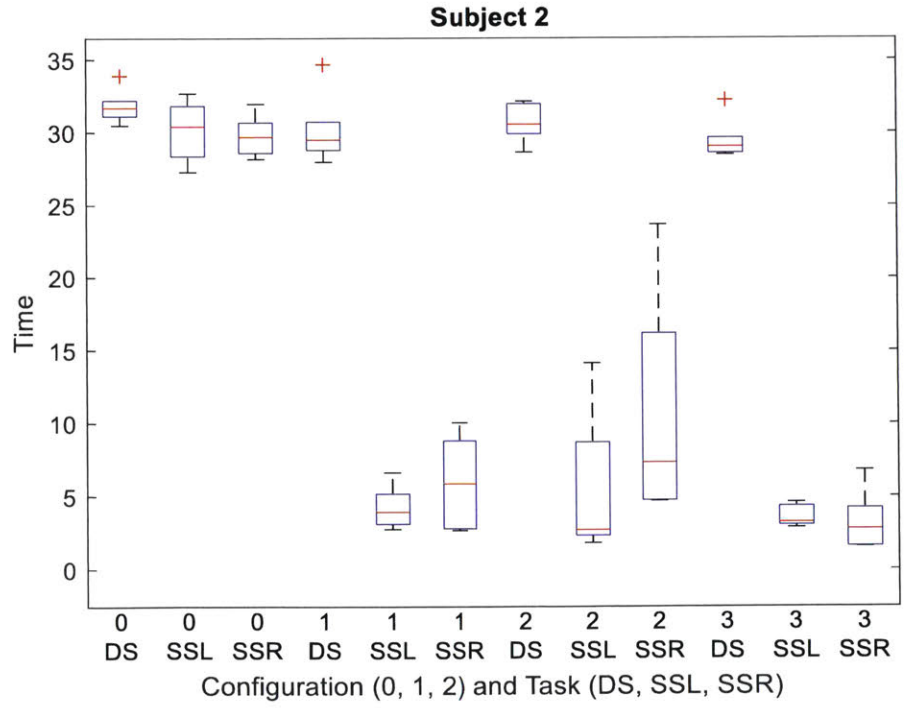

Figure 47: Time, Subject 2

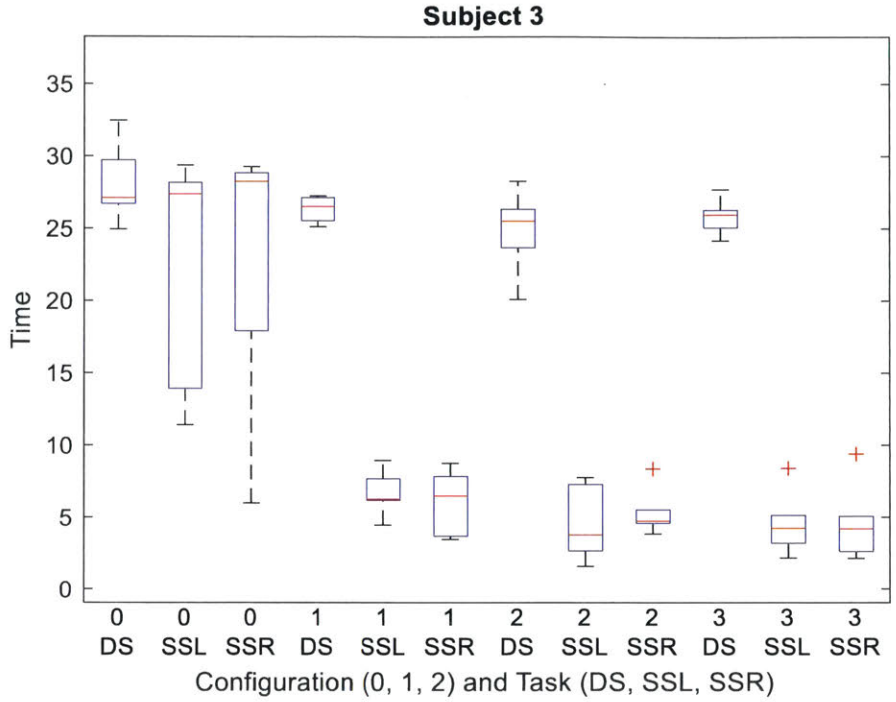

Figure 48: Time, Subject 3

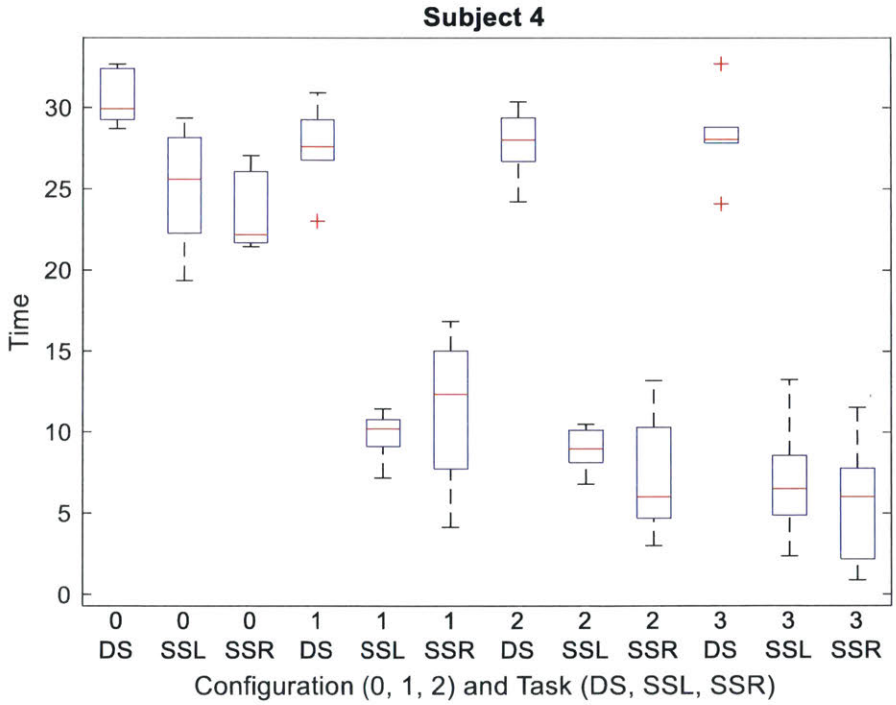

Figure 49: Time, Subject 4

D. Table of Figures

E. Keywords

1. Extravehicular Activity (EVA)
2. Space Suit Assembly (SSA)
3. Kinematics
4. Dynamics
5. Tightly-Coupled
6. Joint Torques
7. Joint Hysteresis
8. Functional Motion Envelope
9. Range of Motion (ROM)
10. Soft-Goods
11. Programmed Motions
12. Degrees-of-Freedom (DOF)
13. Self-Support
14. Indexing
15. Fleet Sizing